Structure and cooling history of the Malton Gneiss, southeastern British Columbia, using the $^{40}Ar/^{39}Ar$ method

by

Iain C. Pirie

Submitted in partial fulfillment of the requirements
for the degree of
Honours Bachelor of Science

at

Dalhousie University
Halifax, Nova Scotia
April 2000

Dalhousie University

Department of Earth Sciences
Halifax, Nova Scotia
Canada B3H 3J5
(902) 494-2358
FAX (902) 494-6889

DATE April, 2000

AUTHOR Iain C. Pirie

TITLE Structure and cooling history of the Malton Gneiss, southeastern British Columbia, using the $^{40}Ar/^{39}Ar$ method.

Degree B.Sc. Convocation May 23 Year 2000

Permission is herewith granted to Dalhousie University to circulate and to have copied for non-commercial purposes, at its discretion, the above title upon the request of individuals or institutions.

for my family

Abstract

The Malton complex, located at the northern tip of the Shuswap complex in southeastern British Columbia, is one of several structural culminations in which Precambrian basement is exposed from beneath Neoproterozoic cover sediments. The complexes preserve structure and fabric related to compressional deformation from Middle Jurassic to Late Cretaceous - early Paleocene time which are overprinted by extensional features of mid-Paleocene to Miocene age. Two high angle west-side-down normal faults, the North Thompson-Albreda and Rocky Mountain faults, bound the Malton Gneiss of the Malton complex and define the northern tip of the Shuswap complex. $^{40}Ar/^{39}Ar$ analyses of amphibole and muscovite obtained along two transects oriented perpendicular the Rocky Mountain Fault were conducted in order to constrain the cooling history of the Malton Gneiss. Only one amphibole analysis was successful, yielding a cooling age of 116 ± 3.4 Ma in the hanging wall of the North Thompson-Albreda Fault. Muscovite analyses were generally more successful and yielded cooling ages of 62 ± 0.4 Ma in the hanging walls and 60 ± 0.4 in the footwalls of the North Thompson-Albreda and Rocky Mountain faults. Temperature vs. time plots, combining already existing AFT data with the results of this study, indicate low temperature cooling rates of *ca.* 6 $^{0}C/Ma$ and *ca.* 22 $^{0}C/Ma$ for the Bulldog Gneiss (located in the footwall of the Rocky Mountain Fault) and the western Malton Gneiss respectively. A high temperature cooling rate of *ca.* 3 $^{0}C/Ma$ is estimated for the hanging wall of the North Thompson-Albreda fault. The relatively faster cooling rate of the Malton Gneiss in comparison to the Bulldog Gniess is likely the combined result of differential vertical offset on the North Thompson-Albreda Fault, differential erosion in Paleocene-Oligocene(?) time, and cooling by fluid flow along the fault. Muscovite cooling ages are 10-20 Ma less than biotite from the Monashee complex and cooling rates markedly slower than those described for the southern complexes of the Shuswap. The results of this study indicate an older cooling age, a slower cooling rate, and different exhumation mechanisms exist for the Malton Gneiss in comparison to the southern complexes of the Shuswap.

Table of Contents

Structure and cooling history of the Malton Gneiss, southeastern British Columbia, using the $^{40}Ar/^{39}Ar$ method

Acknowledgments

This project would not have been completed without the support and contributions of a number of people to whom I am truly indebted:

I would like to thank my advisor, Becky Jamieson at Dalhousie University, for accepting the great challenge of taking me on as her honours student. I also thank Becky for providing funding throughout the project, her valued critiquing of chapter material, as well as guiding me through the rigours of project work.

Thanks also to Olivier Vanderhaeghe at Université Henri Poincaré Nancy 1, for kicking off the project and, perhaps the greatest feat of all, surviving 18 days of field work with me in August of 1998. Olivier should be commended for his patience!

I would not have made it very far in this project if not for the support provided by the staff and faculty of the Department of Earth Sciences at Dalhousie University. Thanks go to Charlie Walls and Tom Duffett for computer and network support, Gordon Brown for producing, and on occasion, fixing my thinsections, Bob McKay for his help with the electron probe microanalysis, and Milton Graves for his photographic expertise. Special thanks to Keith Taylor for instruction on sample preparation, performing the $^{40}Ar/^{39}Ar$ analyses, and his patience while plotting spectra time and again for me, and to Pete Reynolds for walking me through the outcome of the $^{40}Ar/^{39}Ar$ analyses and reviewing all drafts of Chapter 3.

Thanks to Marcos Zentilli for coordinating the thesis project and still having time to address all my questions. Above all, thanks to Marcos for his ever optimistic outlook and positive attitude, and guidance concerning life beyond a career as an undergraduate.

Special thanks to Mike McDonough at Petro Canada and the Geological Survey of Canada, Calgary, for providing me with digitized geologic/structural maps. Thanks to Crystal Kennedy at the Nova Scotia Department of Natural Resources for sacrificing her time and work space to help me digitize the rest.

Thanks to Jim Crowley at the University of Calgary for guiding us at Frenchman Cap and providing an overview of previous work done in that area, while at the same time helping us dodge a few forest fires. Thanks to Britt Norlander for providing the sense and means to get off the mountain and away from the fire.

Finally, thanks to the countless people who provided encouragement along the way.

Chapter 1: Introduction

1.1: Purpose and scope of this study

An overview of the Cordilleran literature reveals numerous studies on the Monashee and Valhalla complexes of the Shuswap complex. These studies investigate tectonism, metamorphism, plutonism and geochronology associated with the complexes. The Shuswap complex (Carr, 1995) of southeastern British Columbia contains three major structural culminations; the Malton, Monashee, and Valhalla complexes (Figure 1). Relatively little is known about the Malton Gneiss of the Malton complex at the northern tip of the Shuswap complex in comparison to these other complexes. The Malton complex (Malton, Yellowjacket, and Bulldog gneisses), located in and adjacent to the northern Shuswap complex (Figure 2), has not received due attention in Cordilleran literature in terms of geochronology. Data obtained in this study are used to improve the existing database for the Malton Gneiss. This study used field mapping and petrography, combined with literature review, and $^{40}Ar/^{39}Ar$ analysis of samples collected from the study area to address the following:

1) The relation of the Malton complex to the other complexes of the Shuswap is not well defined. There is some evidence to suggest that extension acted differently in the vicinity of the Malton complex in comparison to the southern complexes (van der Velden and Cook, 1996). Structural data combined with literature review were used to define the nature of the tectonic history of the Malton Gneiss and compare/contrast it to gneisses of other complexes in the Shuswap complex.

2) Substantial isotopic data exist for the Omenica belt, but the data are limited in the area of the Malton Gneiss. Specifically, the cooling history of the Malton Gneiss and its relation to extension have not previously been defined. By identifying the timing of cooling of the various units in the area of the Malton Gneiss and combining this information with structural data, an attempt to further constrain the exhumation history of the Malton Gneiss has been made.

The significance of metamorphic core complexes has been of interest in studies of the evolution and structure of the North American Cordillera since they

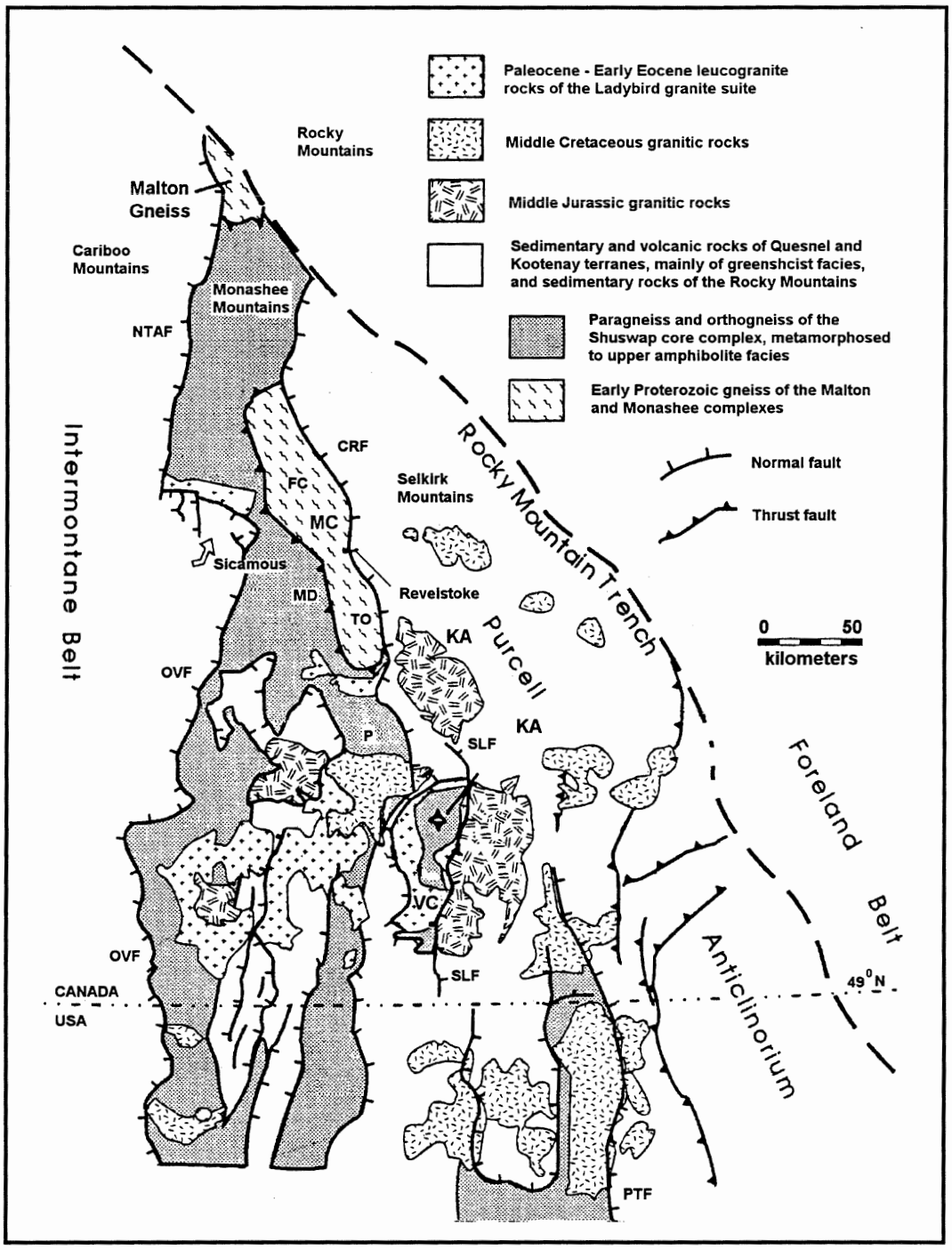

Figure 1: Tectonic map of southern Omineca belt, modified from Parrish et al (1988) and Wheeler and McFeely (1991). The southern Omineca belt is bounded on the east by the Southern Rocky Mountain Trench and the west by the North Thompson-Albreda fault (NTAF), in the area of the Malton Gneiss. CRF – Columbia River fault; OVF – Okanagan Valley fault; SLF – Slocan Lake fault; PTF – Purcell Trench fault; MC – Monashee, and VC – Valhalla complexes; FC – Frenchman Cap; TO – Thor-Odin; P – Pinnacles; MD – Monashee decollement; KA – the Kootenay Arc

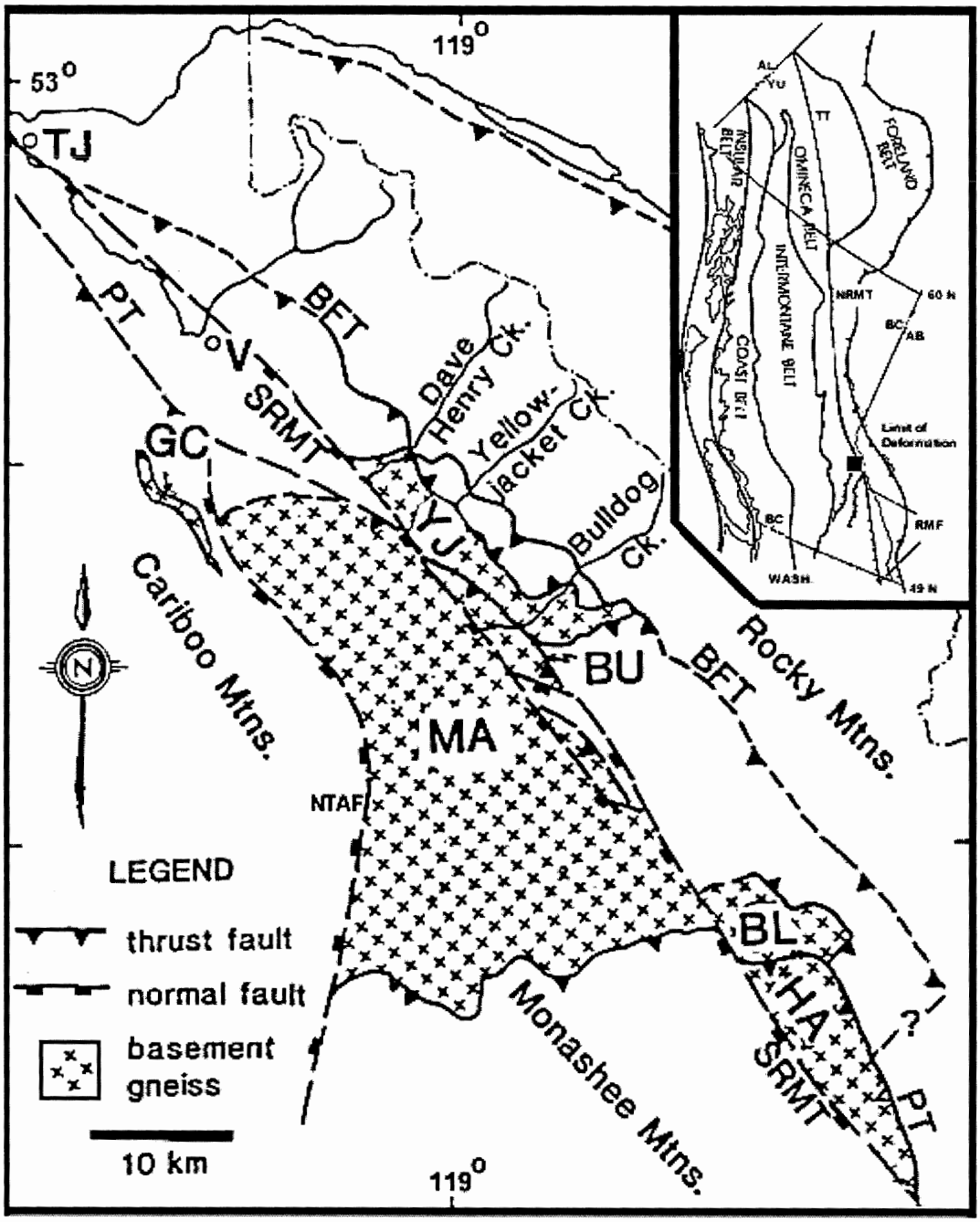

Figure 2: Generalized geological map of the Malton complex (modified from McDonough and Parrish, 1991; Monger, 1993). TT – Tintina Trench; NRMT – Northern Rocky Mountain Trench; NTAF – North Thompson-Albreda fault; SRMT – Southern Rocky Mountain Trench (Rocky Mountain Fault); BFT – Bear Foot thrust; PT – Purcell thrust; MA – Malton Gneiss; YJ – Yellowjacket Gneiss; BU – Bulldog Gneiss; BL – Blackman Gneiss; HA – Hugh Allan Gneiss; TJ – Tete Jaune Cache; V – Valemount. Neoproterozoic Windermere Supergroup metasedimentary rocks are shown in white.

were first identified in the late 1970's - early 80's (e.g., Coney, 1979; Armstrong, 1982). Initially the tectonic significance of the complexes was debated in terms of extension vs. compression. In the Canadian Cordillera, it is now widely viewed that the complexes preserve largely compressional ductile fabrics of Jurassic through early Eocene age overprinted by extensional brittle deformation structures of mid to late Eocene age (Coney and Harms, 1984; Tempelman-Kluit and Parkinson, 1986; Brown and Journeay, 1987; Parrish et al., 1988). Eocene extension has become well documented throughout the Cordillera but the driving mechanisms and timing of extension remain a topic of considerable debate. Much of the debate surrounding mechanisms of extension remains model-driven and is beyond the scope of this study.

Previous isotopic work conducted by others suggest the Malton Gneiss is of the same affinity as gneisses located in the more southern Monashee and Valhalla complexes. However, $^{40}Ar/^{39}Ar$ results obtained in this study suggest that extension acted differently in the area of the Malton complex. This study concludes that Eocene-Oligocene extensional features in the area of the Malton complex played a significant role in the exhumation of the Malton Gneiss, thereby differentiating the Malton Gneiss from other complexes of the Shuswap complex in terms of timing and rate, and probably mechanisms, of exhumation.

1.2: Cordilleran overview

The Canadian Cordillera has been divided into five physiographic belts (inset, Figure 2) oriented parallel to the western continental margin of North America (Armstrong et al., 1977; Monger et al., 1982). These belts have been identified on the basis of lithology and tectonic significance. Compressional tectonics affected the Cordillera from Cretaceous to Eocene time when extension took place. Eocene extension took place along a number of normal faults and extensional shear zones and was associated with magmatism and the deposition of sediments such as those in the Rocky Mountain Trench.

Northeasterly directed telescoping of passive margin and marine sediments of the paleocontinental North American western margin was initiated

in mid-Jurassic time as a result of accretion of an allocthonous terrane in the late Early Jurassic (Brown et al., 1986). This terrane was originally termed Super Terrane I (Monger, 1982), and later termed the Intermontane superterrane (Price et al. 1985).

The folded and thrusted passive margin sediments are referred to as the physiographic Rocky Mountain belt (RMB). Immediately west of the RMB is the Omineca Crystalline belt (OCB), one of two metamorphic and plutonic welts in the Canadian Cordillera, the other being the Coast Plutonic Complex (CPC). The OCB straddles the boundary between the continental margin of North America and the composite Intermontane superterrane and contains the core complexes of the Canadian Cordillera (Monger et al., 1982; Coney and Harms, 1984). The general structure of the southern Canadian Cordillera was summarized by Clowes et al. (1987), Cook et al. (1988), Varsek et al. (1991), Cook et al. (1992), and Carr (1995). Beneath the Omineca belt, the Moho is generally planar despite surface topographic relief (Cook, 1992, 1995; Carr, 1995).

The Rocky Mountain Fault, located within the Southern Rocky Mountain Trench, and North Thompson-Albreda Fault (Figure 2) are products of Eocene extension and are of particular interest to this study (Chapter 2). Both Jurassic to Eocene compressional shear zones and early to middle Eocene extensional shear zones are listric into the lower crust or Moho under the Intermontane belt, interpreted to have acted as a zone of detachment during both compression and extension (Cook et al., 1992).

1.3: Geology and tectonics of the Omineca belt

The development of the Omineca belt involved both compressional and extensional tectonic histories, summarized in Figure 3 by Cook et al. (1992). Each is considered separately here in order to differentiate structures associated with each.

1.3.1: Compressional history

The Monashee complex, located in the central area of the Shuswap complex (Figure 1), is the basis for much of the interpretation of the history of the

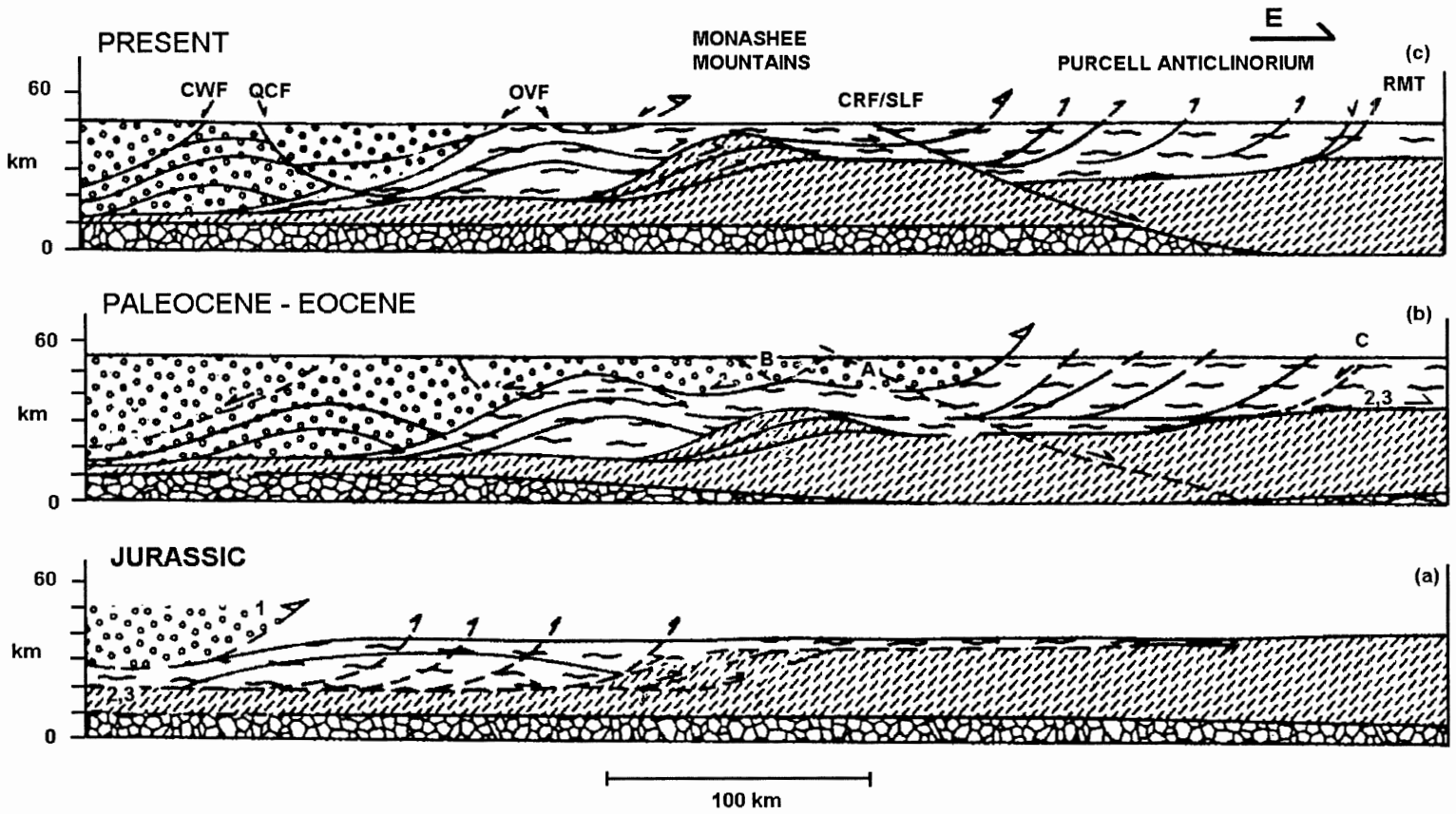

Figure 3: Schematic illustration of the crustal evolution of the southern Canadian Cordillera, modified after Cook et al. (1992). (a) Passive margin development from Proterozoic to Mesozoic, (b) contraction during two major compressional episodes in the Mesozoic and early Tertiary, (c) extension during the middle Tertiary. Faults in the Purcell Anticlinorium (c) and illustrated in (b) and (a) are suggested compressional features. CRF/SLF and A – Columbia River / Slocan Lake fault system; B – Okanagan Valley / Eagle River fault system; RMT and C – Rocky Mountain Trench (extensional feature); 1 – Intermontain supperterrane suture; 2, 3 – Sole thrust, Monashee decollement; CWF – Coldwater Fault; QCF – Quilchena Creek Fault; OVF – Okanagan Valley Fault.

Omineca belt. It was interpreted by Brown and Journeay (1987) to be a crustal-scale duplex developed during late Mesozoic crustal thickening. The upper boundary of the Monashee complex, the Monashee décollement, was identified by Brown et al. (1986) as the shear zone which decoupled the cover from its basement, and accounted for at least 80 km of shortening by the middle Late Jurassic. The Monashee décollement has been interpreted as the westward continuation of the sole thrust (Figure 3) that underlies the Foreland belt (Cook et al., 1992; Brown et al., 1992; Carr, 1995; Digel et al., 1998).

Early displacement along the Monashee décollement carried upper-plate rocks of the Shuswap complex eastward onto the Monashee complex during Middle Jurassic peak regional metamorphism (Brown and Journeay, 1987). Exhumation of the Monashee complex during this period is estimated to have been between 10 and 15 km (Journeay, 1985, 1986, cited in Brown and Journeay, 1987).

Reactivation of the Monashee décollement as a thrust is believed to have occurred sometime in the Late Cretaceous or early Tertiary (Journeay, 1985, 1986). Hotter and deeper tectonic levels of the Shuswap complex were thrust upward and eastward onto cooler and tectonically shallower levels of the Monashee complex (Brown and Journeay, 1987). Back-folding and west-directed thrusting of continental margin rocks over the Intermontane superterrane occurred near the west edge of the Omineca belt (Brown et al., 1986, Price, 1986). Parrish et al. (1988) noted that shortening between Late Jurassic and Paleocene time resulted in high-grade diachronous metamorphism, attained in Late Cretaceous-Paleogene time, and development of east verging structures (folds and faults) which affected Precambrian crystalline basement and overlying metasedimentary rocks, now exposed in the Omineca belt. On a more regional scale, strike-slip faulting in the western Intermontane and Insular (?) Belts (Gabrielse, 1985; Cook et al., 1992) and plutonism in the Omineca belt were associated with compression in the Cordillera during the mid-Cretaceous through early Tertiary (Cook et al., 1992), the result of oblique subduction from

the west (McDonough and Simony, 1988, 1989; Struik, 1993).

Reactivation of the Monashee décollement was probably the result of accretion of the Pacific Rim and Olympic terranes through Late Cretaceous and early Tertiary time (Monger, 1982), following accretion of a second composite terrane, the Insular superterrane (Price et al., 1985), to the continental margin of North America in the Late Jurassic. Cumulative shortening and uplift from mid-Late Jurassic to early Tertiary brought basement rocks of the Monashee complex up from a maximum depth of 25 km to minimum depths of between 10 and 12 km (Brown and Journeay, 1987).

Diachronous thermal metamorphism is described for the Shuswap complex by a number of authors (Carr, 1995; Digel et al., 1998; Gibson et al., 1999). Peak thermal metamorphic conditions were attained in the central and southern Shuswap complex through Middle Jurassic to early Tertiary time. Geochronology studies have revealed Early Proterozoic and Late Cretaceous - Eocene metamorphism in basement rocks of the Monashee complex, and suggest that these rocks were located to the east of the metamorphic front prior to the Late Cretaceous (Carr, 1995).

The Monashee complex preserves an inverted diachronous metamorphic field gradient within the uppermost footwall and immediate hanging wall of the Monashee décollement (Crowley and Parrish, 1999; Gibson et al., 1999). The inverted field gradient is defined by a zone of silimanite + K-feldspar + melt, present at the highest structural level, underlain by a zone of kyanite + stable muscovite. At deeper structural levels the metamorphic assemblages appear to exhibit a normal gradient. Digel et al. (1998) proposed that the inversion was the result of deformation of isograds by east-directed shear strain and attenuation in the footwall, leading to relative lateral transfer of rocks preserving evidence of inverted diachronous metamorphism.

Niether Digel et al. (1998) nor Crowley and Parrish (1999), suggested that overthrusting of hotter rocks onto cooler rocks was responsible for the metamorphic inversion. Crowley and Parrish (1999) concluded that heat was

generated from a deeper source which resulted in what are now upper crustal rocks reaching peak metamorphic conditions before structurally lower crustal rocks. Timing of this event was prior to overthrusting of the now structurally lower crustal rocks by the current upper crustal rocks. Details concerning metamorphism in the area of the Malton Gneiss are presented in Chapter 2.

1.3.2: Extensional history

East-west extension in the Cordillera is well documented throughout Canada and the United States. However, the mechanisms of extension and exhumation of the core complexes have been widely debated. Only extension affecting the Canadian Cordillera is discussed here as extension within the southwestern United States is quite different and beyond the scope of this study.

Molnar et al. (1993) identified three major processes which may explain a change from crustal shortening and thickening to extension: 1) a sudden increase of relief as an isostatic response to removal of the lithospheric root of the orogen; 2) a reduction in compressive forces applied to the margins of the mountain range; 3) a change in the rheology of the lithosphere leading to mechanical weakening and gravitational collapse.

England (1982) and Molnar and Chen (1983) suggested that thickened crust will spread laterally because of gravitational instability if there is sufficient topographic head and sufficient lowering of crustal viscosity. This would require that certain boundary conditions were met, such as a low compressive stress field and laterally confining regions that were weaker than the area of thickened crust (Coney and Harms, 1984).

Extensional features in the Canadian Cordillera formed during Late Cretaceous to Miocene time, beginning at about the same time as thrusting stopped (Coney and Harms, 1984; Tempelman-Kluit and Parkinson, 1986; Brown and Journeay, 1987; van der Velden and Cook, 1996; Johnson and Brown, 1996). Thickened crust (50 to 60 km thick) west of the foreland fold and thrust belt, formed during Mesozoic compression, became the site of deep-seated crustal extension during Eocene to Miocene time (Figure 3) (Coney and

Harms, 1984) leading to exhumation of the core complexes in the foot-walls of the normal faults (Cook et al., 1992).

In the Omineca belt, extension is believed to have been accompanied by a pulse of magmatism in the Cenozoic (generated in response to a pulse of crustal thickening *ca.* 52 Ma), which reduced crustal viscosity in the Eocene and again in the Oligocene-Miocene, and by a lowering of intraplate convergent stress fields due to changing plate kinematics (Coney and Harms, 1984; Brown and Journeay, 1987; Carr, 1995; Vanderhaeghe and Teyssier, 1997). However, ductile extensional faulting and associated plutonism evident in southern core complexes of the Shuswap complex, such as the Valhalla complex (Figure 1), have a debated association with extensional processes identified in the more northern Monashee complex (Brown and Journeay, 1987; Vanderhaeghe and Tessyier, 1997).

In the Thor-Odin dome of the Shuswap complex (Figure 1), Vanderhaeghe and Teyssier (1997) proposed that following crustal thickening, thermal relaxation and partial melting of the mid to lower crust resulted in mechanical weakening of the crust and the initiation of orogenic gravitational collapse accommodated by normal faulting of the brittle upper crust. Orogenc gravitational collapse occurs when thickened crust becomes unstable under its own weight, accompanied by a decrease in crustal viscosity and change in boundary conditions (defined above) or change in the regional stress field, and collapses, spreading laterally. Vanderhaeghe and Teyssier (1997) focus on the role of crustal anatexis in orogenic gravitational collapse, manifest in the form of granitoids and migmatites that weaken the mid- to upper crust. Similar ideas have been proposed by Parrish (1988) and Carr (1989).

Alternate mechanisms which may have contributed to orogenic collapse include plate motion reorganization in Eocene time, resulting in a decrease in compressional forces (Engebreston et al., 1985), mantle delamination approximately 50 Ma ago that resulted in increased geothermal gradients (Bardoux and Mareshal, 1994), in part, represented by volcanism.

North of the Thor-Odin dome, at the latitude of the Monashee complex, Tempelman-Kluit and Parkinson (1986) identified an Eocene crustal shear (the Okanagan Valley Fault) with large east-west extension at the western margin of the Shuswap complex. They suggested that the core complex rose isostatically in response to unroofing caused by westward lateral displacement of the upper plate. Tempelman-Kluit and Parkinson (1986) noted that the shear zone cuts and offsets some granites in the area. According to Tempelman-Kluit and Parkinson (1986), steeply and gently dipping extensional faults which cut the upper plate but are absent in the lower plate (Brown and Journeay, 1987) are mechanically linked to the shear zone and are about the same age. Johnson and Brown (1996) have proposed approximately 45 km of Eocene east-west extension in the Omineca belt and attribute 30 km of extension to two regional listric normal faults, the Okanagan and Eagle River faults (Figure 1).

The Columbia River Fault, bounding the Shuswap complex to the east, is interpreted as a ductile-brittle normal fault of Early Eocene age (Parrish et al., 1988). The Eocene Okanagan Valley Fault (Johnson and Brown, 1996), bounding the Shuswap complex to the west, is believed to continue, or to splay, north into the North Thompson-Albreda Fault which in turn is truncated by the Rocky Mountain Fault (Campbell, 1968; Murphy, unpublished data, 1986; cited in Parrish et al., 1988).

Large-scale, intracontinental transcurrent faults include the Northern Rocky Mountain and Tintina Trench faults (inset, Figure 2), Fraser River-Straight Creek faults, and Pinchi Fault (Price and Carmichael, 1986). Dextral slip along these fault systems was interpreted by Price and Carmichael (1986) to have occurred in Late Cretaceous-Paleogene time, the resulte of oblique subduction of the Pacific plate below the western margin of the North American plate. It has been suggested that east-west crustal extension during early and middle Eocene time was caused by strike-slip displacement along the Tintina-Northern Rocky Mountain Trench fault zone (Price and Carmichael, 1986; Struik, 1993; inset, Figure 2) that resulted in a change from south to southwesterly directed fault

motion and en echelon fault zones (Fraser River-Straight Creek Fault zone).

Chapter 2: Geology and structure of the study area

The structure of the study area between the latitudes of $52^0$35'N and $52^0$45'N was studied in order to aid in sample selection and interpretation of the Ar apparent age spectra obtained in this study. Figure 4 illustrates structure within the study area. Figures 5 and 6 are schematic cross-sections along A-A' and B-B'. Structural analysis was accomplished through three methods: 1) literature review; 2) field mapping; 3) petrography of thin sections.

2.1: Geology of the Malton complex

The Malton complex, located at the northern tip of the Shuswap complex, consists of three Precambrian basement gneisses (Van Den Driessche and Maluski, 1986; Chamberlain et al., 1980; Parrish and Armstrong, 1983, cited in McDonough and Simony, 1988): the Yellowjacket Gneiss, Bulldog Gneiss, and Malton Gneiss (McDonough and Simony, 1988) (Figure 2). McDonough and Simony (1988) provided an overview of the structure, lithology, and metamorphism of the Malton complex.

Both the Bulldog and Yellowjacket gneisses are located in the immediate footwall of the Rocky Mountain Fault, east of the Malton Gneiss, and are believed to have acted as basement highs on which the Miette Group, a thin facies of Neoproterozoic metasediments in the Windermere Supergroup (Figure 7), was deposited (McDonough and Simony, 1988). The Miette Group was described by Van Den Driessche and Maluski (1986) as consisting of conglomerates, schists, and quartzites.

The gneiss bodies are characterized by thin slices of gneiss and parautochthonous cover, caught up in east-northeast directed thrust faults. The Yellowjacket gneiss, transported eastward on the oblique-slip Bear Foot Thrust (Figure 2), is composed of a minimum of four thin slices of granodioritic, augen-bearing orthogneiss and slivers of metasediment. The Bulldog Gneiss, later carried over the Yellowjacket Gneiss and its cover by the Purcell Thrust (Figure 2), is composed of banded paragniess and amphibolitic gneiss, with minor orthogniess, younger amphibolite, and metasidiment.

The Malton Gneiss lies west of the Bulldog Gneiss and west of the Rocky

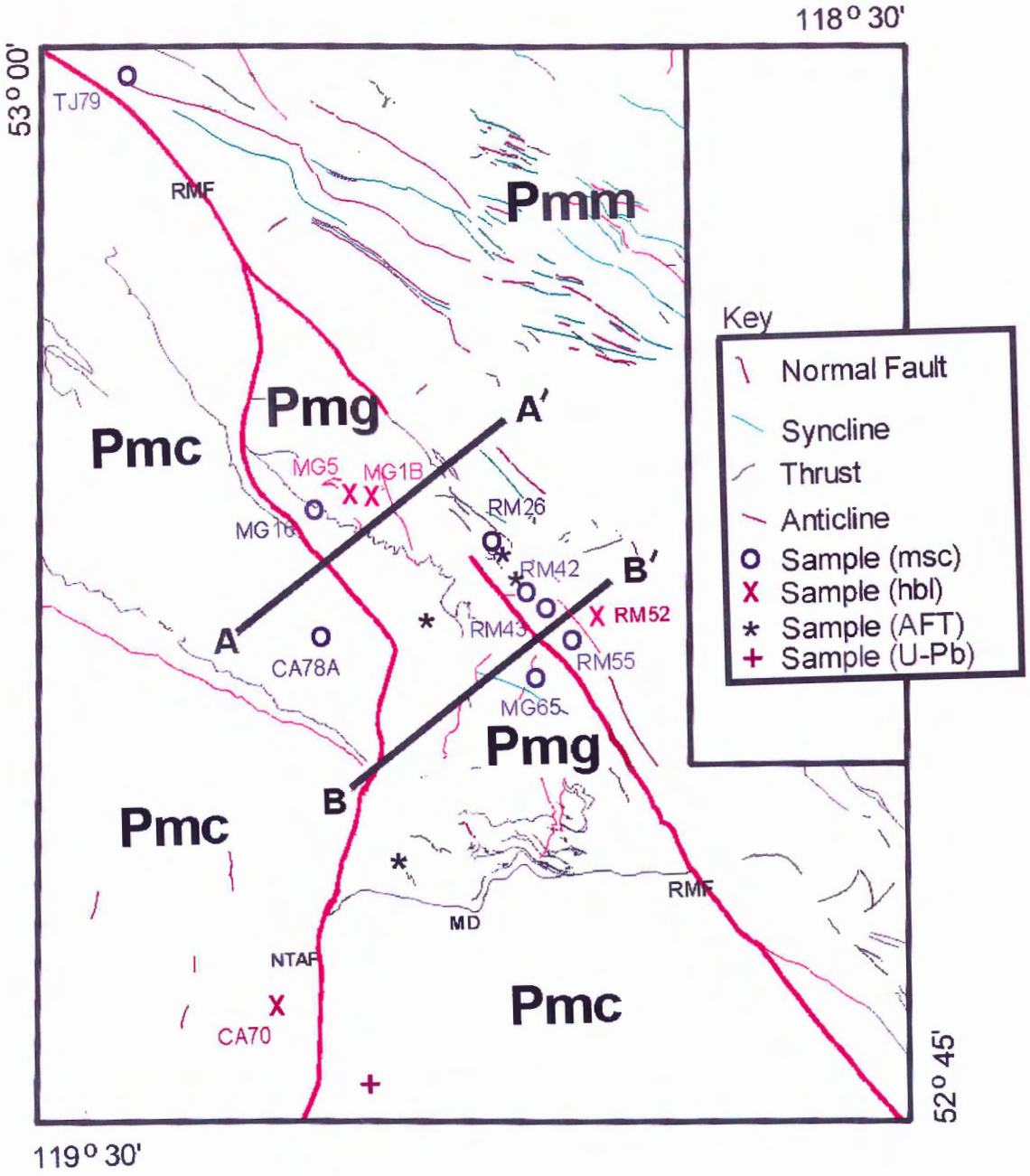

Figure 4: Structure of the northern Shuswap complex (compiled and modified from McDonough and Morrison, 1990; McDonough and Mountjoy, 1990; McDonough and Murphy, 1994; McDonough et al., 1991a, 1991b) and sample locations. Pmc – Mica Creek succession; Pmg – Malton Gneiss; Pmm – Miette Group; NTAF – North Thompson-Albreda fault; RMF – Rocky Mountain fault; MD – Malton Decollement. msc – Muscovite; hbl – hornblende; AFT – Apatite Fission Track (McDonough et al., 1995); U-Pb – zircon, monazite (Digel et al., 1998).

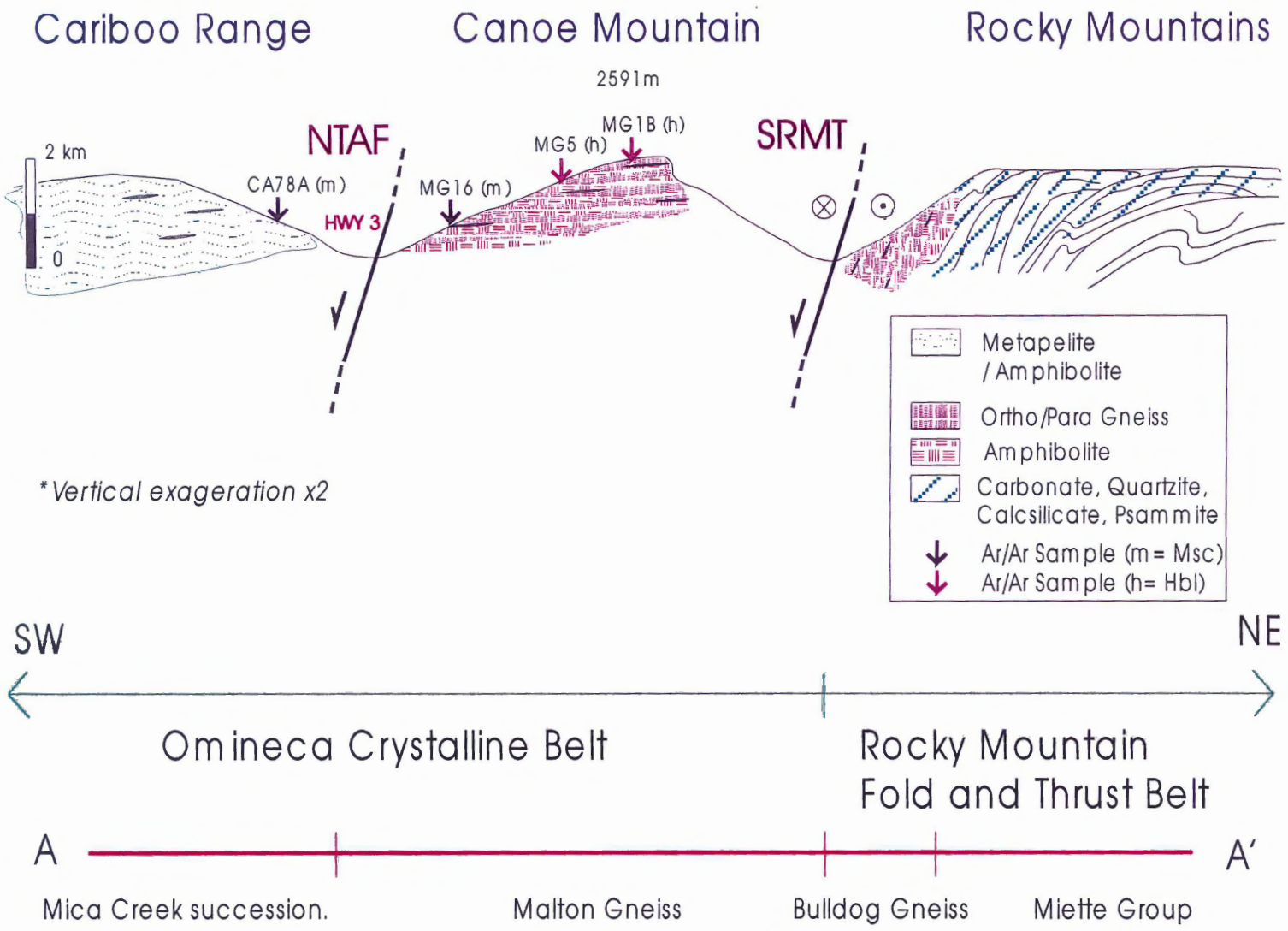

Figure 5: Schematic cross-section of A-A' locating the various units and sample locations in the study area.

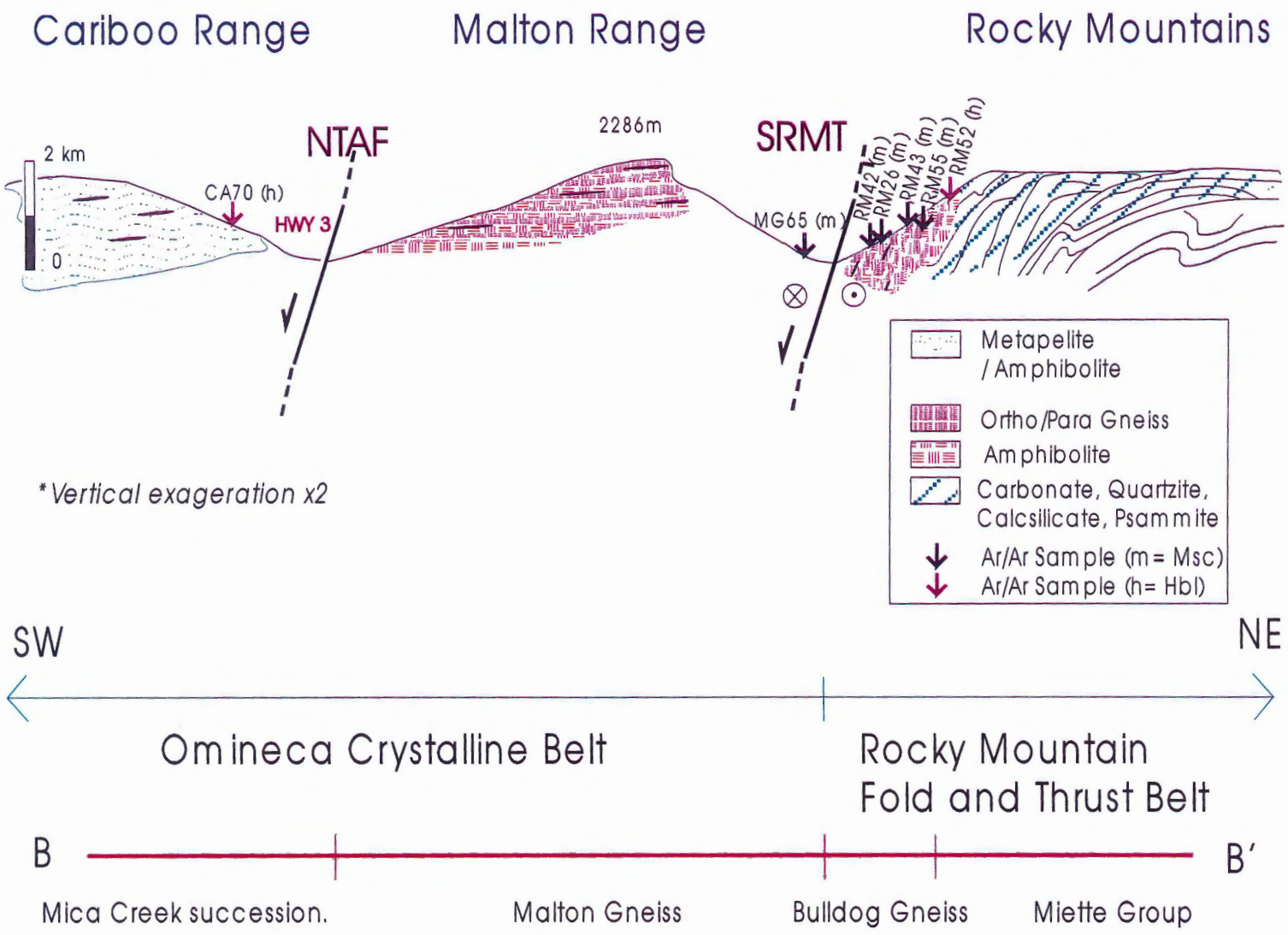

Figure 6: Schematic cross-section of B-B' locating the various units and sample locations in the study area.

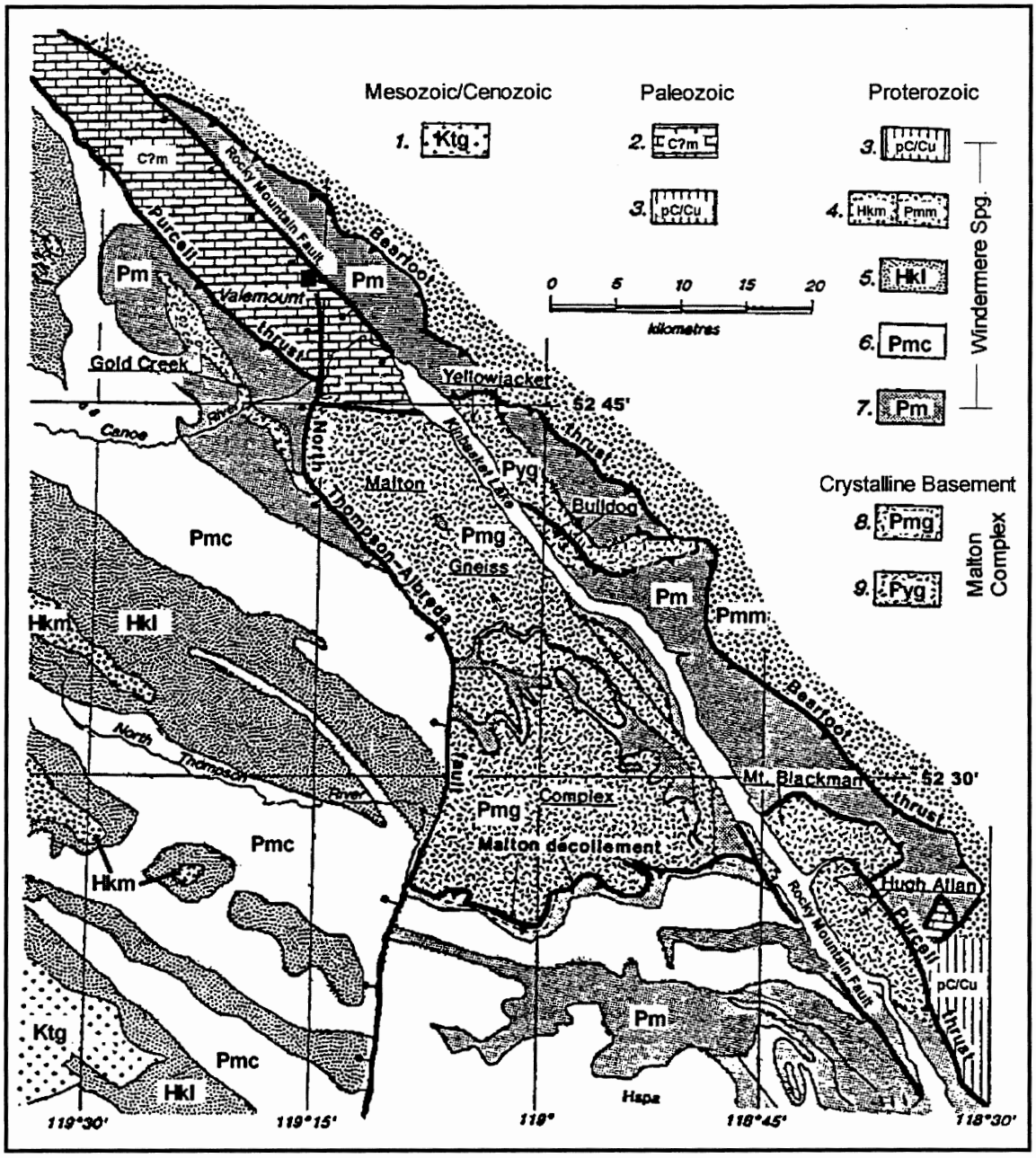

Figure 7: Geological map of the Valemount area, modified after compilation by D. C. Murphy (from Murphy and McDonough, 1990). The geology south of the Malton Gneiss shows the distribution of Mica Creek succession units; Pm – lower grit and pelite of Mica Creek succession; Pmc – Semipelite-amphibolite unit; Hkl – lower Kaza; Hkm – middle Kaza; Ktg – Cretaceous granite; Pmg – Paleoproterozoic Malton Gneiss; Pyg – Paleoproterozoic Yellowjacket Gneiss; Pmm – middle Miette; pC/Cu – undifferentiated Neoproterozoic to Upper Cambrian strata; C?m – Middle Cambrian ? carbonate.

Mountain Fault (Figure 2). Both the Bulldog and Malton gneisses lie within the hanging wall of the Purcell Thrust. Simony et al. (1980) have shown that the detached cover above the Malton Gneiss may be mapped continuously into Horsethief Creek Group strata of the Mica Creek area, west of the Malton Gneiss and the Shuswap complex, making the Bulldog succession Horsethief Creek Group equivalent. The Miette Group and Mica Creek succession of the Horsethief Creek Group are part of the Windermre Supergroup surrounding the Shuswap complex (Figure 7). The Mica Creek succession south of the Malton complex is suggested to represent a locus of Neoproterozoic volcanism and rifting of the western margin of Laurentia (Pell and Simony, 1987; Sevigny, 1988; Ross, 1991).

The Malton Gneiss was interpreted by McDonough and Simony (1988) to be part of the same complex as the Bulldog Gneiss, based on similarity of gneiss and Windermere Supergroup cover lithologies. Both gneisses consist of four lithologic units: 1) Leucocratic, granitic augen gneisses and associated aplite; 2) melanocratic, amphibolitic gneisses with interlayered quartz-rich paragneisses; 3) weakly foliated, leucocratic L-tectonite having a hornblende + biotite lineation; 4) dykes and tectonic pods of amphibolite, and schistose mafic dykes.

Leucocratic orthogneiss has been interpreted to have intruded the paragneiss of the Malton Gneiss by 2000 Ma and is nearly the same age as orthogneiss present in the Bulldog Gneiss (Parrish and Armstrong, 1983). This magmatic event occurred too early to play a role in compressional or extensional events within the Omineca belt, but its presence supports correlation of various gneissic bodies within the Malton complex.

Other similarities linking gneissic units include a homogeneous body of augen gneiss located in the Malton Gneiss (Morrison, 1982) which strongly resembles augen gneiss of the Yellowjacket Gneiss. The cover sequences of the gneisses are of the same affinity (Windermere Supergroup), stratigraphic position, and thickness (McDonough and Simony, 1988) (Figure 3).

The basement-cover contact is interpreted to pre-date peak metamorphic

conditions Paleozoic, whereas the Bear Foot Thrust is interpreted as pre- to syn peak metamorphic conditions, pre-dating dextral motion on transcurrent faults identified in the northern Canadian Cordillera (McDonough and Simony, 1988). The staurolite - kyanite and garnet isograds in the Miette Group (Figure 8) are not offset by the Bear Foot Thrust. Post-dating the Bear Foot Thrust, the Purcell Thrust was interpreted by McDonough and Simony (1988) as postmetamorphic, based on porphyroblast - foliation relationships from the footwall of the fault. In the Selkirk, Monashee, and Cariboo Mountains, regional Mesozoic isograds strike generally northwest-southeast; however, south of the Malton Gneiss that pattern is deflected into an east-west trend, parallel to the southern boundary of the Malton Gneiss (Digel et al., 1998). Digel et al. (1998) interpreted the reorientation of the isograds as a response to thickening of the Malton Gneiss, as basement slices (including the Malton Gneiss) from north of a north-facing lateral ramp were forced up relative to adjacent cover rocks to the south during reactivation of the basal thrust or sole thrust in the Late Cretaceous.

McDonough and Simony (1988) proposed that a bimodal distribution in isotopic dates obtained from basement gneisses in the Omenica belt suggests that the North American basement ($\leq$2000 Ma) was intruded by plutons by *ca.* 750 Ma. However, plutonism identified in the Monashee and Selkirk Mountains at 135-100 Ma and 63 Ma (Scammell, 1993) has not been recognized in the Miette Group east of the Malton complex. Jurassic metamorphism and plutonism have been identified further south in the Cordillera (Archibald et al., 1983) but have not been demonstrated in the area of the Malton and Monashee complexes, possibly due to overprinting by high-grade Cretaceous metamorphism and anatexis.

Granitic rocks characterize the middle crustal zone at the latitude of the Monashee complex and many have been dated as Paleocene-Eocene in age (Carr, 1989, 1990, and Carr and Brown, 1990; Cook et al., 1992). They are associated with pegmatites in the hangingwalls of thrusts and the footwalls of normal faults, and have no known extrusive equivalents recognized at higher

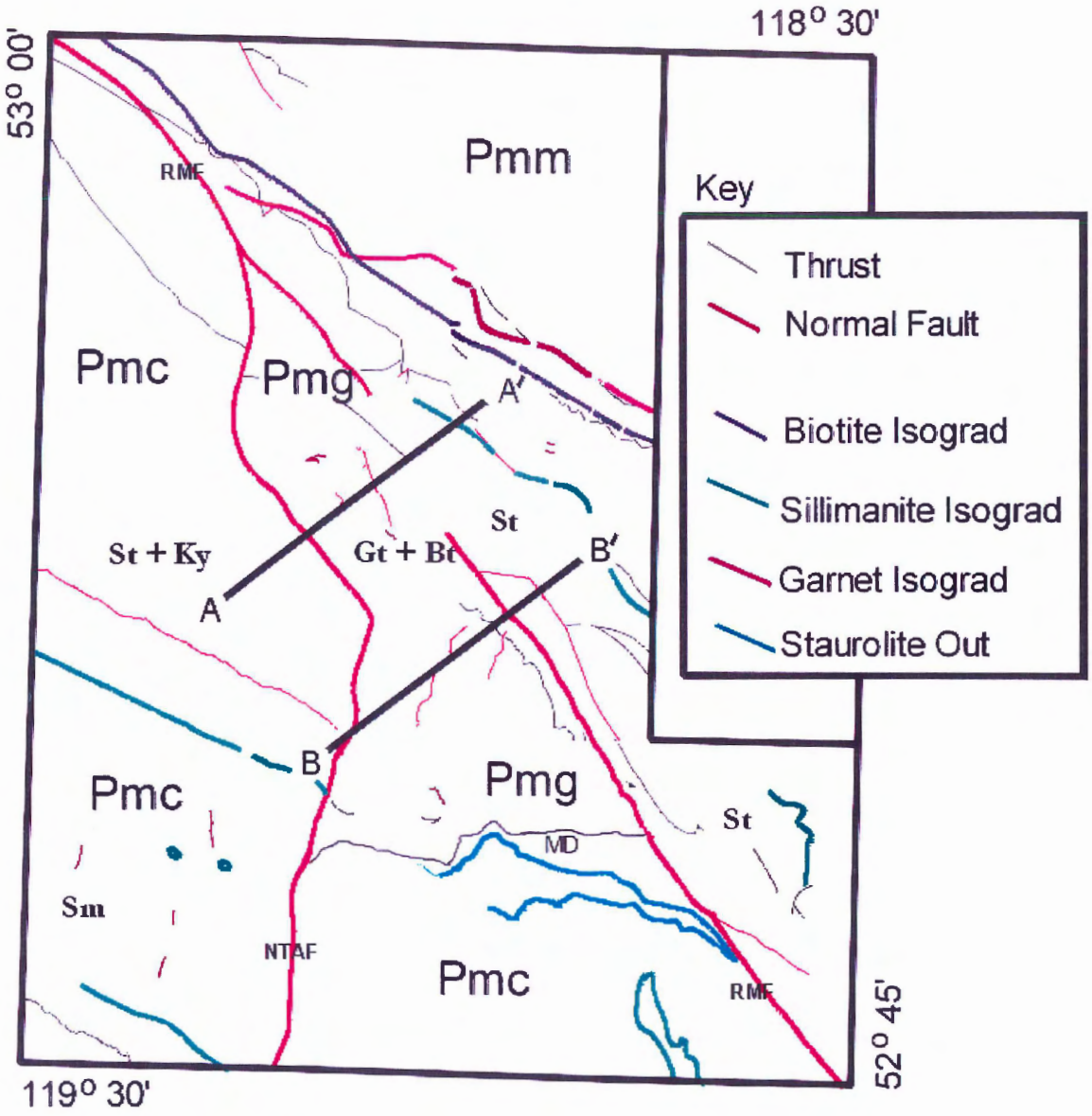

Figure 8: Metamorphic isograds and normal faulting in the northern Shuswap complex (compiled and modified from McDonough and Morrison, 1990; McDonough and Mountjoy, 1990; McDonough and Murphy, 1994; McDonough et al., 1991a, 1991b). Pmc – Mica Creek succession; Pmg – Malton Gneiss; Pmm – Miette Group; NTAF – North Thompson-Albreda fault; RMF – Rocky Mountain fault; MD – Malton Decollement. St – staurolite; Ky – kyanite; Sm – sillimanite; Gt – garnet; Bt – biotite.

structural levels (Parrish et al., 1988; Carr, 1992, 1995).

There have been numerous studies of other basement exposures and their associated cover in the Shuswap complex, including Frenchman Cap Dome and Thor-Odin Dome of the Monashee complex, and the Valhalla complex (Archibald et al., 1983; Parrish and Armstrong, 1987; Currie, 1988; Scammell, 1991, 1992, 1993; Carr, 1992; Brown et al., 1992; Parrish, 1995; Crowley and Parrish, 1999). In contrast, there are relatively few geochronologic data from the Malton Gneiss and its cover. The results of many of these studies are summarized in Table 1.

2.1.1: Structural geology

The study area lies within a structurally complex area of the Canadian Cordillera with a protracted history of compression, extension, and transcurrent tectonic activity. Figure 9 illustrates the structural relationships in cross-section between the Miette Group of the Rocky Mountains, the Malton Gneiss (geographically central to the study area), and the Mica Creek succession of the Cariboo Mountains to the west (McDonough, 1991).

A décollement underlying these units, the Rocky Mountain sole thrust (Figure 3), has been interpreted as a basal detachment that formed above the cratonic basement (Bally et al., 1966) by Mesozoic telescoping of the overlying Upper Proterozoic and younger strata of the foreland fold and thrust belt (Brown and Read, 1983; McDonough and Simony, 1988). The Monashee décollement, bounding the Monashee complex to the south (Figure 1), is interpreted as the western continuation of the sole thrust (Brown et al. 1992; Cook et al., 1992).

The tectonic history of the northern Shuswap complex appears to have evolved independently of two moderate to steeply dipping west-side-down normal faults, the North Thompson-Albreda Fault (NTAF) and the Rocky Mountain Fault (RMF), which is seated in the Southern Rocky Mountain Trench (Figure 2). The Southern Rocky Mountain Trench continues north of the Shuswap complex, through the locality of Tête Jaune Cache, transecting the Windermere Supergroup and marking the boundary

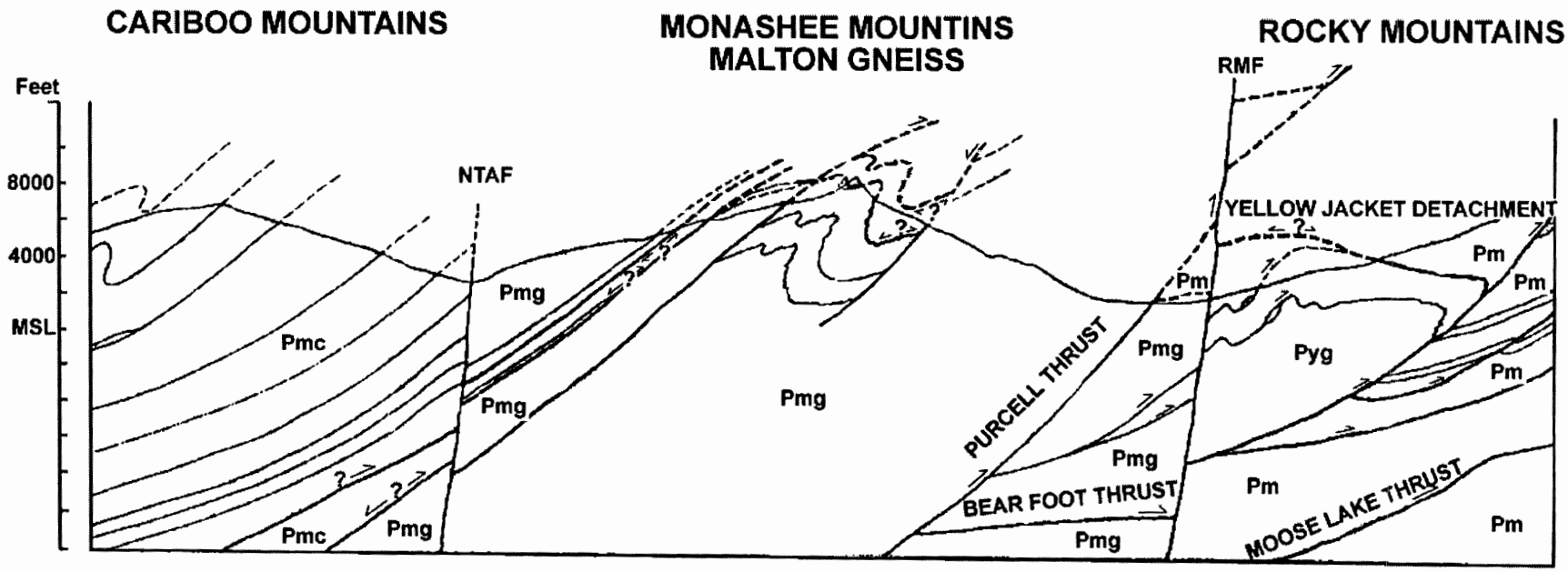

Figure 9: Cross section at the latitude of the Malton complex. Modified from McDonough et al., 1991. Note the steep dip of the North Thompson-Albreda and Rocky Mountain faults, implying that they are late structures and are unlikely to be directly involved in exhumation of the Malton Gneiss. Directions related to thrusting and faulting are adapted from McDonough, 1991. NTAF – North Thompson-Albreda Fault; RMF – Rocky Mountain Fault; Pmc – Mica Creek succession; Pmg – Malton Gneiss; Pyg – Yellowjacket Gneiss; Pm – Miette Group.

Table 1: Summary of previous isotopic data obtained near to and with implications to the tectonic development of the Malton Gneiss

Isotopic Age	Location	Method	Source	Comments
2200 Ma	Monashee complex	-	Brown et al. (1986)	Similar to the Malton Gneiss
≤2000 Ma ~750 Ma	Malton Gneiss " 	*U-Pb* -zircon -zircon	Parrish and Armstrong, (1983) "	Bimodal distribution suggesting an intrusive event
163 Ma 174 Ma 174 Ma	Cariboo Mts. Pluton Pluton Orthogneiss	*Rb-Sr* -WR isochron *U-Pb* -zircon -titanite	Pigage (1977), Gerasimoff (1988), Mortensen et al. (1987)	Peak metamorphic conditions attained in the Cariboo Mountains at lat. of Malton Gneiss
165 Ma	Kootenay Arc	*K/Ar* -hornblende	Archiblad et al. (1983)	Peak metamorphic conditions
155 Ma 147 Ma	Phyllites Hanging Wall of OVF	*K/Ar* -hornblende -biotite	Mathews (1981) "	Cooling ages
135-100 Ma	Monashee Mountains	*U-Pb* -zircon, monazite	Sevigny et al. (1989)	Plutonism: Pulses 1a & 1b
112 Ma	st-ky zone of Bulldog Creek	*K/Ar* -biotite	McDonough and Simony (1988)	Cooling age from amphibolite facies metamorphism
102-52 Ma	Gneiss Footwall of OVF	*K/Ar* -hornblende	Mathews (1981)	Cooling age
100 Ma	Monashee Mountains	*U-Pb* -monazite / titanite	Scammell (1993)	Peak metamorphic conditions
100 ± 2 Ma 78 ± 2	Tête Jaune Cache	$^{40}Ar/^{39}Ar$ -biotite -muscovite	Van Den Driessche and Maluski (1986)	Cooling age
76.3 ± 5.8 Ma	Northern Monashee Mountains	*K-Ar* -hornblende	Sevigny et al. (1990)	Cooling age

Table 1, continued

Isotopic Age	Location	Method	Source	Comments
70-62 Ma	Miette Group	*Apatite Fission Track*	McDonough et al. (1995)	Closure age (105 ± 10°C)
~65 Ma	Northwestern Selkirk Mountains	$^{40}Ar/^{39}Ar$ -biotite	Colpron (1996)	Cooling below 280-300°C
65-59 Ma	Mount Cheadle - Mica Dam	*U-Pb* -zircon, monazite and titanite	Digel et al. (1998)	Sillimanite overprint (M2)
65 Ma 55 ± 1 Ma	Purcell Anticlinorium	$^{40}Ar/^{39}Ar$ -Muscovite -biotite	Archibald et al. (1984)	Cooling ages
63 Ma (71-57 Ma)	Northern Monashee Mountains	*U-Pb* -zircon, monazite	Scammell, (1993)	Plutonism: Pulse 2 (middle crust)
60-55 Ma	Thor-Odin Monashee complex	$^{40}Ar/^{39}Ar$ -hornblende	Vanderhaeghe (1997)	Cooling age
~60-52 Ma	Frenchman Cap Monashee complex	*U-Pb* -metamorphic zircon	Parrish (1995) and references therein	Metamorphic cooling age
58.0 ± 4.0 Ma	Cariboo duplex (paragneiss)	*U-Pb* -titanite	Carr (1995)	Monashee décollement
52-44 Ma	Gneiss Footwall of OVF	*K/Ar* -biotite	Mathews (1981) and Vanderhaeghe (1997)	Cooling age
51.4 ± 3.5 Ma	Northern Monashee Mountains	*K-Ar* -muscovite	Sevigny et al. (1990)	age attained cooling (closure) temperature
50 Ma	West Malton Gneiss	*Apatite Fission Track*	McDonough et al. (1995)	Closure age (105 ± 10°C)
25-24 Ma	East Malton & Bulldog / Yellowjacket gneisses	*Apatite Fission Track*	McDonough et al. (1995)	Closure age (105 ± 10°C)

between two physiographic belts of the Cordillera, the Rocky Mountain Fold and Thrust belt to the east and the Omenica Crystalline belt to the west (Monger et al., 1982) (inset, Figure 2).

Marking the western boundary of the Shuswap complex is the NTAF, juxtaposing the Malton Gneiss of the Malton complex to the east with metasediments of the Mica Creek succession (Figure 7), part of the Windermere Supergroup, to the west (Murphy and McDonough, 1990). Sediments of the Mica Creek succession have undergone Mesozoic high-grade metamorphism and anatexis (Ghent et al., 1982; Sevigny et al., 1990; Digel et al., 1998). The NTAF is truncated by the RMF at the northern boundary of the Shuswap complex.

Marking the eastern boundary of the Shuswap complex is the RMF. Metamorphic grades of the Malton complex, including the overlying cover of the Yellowjacket and Bulldog gneisses, are middle amphibolite facies with kyanite ± staurolite bearing assemblages (Figure 6; McDonough, 1984; McDonough and Simony, 1988; Sevigny and Ghent, 1989). McDonough and Simony (1988) recognized two phases of metamorphism responsible for recrystallization of the staurolite- and kyanite- bearing metasediments of the Miette Group (Campbell, 1968). The prograde phase attained middle amphibolite facies during Mesozoic deformation. Retrograde lower greenschist facies metamorphism accompanied Eocene extension and cataclasis along the RMF (McDonough, 1984; McDonough and Simony, 1988). Cataclasis in the RMF also locally produced highly altered greenschist facies zones in both gneiss bodies (McDonough and Simony, 1988). To the east of the Malton complex, the Miette Group of the Windermere Supergroup (Figure 7) is dominated by greenschist facies metamorphism.

Van Den Driessche and Maluski (1986) presented a discussion on structure and metamorphism in the area of Tête Juane Cache (Figure 2). In this area, the Miette Group is described as a detrital Precambrian suite, characterized by a subvertical folliation and subhorizontal stretching lineation parallel to the fold axes. These fabrics were interpreted to result from dextral

crustal-scale shear, parallel to the SRMT and Purcell Thrust.

The Valemount strain zone (VSZ; McDonough and Simony, 1989) is a narrow zone of high orogen-parallel strain that affects the pebble conglomerate of the Miette Group. This structure marks the eastern limit of a wide zone of orogen-parallel fabrics distributed throughout the Omineca and Rocky Mountain belts (McDonough and Simony, 1989).

The parallelism of stretching lineations and fold axes were interpreted by McDonough and Simony (1989) as the product of significant transverse shortening during slightly oblique subduction. They suggest that orogen-parallel lineations are not representative of relative plate motions between North America and accreted terranes, but probably are a function of footwall buttressing of thrust sheets. Thus the southern Rocky Mountain belt and the Omineca belt are linked via an oblique-slip thrust regime that is tectonically unrelated to the Southern Rocky Mountain Trench (McDonough and Simony, 1989).

2.1.2: The Southern Rocky Mountain Trench

The Southern Rocky Mountain Trench (SRMT) is a valley marking the physiographic boundary between the Rocky Mountain and Omenica belts. The origin and tectonic significance of the SRMT are quite controversial.

The SRMT is interpreted by some authors to be the locus of one of several en echelon strike-slip faults (Van Den Driessche and Maluski, 1986; Struik, 1993) linked by extensional pull-aparts and locally represented by metamorphic core complexes (Van Den Driessche and Maluski, 1986). Other authors have interpreted the SRMT to be the surface expression of the RMF (McDonough and Simony, 1988; van der Velden and Cook, 1994, 1996). They described the RMF as a west-side down listric normal fault of Eocene age along which there is no documented strike-slip movement. Brown et al. (1993) identified a component of local oblique slip on northwest-trending normal faults, including the RMF, and suggested this was the result of dip-slip on northeast trending faults, such as the NTAF.

The amount of normal-sense offset has been estimated at between 10-12 km for the RMF between 49 ^{0}N - 49 ^{0}30'N and only a few kilometers at 50 ^{0}15'N

(van der Velden and Cook, 1994, 1996). The reduction in displacement northward was interpreted by van der Velden and Cook (1996) to be the result of shortening transfer via the Rocky Mountain sole thrust beneath the Purcell anticlinorium to the Slocan Lake Fault (Figure 1). Estimates of displacement across the NTAF are from 1-3 km of normal-sense offset (Currie, 1988; Walker, 1989). The role played by the RMF in the development of structure in and north of the Shuswap complex is not well understood. Metamorphic isograds west of the Shuswap complex (Figure 8) are generally discordant to brittle structures such as the RMF and NTAF, whereas east of the Malton Gneiss isograds are broadly parallel to the RMF.

In this study, $^{40}Ar/^{39}Ar$ geochronology, combined with field mapping, is used to constrain the timing of cooling in the area of the northern Shuswap complex. Specifically, questions concerning the timing of movement on the RMF and NTAF in relation to exhumation of the Malton Gneiss have been addressed.

2.2: Field mapping

Structural mapping of the Shuswap complex by the author and O. Vanderhaeghe was conducted over 18 days in August of 1998, 7 of which were spent in the study area. The field observations obtained were used to supplement data from local and regional mapping projects conducted by others prior to this study. The objective was to become familiar with local structural relationships and the mineralogy and texture of the various units, and to collect samples appropriate for argon analysis.

2.2.1: Methodology

Strike and dip measurements were obtained for foliations defining primary features, such as bedding planes, and ductile deformation fabrics. Measurements of lineations were obtained using mineral alignment, stretched minerals, and fold axes as the defining criteria. Brittle deformation features, such as fault planes and fractures or joints, were measured. Slickensides were measured as lineations for brittle deformation features. Oriented samples were obtained where microfabric was of interest. Stereonets plotted from structural data measured in the study area are presented in Figures 10 and 11.

2.2.2: Field observations

Insufficient mapping was conducted in this study to locate metamorphic isograds. Mapping did permit verification of the metamorphic grade of the units present in the study area as described previously by others.

The Malton Gneiss is characterized by a gentle to moderately dipping gneissic foliation (Figures 10 and 12). It is unclear whether this foliation is Proterozoic or related to the stacking of crustal slices during Mesozoic compression (Figures 3 and 9) or both. In the Malton Gneiss, shear strain is manifest, in part, as sheath folds oriented perpendicular to the Rocky Mountain Fault and transposed bedding (Figure 13). This orientation is nearly orthogonal to folding in the Miette Group of the Rocky Mountains and the Mica Creek succession of the Cariboo Mountains. This suggests that either compressional features exposed in the Malton Gneiss and surrounding units are unrelated, or timing of ductile deformation differed between the time of stacking of the basement slices and Mesozoic compression of the overlying cover sequences, or deformation mechanisms were different. Brittle structures, superimposed on the ductile deformation features, are moderate to steeply dipping, striking between south and west (Figure 10). Measurements conducted in the field probably caused this deformation.

In the immediate footwall of the RMF, along the east shore of Kinbasket Lake (Figure 7) cataclastite and mylonite zones are common in rocks of the Malton complex (Yellowjacket and Bulldog gneisses) and the overlying Miette Group. Augen gneiss of the Malton complex contains rotated delta-porphyroclasts which indicated dextral sense of shear (Figure 14). The gneissic foliation in the amphibolite facies Bulldog Gneiss in the Rocky Mountains dips moderately to the northeast and southwest (Figure 11). Discordance of these measurements suggests that these shear fabrics may be related, at least in position, to folds within the Miette Group, or that they are not equivalent.

The amphibolite facies metasediments of the Mica Creek succession, located in the Cariboo Mountains, resemble the greenschist facies metasediments of the Miette Group of the Rocky Mountains in structure and

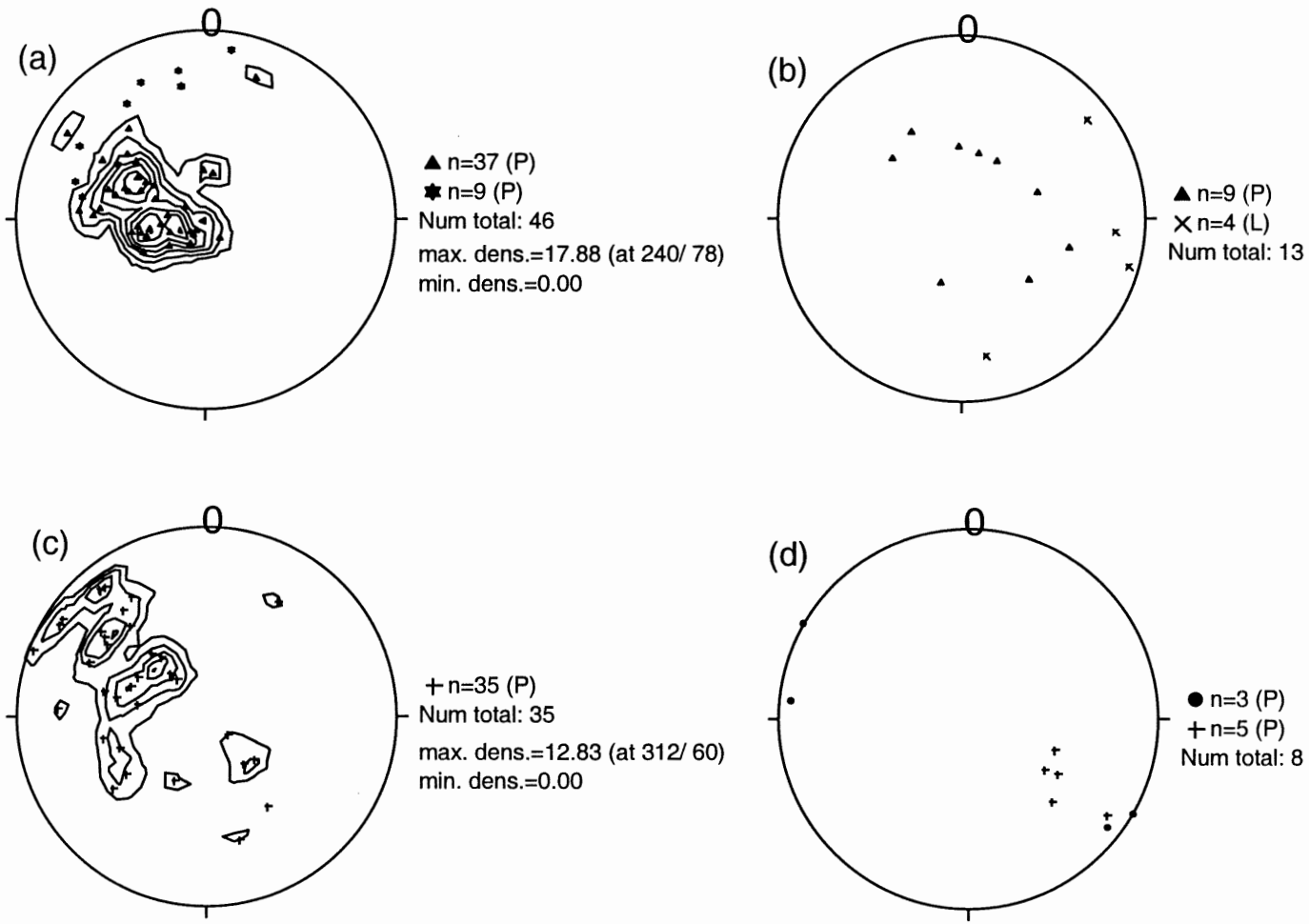

Figure 10: Equal area projection, lower hemisphere. Contours at 2.5, 5.0, 7.5, 10.0, 12.5. (a) – Malton Gneiss; (b) – Mica Creek succession; (c) – Miette Group, east of Malton Gneiss; (d) – Miette Group, Tete Jaune Cache location. ▲ = gneissic folliation data; ✡ = Fault/fracture plane data; **x** = Fold axes data; **+** = S_0 data. Data obtained by author and O. Vanderhaeghe.

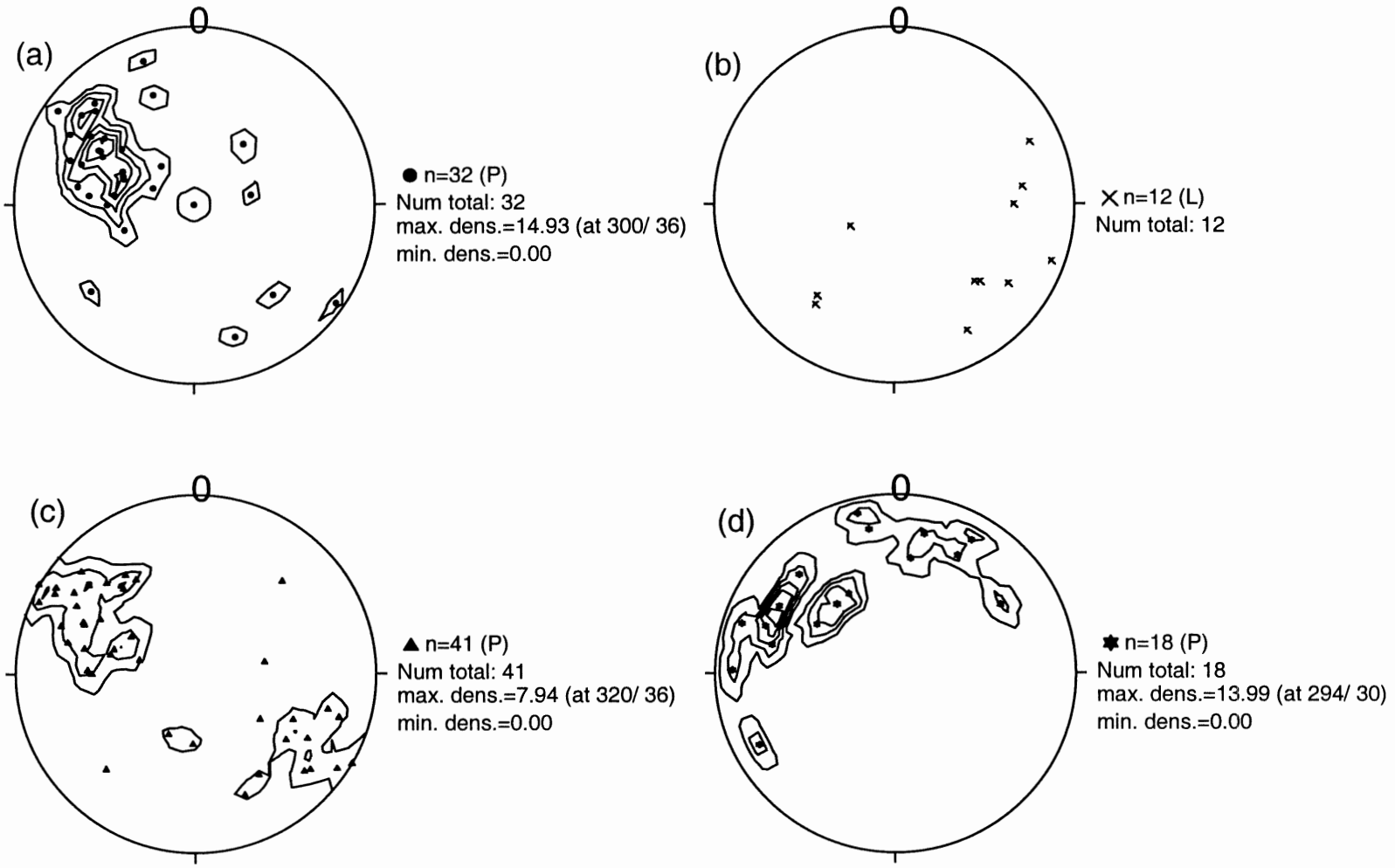

Figure 11: Equal area projection, lower hemisphere. Contours at 2.5, 5.0, 7.5, 10.0, 12.5. (a) & (b) – Miette Group, west of Malton Gneiss (c) & (d) – Bulldog Gneiss. ▲ = gneissic folliation data; ✡ = Fault/fracture plane data; **x** = Fold axes data; ● = S_2 data. Data obtained by author and O. Vanderhaeghe.

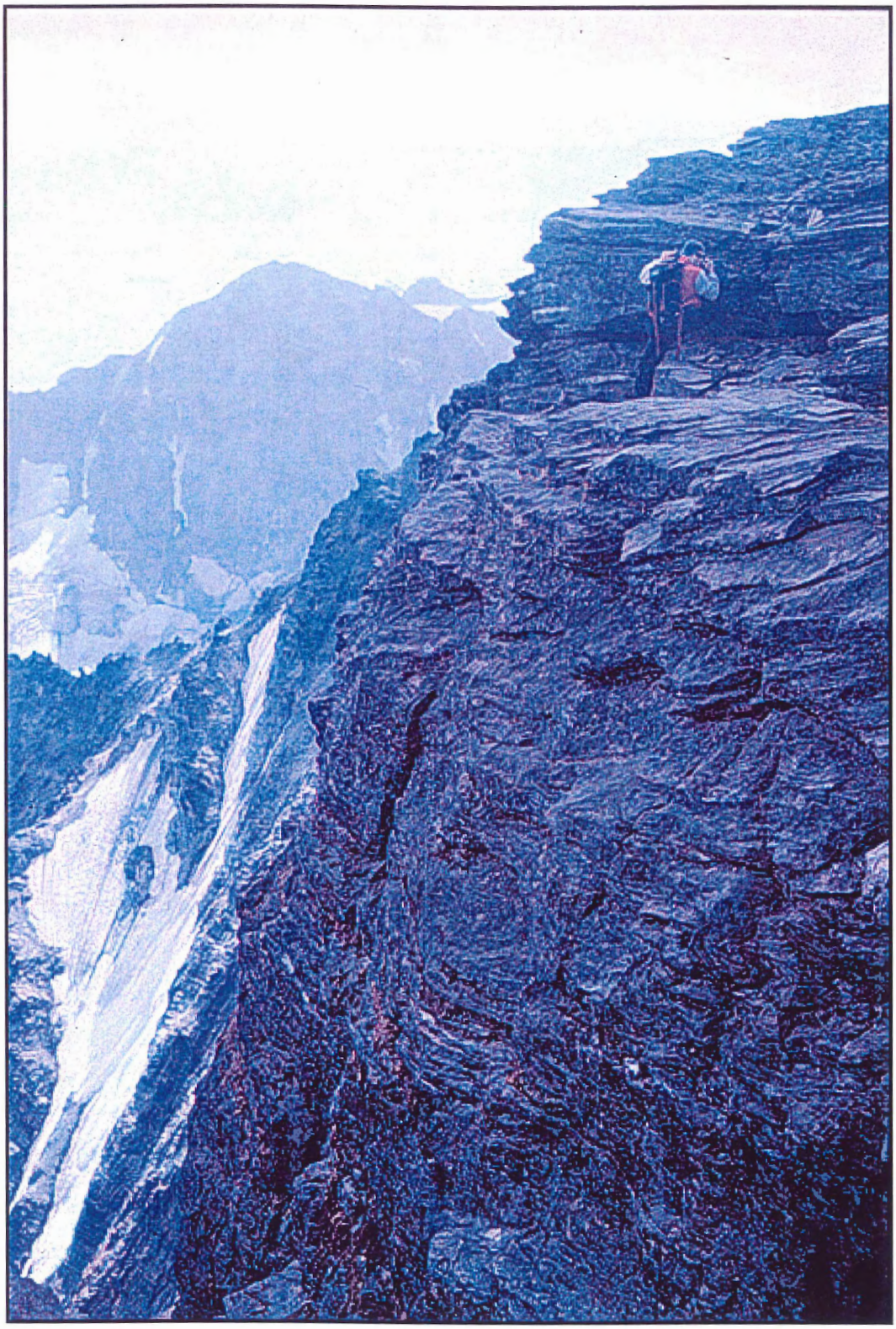

Figure 12: Malton Gneiss, facing south-southwest. Gneissic foliation is gently dipping and fold axes are oriented such that they strike perpendicular to cliff face.

Figure 13: Folding in the eastern Malton Gneiss, facing north-northeast. Elsewhere in the Malton Gneiss, sheath folds and large-scale (2-3 m) boudins are present. Fold axes are oriented perpendicular the Rocky Mountain Fault. Note Marmot at top for scale.

Figure 14: Augen gneiss, located in the Malton complex on the eastern shore of Kinbasket Lake; footwall of the Rocky Mountain Fault. Using rotational criteria, sigma grains (augen feldspars) indicate minor dextral shear perpendicular the lineation (strike-slip). South is to the right.

fabric (Figures 10 and 11). Fold axes are generally oriented southeast, consistent with compressional structures present in the Rocky Mountains. Gneissic foliations are gently dipping and appear to be undulose, resulting in a wide range of dip directions. Brittle deformation features were not mapped sufficiently to warrant presentation here.

At Tête Jaune Cache, Miette Group metasediments are metamorphosed to upper greenschist / lower amphibolite facies. Bedding (S_0) is subhorizontal with mild to moderate dip to the northwest (Figure 10). S_1 is crenulated in mica-rich layers such that S_2 (crenulation cleavage) parallels S_0.

Mapping in the greenschist facies metasediments of the Miette Group in the Rocky Mountain Fold and Thrust belt revealed the following structures, which are probably related to compression. At some distance west of the SRMT bedding dips to the southeast within thrust sheets and folding is generally open (Figures 11 and 15). Closer to the SRMT, duplexes and incipient duplex structures are common. In mica schists near the SRMT, S_1 generally dips moderately to the southeast. Fold axes strike southeast, roughly parallel to the SRMT. Near the SRMT bedding approaches vertical where folds are tighter (Figure 16).

Superimposed on the compressional structures of the Miette Group are brittle structures, most likely related to extension. Measurements of fault and fracture planes are shown in Figure11. Brittle structures are moderate to steeply dipping, oriented between southeast and southwest. Variation in orientation is most likely the result of measurements of joint planes.

2.3: Petrography

2.3.1: Methodology

Thin sections were cut parallel and perpendicular to the major planar deformation fabric of the samples. Where lineations were present, cuts were made parallel to the lineation in order to observe in a favourable orientation (e.g., Simpson and Schmid, 1983; Hanmer and Passchier, 1991). Petrographic criteria (the amount of deformation and relationship, size, and abundance of minerals) were used to determine the samples best suited for Ar analysis.

Figure 15: Subhorizontal bedding exposed in the Miette Group. This outcrop is located at the greatest distance east of the Rocky Mountain Fault within the study area. Photo taken facing southeast.

Figure 16: Folding within the Miette Group tightens near to the Rocky Mountain Fault, along the eastern shore of Kinbasket Lake. Fold axes are generally vertical. Photo taken facing southeast.

Polished thin sections were made from the samples chosen for Ar analysis. Thin section photographs and backscattered electron images (BSI) of the amphiboles analyzed using the $^{40}Ar/^{39}Ar$ method are presented with petrographic descriptions in Appendix A. Electron probe microanalysis was used to measure the K_2O content of the amphiboles and to identify any chemical zoning. The results of the microprobe analyses were used for amphibole classification (Appendix B). Results from analyses investigating chemical zoning are available in Appendix C. A general summary of sample petrography is provided below.

2.3.2: Petrographic observations

The mineralogy of the Malton complex (MG5, MG1B, RM52) is consistent with that of a syenite, consisting of calcic amphibole + K-spar + biotite + titanite + epidote + minor quartz and spongy garnet. This was reflected by the high potassium content of the amphiboles analyzed with the microprobe (Appendix B and C). There is a well defined fabric (aligned amphiboles, planar biotite, stretched feldspar) related to the gneissic foliation. Some epidote contains allanite cores. The mineralogy constrains the metamorphic grade of the samples from the Malton complex to lower amphibolite facies.

Similar to the Malton complex, the mineralogy of the Mica Creek succession (CA70B) resembles a syenite, containing amphibole + biotite + some K-feldspar + large, spongey garnets. In contrast to the Malton complex, the fabric is somewhat recrystallized. The absence of epidote and presence of garnet constrains the metamorphic grade to amphibolite facies. Sample CA78A (obtained for muscovite) also displays a recrystallized mineral assemblage. Minerals in both thin sections are coarse-grained. The presence of kyanite in the Mica Creek succession constrains metamorphism to middle amphibolite facies.

Muscovite + K-feldspar + plagioclase + quartz characterize the mineral assemblage of the Miette Group at Téte Jaune Cache (TJ79). Muscovites are largely crenulated and exhibit some recrystallization. A metamorphic grade of upper greenschist / lower amphibolite facies is defined for the metasediments at this locality.

Kyanite ± staurolite in the Miette Group, east of and near to the RMF, constrain the metamorphic grade to middle amphibolite facies. The level of recrystallization decreases with distance east from the Rocky Mountain Fault. Samples in the immediate footwall of the RMF exhibit retrograde metamorphism, probably related to cataclasis or mylotonization. Muscovite from these samples is generally highly deformed and recrystallized.

Chapter 3: Geochronology

3.1: The $^{40}Ar/^{39}Ar$ Method

The $^{40}Ar/^{39}Ar$ method is used to obtain information on the cooling history of a sample that is of interest to the study. Closely related to $^{40}Ar/^{39}Ar$ method is the concept of closure temperature. The $^{40}Ar/^{39}Ar$ method, closure temperature, and methods of interpreting $^{40}Ar/^{39}Ar$ spectra, are briefly reviewed below.

3.1.1: Basic principles

This dating method is based on the ratio of the radiogenic daughter isotope (^{40}Ar) to parent isotope (^{40}K). McDougall and Harrison (1988) provide a discussion of the $^{40}Ar/^{40}K$ and $^{40}Ar/^{39}Ar$ isotopic systems and their limitations. A brief summary is provided here.

^{40}K decays to both ^{40}Ca and ^{40}Ar. For the ^{40}Ar branch, ^{40}Ar, the radiogenic daughter isotope is measured. The ^{40}Ca branch is not suitable for geochronological purposes because the large amount of naturally occurring ^{40}Ca saturates the analysis and makes it difficult to detect the small amounts of this isotope produced by ^{40}K decay.

The age equation is used to calculate an apparent age based on the rate of radioactive decay of an isotope. The general form of the age equation used in the K-Ar method is given by McDougall and Harrison (1988):

$$t = 1/\lambda \ln[1 + (\lambda/\lambda_e+\lambda'_e)(^{40}Ar/^{40}K)] \quad (1)$$

where **t** is the apparent age and the various radioactive decay constants are represented by λ, λ_e, and λ'_e. The half-life for ^{40}K is reported by McDougall and Harrison (1988) as 1250 million years.

The $^{40}Ar/^{39}Ar$ method is a form of isotopic analysis that has evolved from the $^{40}K/^{40}Ar$ method (McDougall and Harrison, 1988; Reynolds, 1992). Having surpassed the $^{40}K/^{40}Ar$ method in popularity in the late 1970's, the $^{40}Ar/^{39}Ar$ method is currently one of the most widely used isotopic systems for obtaining apparent ages (Reynolds, 1992).

Preference for $^{40}Ar/^{39}Ar$ over the $^{40}K/^{40}Ar$ technique has arisen due to the possibility of measuring the ratio of daughter to parent in a single isotopic analysis, overcoming the requirement for a separate potassium analysis (McDougall and Harrison, 1988). A separate analysis not only requires additional time at additional cost but also depends on sample homogeneity. Another benefit of the $^{40}Ar/^{39}Ar$ system is that a substantially smaller amount of material is required for analysis (McDougall and Harrison, 1988; Reynolds, 1992). Reynolds (1992) further attributes the decrease in material required for dating to the development and use of more sensitive mass spectrometers in recent times. Both an increase in sensitivity of mass spectrometers and the need for only one analysis imply that isotope ratios, and hence age, can be measured more precisely than in the $^{40}K/^{40}Ar$ system (Merrihue and Turner, cited in Harper, 1973; McDougall and Harrison, 1988).

Reynolds (1992) described how the $^{40}Ar/^{39}Ar$ system is derived from the $^{40}K/^{40}Ar$ system and how it is applied to geological samples. In summary, potassium-bearing minerals are exposed to a neutron flux in a nuclear reactor, such as the one at McMaster University, Hamilton, Ontario, converting some of the ^{39}K to ^{39}Ar as described by the fast neutron reaction $^{39}K(n,p)^{39}Ar$. The age equation then takes the form:

$$t = 1/\lambda \ln(1 + J^{40}Ar^*/^{39}Ar_K) \qquad (2)$$

where t = age; J is a function of the neutron flux, the neutron capture cross-section, the irradiation time, the decay constants and the isotopic composition of potassium (i.e., the ratio of $^{39}K/^{40}K$; McDougall and Harrison, 1988). The half-life for ^{39}Ar is reported by McDougall and Harrison (1988) as 269 years.

Analysis typically proceeds by heating the sample in a stepwise manner. The ^{39}Ar released in each step is analyzed to determine the $^{40}Ar/^{39}Ar$ and other isotopic ratios (Schaeffer, 1982). A plot of apparent age versus fraction of ^{39}Ar released is called an age spectrum.

Errors are reported at the 2-sigma level and include the uncertainty in the irradiation parameter, J (determined to be between 0.00224 and 0.002269 (± 0.5%) for amphiboles in this study), but do not incorporate uncertainty in the assumed age of the flux monitor. An age plateau is defined where contiguous steps containing 50% or more of the total gas evolved exhibit no differences in apparent age beyond the ones expected from experimental uncertainties.

3.1.2: Closure temperatures

Closure temperature is the temperature at which a cooling mineral becomes effectively closed to argon loss (equation **(4)**). If a mineral forms below its closure temperature, the apparent age is interpreted to be a growth age (McDougall and Harrison, 1988). If a mineral grew or recrystallized at a temperature greater than the closure temperature, the apparent age is interpreted to be a cooling age. When a pre-existing mineral is heated to or above its closure temperature such that Ar diffusion occurs, it is said to be reset. McDougall and Harrison (1988) note that if the sample has been reset, only the post-metamorphic peak or post-deformation event history is recorded by this isotopic system.

The movement of Ar in or out of a crystal lattice may be described by the Arrhenius equation of diffusion:

$$D = D_o^{(-E/RT)} \qquad (3)$$

Where D = diffusion coefficient; D_o and E are the frequency factor and activation energy, respectively; R = gas constant; T = the absolute temperature (McDougall and Harrison, 1988).

Dodson (1973) derived the following expression for closure temperatures:

$$T_c = (E/R) / [\log_e ([A R T_c^2 (D_o/a^2)] / [E(dT/dt)])] \qquad (4)$$

where T_c = closure temperature; A = constant that depends on the assumed

diffusion geometry; a = effective diffusion radius; dT/dt = the cooling rate at T_c. Note that a slow cooling rate results in a low closure temperature. Table 2 presents the closure temperatures for muscovite, biotite, hornblende and K-feldspar. These values are model based and may vary according to model. For example, McDougall and Harrison (1988) suggest a closure temperature of 350 ^{0}C for muscovite. Although the values are presented to a high degree of precision, laboratory investigations typically indicate a variation of ±50 ^{O}C in closure temperature for these minerals.

Table 2: T_c of minerals commonly used in the $^{40}Ar/^{39}Ar$ system

Mineral	Closure Temperature (Tc)	Comments
Amphibole*	531 ^{0}C ~490 ^{0}C	For a cooling rate of 50 ^{0}C/Myr For a cooling rate of 5 ^{0}C/Myr
Muscovite*	378 ^{0}C 337 ^{0}C	For a cooling rate of 50 ^{0}C/Myr For a cooling rate of 5 ^{0}C/Myr
Biotite*	333 ^{0}C (Ann_{56}), 431 ^{0}C (Ann_4) 301 ^{0}C (Ann_{56}), 395 ^{0}C (Ann_4)	For a cooling rate of 50 ^{0}C/Myr For a cooling rate of 5 ^{0}C/Myr
Feldspar^	125-185 ^{0}C (microcline), ≤ 315 ^{0}C (orthoclase)	Low Temp.

*Obtained from Lister and Baldwin (1995)
^Obtained from Harrison and McDougall (1982) and Heizler and Harrison (1988)

3.1.3: Methods of interpretation

McDougall and Harrison (1988) illustrate spectra which represent three different possible outcomes of $^{40}Ar/^{39}Ar$ analysis (Figure 17). Each spectrum has characteristics diagnostic of specific histories with respect to argon retention.

Excess argon is defined by McDougall and Harrison (1988) as the component of ^{40}Ar incorporated into samples by processes other than by in situ radioactive decay of ^{40}K. Excess ^{40}Ar may be introduced into a rock or mineral sample by physical contamination from older material, and may be manifest in an age spectrum by a U-shaped profile. In this case, the minimum age is the most reliable age estimate. Excess argon at the grain boundaries may dramatically increase initial apparent ages in a spectrum. Initial degassing at low temperature may remove a significant fraction of the excess ^{40}Ar and thus

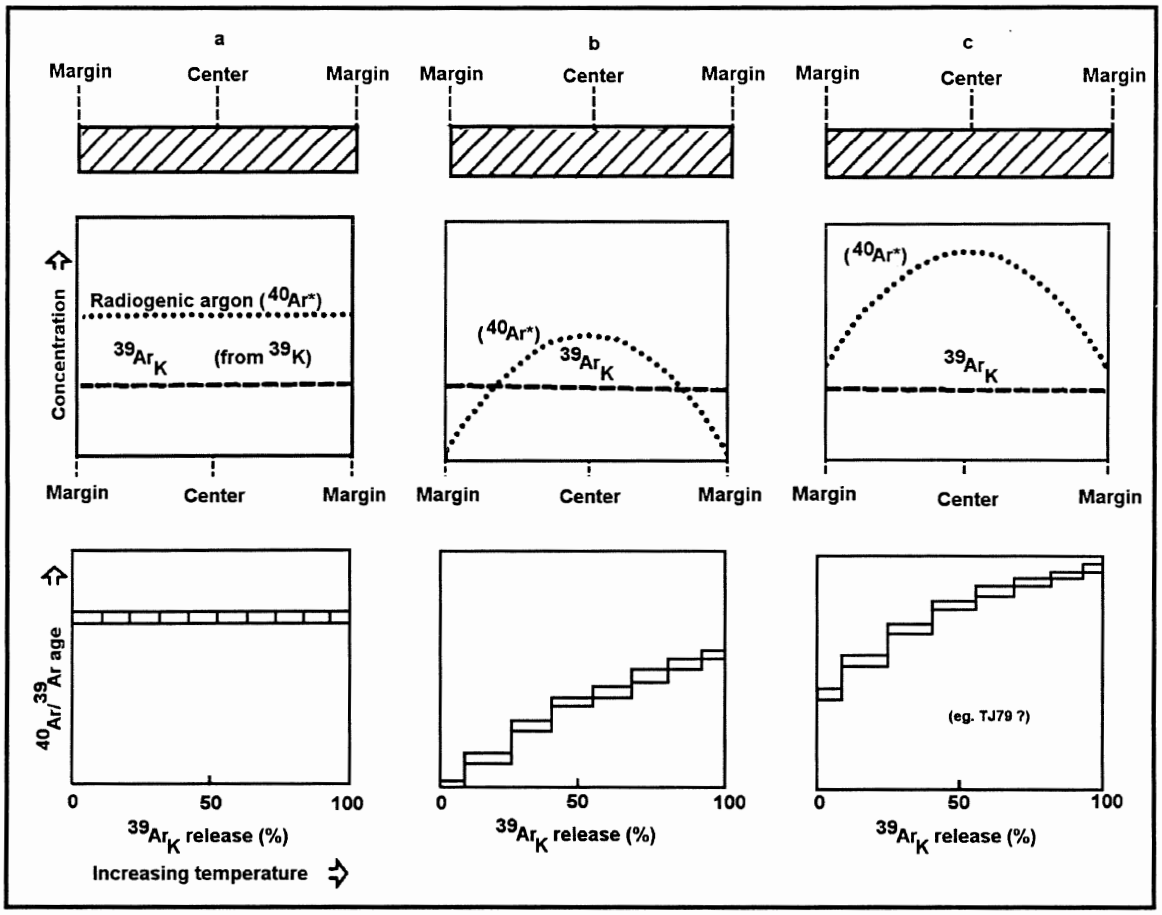

Figure 17: Schematic diagrams showing model $^{40}Ar/^{39}Ar$ age spectra (McDougall and Harrison, 1988, p. 13). Top diagram portrays an idealized crystal in cross section, the middle diagram in each panel shows the concentration of radiogenic argon and neutron-induced $^{39}Ar_K$ across the crystal, and the lower diagram illustrates the $^{40}Ar/^{39}Ar$ age spectrum expected from measurement of argon extracted in successive steps at progressively higher temperature from the idealized crystal. (a) The case of a crystal undisturbed subsequent to initial crystallization and rapid cooling. (b) The case in which partial loss of radiogenic argon has occurred from the crystal in geologically recent times, so that there is a marked gradient of radiogenic argon across the crystal from essentially zero at the grain boundary. (c) The same case as in b, except that significant accumulation of radiogenic argon has occurred since the reheating event owing to the passage of time. A maximum age for the time of reheating is given by the $^{40}Ar/^{39}Ar$ age for the gas released in the first step of the experiment, and a minimum age for the primary crystallization of the crystal is provided by the apparent age measured on the gas released at the highest temperature. Thickness in bars in model age spectra indicates nominal uncertainty in the individual ages.

improve the accuracy of this method relative to the $^{40}K/^{40}Ar$ method (Merrihue and Turner, 1966).

Validity of age data may be tested by plotting the isotopic data in different ways. In cases where excess ^{40}Ar is suspected, a conventional isochron plot ($^{40}Ar/^{36}Ar$ vs. $^{39}Ar/^{36}/Ar$) or an inverse isochron plot ($^{36}Ar/^{40}Ar$ vs. $^{39}Ar/^{40}Ar$) may be able to detect this component and correct for its presence. The conventional isochron technique "is analogous to the Rb-Sr isochron method in which a linear correlation of data from a coeval suite of samples reveals both the geologic age (proportional to the slope of the line) and the initial isotopic composition of the daughter product element (given by the intercept of the line with the daughter element isotope ratio axis)" (McDougall and Harrison, 1988, p. 121). The inverse isochron plot overcomes two problems inherent to the conventional plot (Harrison and McDougall, 1988). In a conventional isochron plot, the isotope measured with the poorest precision, ^{36}Ar, is common to both axes, possibly giving rise to misleading linear correlations. Secondly, samples in which no ^{36}Ar has been detected plot at infinity. Consequently, radiogenically enriched samples will dominate the regression and prevent precise determination of the trapped argon composition. In an inverse isochron plot, ^{40}Ar is used as the reference isotope. Because ^{40}Ar is always the most abundant iotope, it can be measured very precisely and the correlation between errors in the ratios is small. This approach results in a restricted array of data with a negative slope in which the age is given by the x-intercept and the trapped composition corresponds to the y-intercept.

When analyzing hornblende, contamination from biotite may also contribute to error in apparent age. This can be investigated by plotting $^{37}Ar/^{39}Ar$ vs $\%^{39}Ar$ evolved. A low $^{37}Ar/^{39}Ar$ ratio is indicative of biotite contamination as ^{37}Ar is derived directly from Ca, and there is no Ca in biotite. This check is not available for muscovite analysis because it is similar to biotite in K and Ca content. These checks have been performed on the $^{40}Ar/^{39}Ar$ data obtained for the samples of this study (Chapter 4).

3.2: Sample preparation

Samples containing mineralogies useful for Ar analysis were taken from the Miette Group located at Tête Jaune Cache, the Bulldog Gneiss in the Rocky Mountain Fold and Thrust belt (near the RMF), the Malton Gneiss, and the Mica Creek succession in the Cariboo Mountains (Figure 2). The sample locations define two northeast-southwest transects (Figures 8 and 9). Amphibole and muscovite are the two most common minerals present throughout the study area that are datable using the Ar method (Table 2). Collected samples were free of brittle deformation structures and weathering.

Samples were crushed and sieved using U.S. Standard #60 (250 μm) and #120 (125 μm) mesh. The 125 μm separates were then washed with water and acetone and dried under a fumehood for a period of up to 24 hours. Separation of amphiboles from muscovites and other minerals was accomplished using a Frantz electromagnetic separator. Muscovites were further separated from amphibole by repeatedly rolling the amphibole off a dipping piece of paper along which mica was resistant to sliding. Final separation of both amphibole and muscovite was accomplished by hand-picking under a binocular microscope, to produce separates of a few milligrams in mass for muscovites and a few tens of milligrams for amphibole. These separates were individually wrapped in thin aluminum foil and stacked in an aluminum canister with between five and seven interspersed flux monitors. The flux monitor was the hornblende standard MMHb-1 which has an apparent K-Ar age of 520 ±2 Ma (Samson and Alexander, 1987). The canisters were sent to McMaster University for fast neutron irradiation. Upon the return of the samples from McMaster University, isotopic analyses were made by Keith Taylor in the Dalhousie laboratory using a VG3600 mass spectrometer attached to a double-vacuum tantalum resistance furnace.

3.3: $^{40}Ar/^{39}Ar$ results

Apparent age spectra from amphibole are reported in Figure 18. Apparent age spectra from muscovite are reported in Figure 19. Sample location and type is illustrated in Figures 4 through 6. Discussion of the samples is

organized from highest to lowest metamorphic grade with discussion of high-temperature minerals preceding relatively lower-temperature minerals.

CA-70B, amphibole- Samples were obtained from an outcrop of amphibolite located in the mica Creek succession of the Cariboo Range, west of the NTAF. Relative to other amphibole samples, back-scattered imaging revealed the amphibole to be partially recrystallized. $^{40}Ar/^{39}Ar$ analysis resulted in a poorly-defined age gradient, increasing from a minimum of 116 ±3.4 Ma to a maximum of 143 Ma, with an anomalous value of 145 Ma at step 9 of 16, representing 21% of the ^{39}Ar released. $^{37}Ar/^{39}Ar$ analysis indicates initially high potassium values over the first 4 steps, representing 2.2% of the ^{39}Ar released. The remaining spectrum is consistent with degassing of relatively contaminant free amphibole. Of the four spectra obtained from amphiboles, this is the only one interpreted to be geologically significant. The lowest step is interpreted to represent the maximum age for the time of reheating, and a minimum age of crystallization of the amphibole is provided by the apparent age measured at the highest step.

CA-78A, muscovite- Coarse-grained muscovite was obtained from an outcrop of mica schist also located in the Mica Creek succession. A plateau consisting of 13 steps, representing 95% of the ^{39}Ar released, has an apparent age of 62 ±0.4 Ma. The initial three steps, representing 2.4% of the ^{39}Ar released, are not interpreted to be geochronologicaly significant.

TJ-79, muscovite- Samples were obtained from an outcrop of psammite located in the footwall of the RMF, at the location of Tête Jaune Cache. Mica fish are common and biotite and muscovite are locally intergrown. The apparent age spectrum is U-shaped indicating possible excess ^{40}Ar. A minimum age of 83 Ma was obtained over two low temperature steps, representing only 11% of the ^{39}Ar released. Since excess ^{40}Ar appears to be present and the age minimum is poorly defined, it is likely that the result obtained from this analysis is not geochronologically significant. At very best, the above spectrum may be interpreted as a maximum apparent age.

Figure 18:
Apparent age and $^{37}Ar/^{39}Ar$ spectra from amphibole samples. Relative uncertainties are reported at the 1 sigma level, represented by the half-heights of the rectangles. Preferred ages are reported with uncertainties at the 2 sigma level that include error in the irradiation parameter, J (J = 0.00224 and 0.002269 (± 0.5%)).

Figure 19:
Apparent age spectra from muscovite samples. Preferred ages and uncertainties are as in Figure 18.

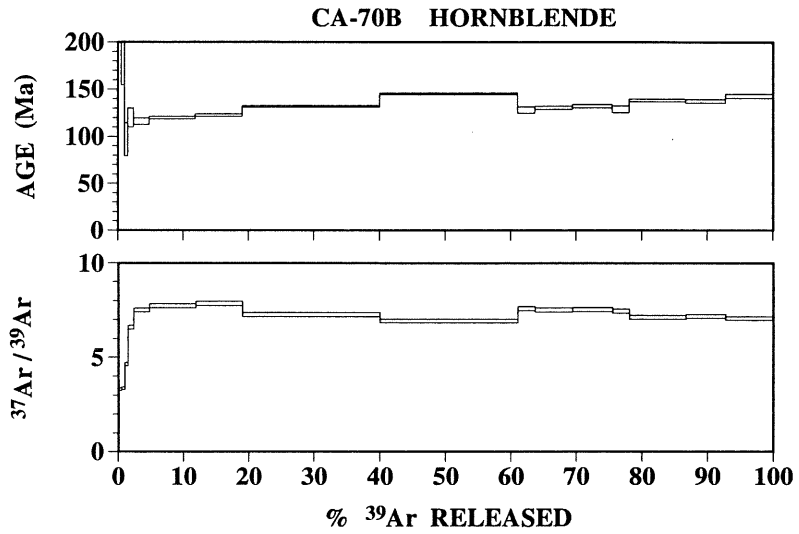
CA-70B HORNBLENDE
AGE (Ma)
200
150
100
50
0
$^{37}Ar/^{39}Ar$
10
5
0
0 10 20 30 40 50 60 70 80 90 100
% ^{39}Ar RELEASED

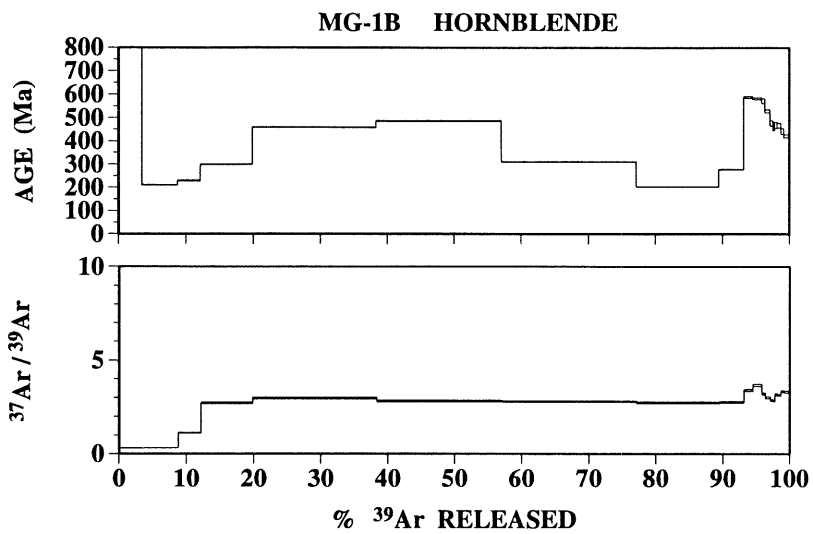
MG-1B HORNBLENDE
AGE (Ma)
800
700
600
500
400
300
200
100
0
$^{37}Ar/^{39}Ar$
10
5
0
0 10 20 30 40 50 60 70 80 90 100
% ^{39}Ar RELEASED

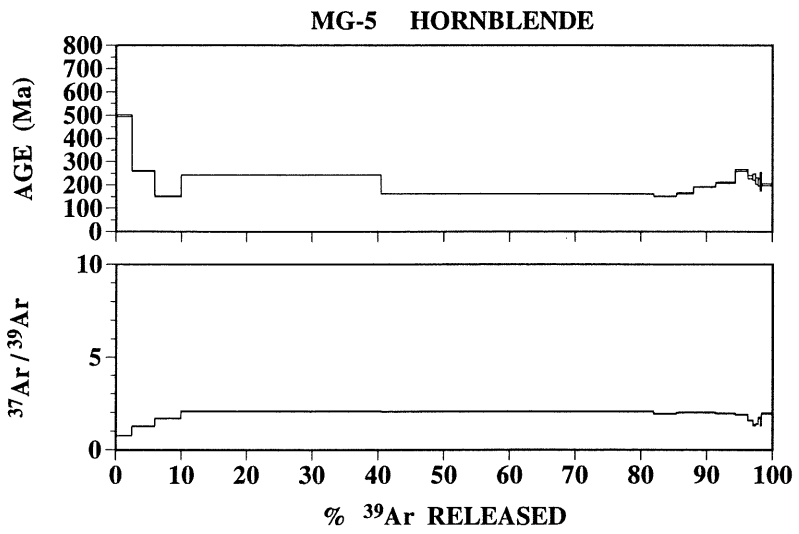
MG-5 HORNBLENDE
AGE (Ma)
800
700
600
500
400
300
200
100
0
$^{37}Ar/^{39}Ar$
10
5
0
0 10 20 30 40 50 60 70 80 90 100
% ^{39}Ar RELEASED

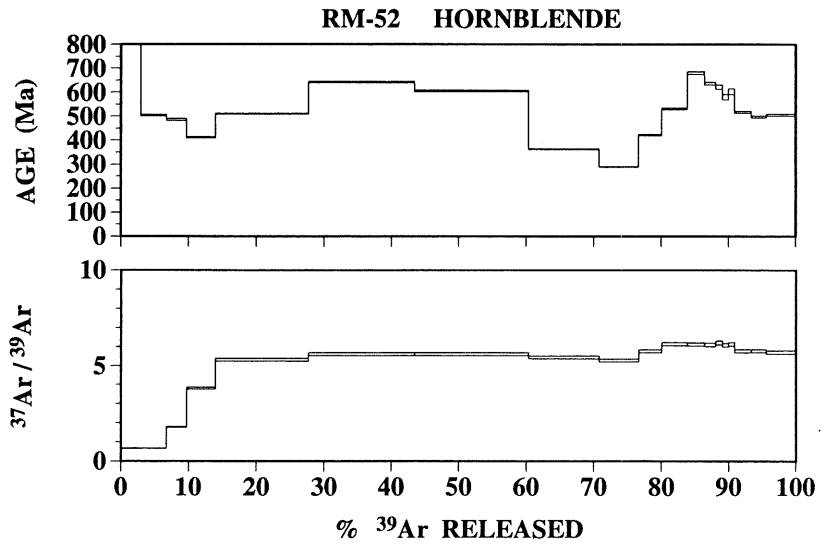
RM-52 HORNBLENDE
AGE (Ma)
800
700
600
500
400
300
200
100
0
$^{37}Ar/^{39}Ar$
10
5
0
0 10 20 30 40 50 60 70 80 90 100
% ^{39}Ar RELEASED

Figure 18

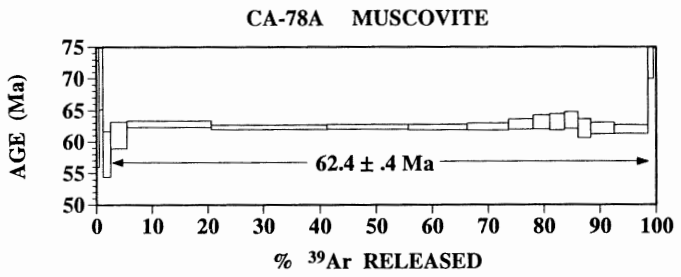
CA-78A MUSCOVITE
AGE (Ma)
62.4 ± .4 Ma
% 39Ar RELEASED

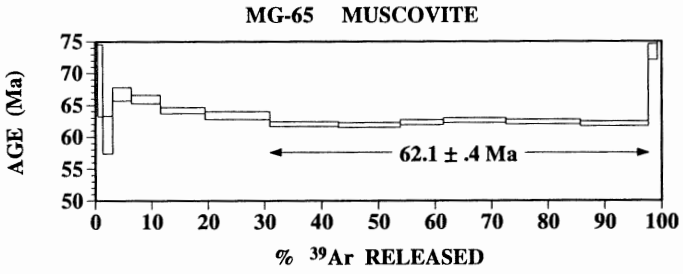
MG-65 MUSCOVITE
AGE (Ma)
62.1 ± .4 Ma
% 39Ar RELEASED

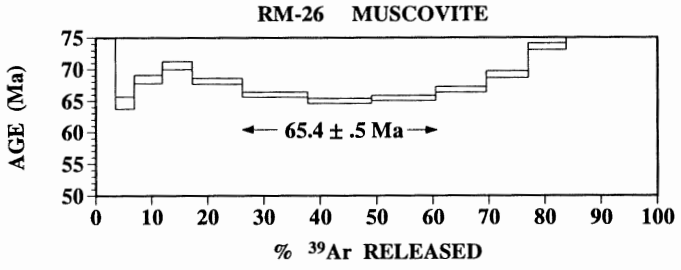
RM-26 MUSCOVITE
AGE (Ma)
65.4 ± .5 Ma
% 39Ar RELEASED

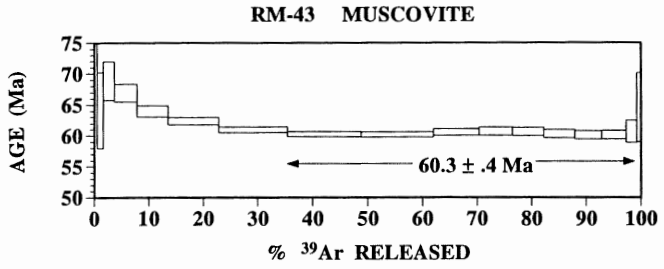
RM-43 MUSCOVITE
AGE (Ma)
60.3 ± .4 Ma
% 39Ar RELEASED

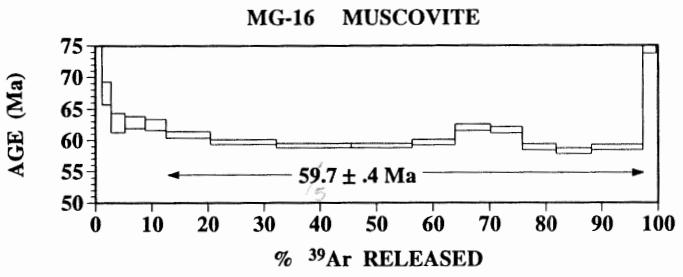
MG-16 MUSCOVITE
AGE (Ma)
59.7 ± .4 Ma
% 39Ar RELEASED

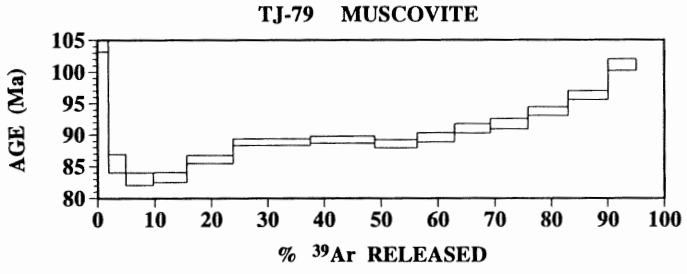
TJ-79 MUSCOVITE
AGE (Ma)
% 39Ar RELEASED

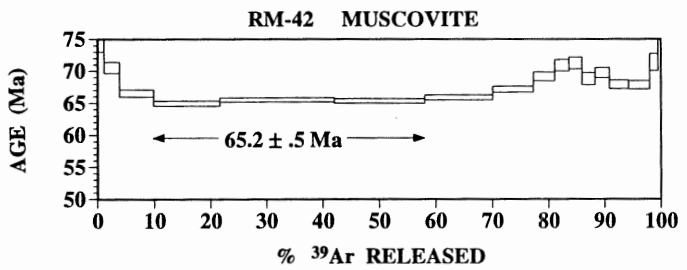
RM-42 MUSCOVITE
AGE (Ma)
65.2 ± .5 Ma
% 39Ar RELEASED

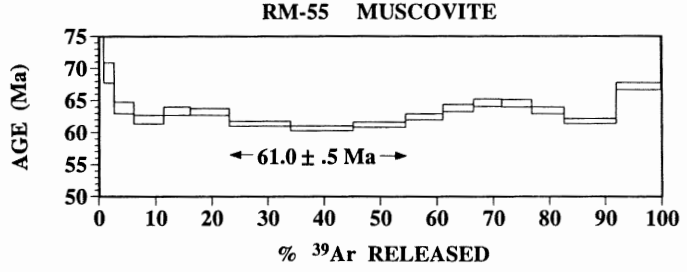
RM-55 MUSCOVITE
AGE (Ma)
61.0 ± .5 Ma
% 39Ar RELEASED

Figure 19

MG-5, amphibole- A sample was obtained from a leucogniess outcropping in the Malton Gneiss, east of the NTAF. $^{40}Ar/^{39}Ar$ analysis resulted in discordant apparent ages. The data are poorly resolved due to 72% of the ^{39}Ar having been released over steps 4 and 5. Maximum and minimum apparent ages are 262 Ma and 151 Ma respectively. The general pattern of all amphibole spectra, with the exception of *CA70B*, is a high-low-high apparent age pattern, the low apparent age occurring in the later part of the spectrum. $^{37}Ar/^{39}Ar$ analysis indicates initially high potassium values over the first 3 steps, representing 10% of the ^{39}Ar released. The remaining spectrum is consistent with degassing of relatively contaminant free amphibole. The $^{40}Ar/^{39}Ar$ analysis are therefore interpreted to be geochronologically inconclusive.

MG-1B, amphibole- A sample was also obtained from an orthogniess outcropping in the Malton Gneiss. $^{40}Ar/^{39}Ar$ analysis resulted in discordant apparent ages, ranging from a maximum of 587 Ma to a minimum of 202 Ma in the latter part of the spectrum. $^{37}Ar/^{39}Ar$ analysis indicates initially high potassium values over the first 3 steps, representing 12% of the ^{39}Ar released. The remaining spectrum is consistent with degassing of relatively contaminant-free amphibole. The $^{40}Ar/^{39}Ar$ analysis is thereforee interpreted to be geochronologically inconclusive.

MG-16, muscovite- Samples were obtained from a mica schist (slice of parautochthonous cover) outcropping in the western Malton Gneiss. The muscovite grains are commonly intergrown with biotite. Initially high apparent ages characterize the first five steps of the apparent age spectrum, over which 12% of the ^{39}Ar was released. Over the following 10 steps, 84% of the ^{39}Ar was released with a mean apparent age of 60 ±0.4 Ma.

MG-65, muscovite- Another sample was obtained from a mica schist outcropping in the Malton Gneiss, located in the immediate hanging wall of the RMF. Biotite is intergrown with and/or rims the muscovite. The apparent age spectrum has high initial apparent age values over the first 7 steps, representing 31% of the ^{39}Ar released. The next 6 steps constitute a plateau over 66% of the

^{39}Ar released at an apparent age of 62 ±0.4 Ma.

RM-52, amphibole- A sample was obtained from an outcrop of amphibolite, located in the Bulldog Gneiss, in the immediate footwall of the RMF. The amphibole is poikiloblastic and is commonly intergrown with biotite. $^{40}Ar/^{39}Ar$ analysis resulted in discordant apparent ages, ranging from a maximum of 680 Ma to a poorly defined minimum of 288 Ma. In the later part of the spectrum. $^{37}Ar/^{39}Ar$ analysis indicates initially low calcium/potassium values over the first 4 steps, representing 14% of the ^{39}Ar released. The rest of the spectrum is consistent with degassing of relatively contaminant-free amphibole. The $^{40}Ar/^{39}Ar$ analysis is therefore interpreted to be geochronologically inconclusive.

RM-26, muscovite- A sample was collected from an orthogneiss outcropping as a section of the Bulldog Gneiss. Plagioclase is locally sericitized and biotite retrograded to chlorite. The apparent age spectrum is U-shaped indicating possible excess ^{40}Ar. A minimum apparent age of 65 ±0.5 Ma was obtained over three steps through which 34% of the ^{39}Ar was released. As for *TJ-79*, this age is interpreted to be the maximum possible value.

RM-42, muscovite- Samples were obtained from a mica schist, located in the footwall of the RMF. Muscovite is weakly crenulated and locally intergrown with biotite. The apparent age spectrum for muscovite from sample *RM-42* is U-shaped, indicating possible excess ^{40}Ar. A minimum apparent age of 65 ±0.5 Ma was obtained over three steps over which 48% of the ^{39}Ar was released. The apparent age represented by these steps is interpreted to be an upper age limit.

RM-43, muscovite- Another orthogneiss of the same general locality as RM-42 was also sampled. In thin section, the sample exhibits substantial retrogression but muscovite is generally medium grained and free of biotite. $^{40}Ar/^{39}Ar$ analysis produced high apparent age values at low temperature where 23% of the ^{39}Ar was released over 6 steps. A plateau representing 76% of the ^{39}Ar released over 10 steps followed the initial high values, indicating an apparent age of 60 ±0.4 Ma.

RM-55, muscovite- Again, muscovite, obtained from a mica schist of the

Miette Group, located east of the RMF, is weakly crenulated and at least partially recrystallized. The spectrum obtained from $^{40}Ar/^{39}Ar$ analysis is discordant with high apparent ages at low temperature. A minimum apparent age of 61 ±0.5 Ma was obtained over three steps through which 31% of the ^{39}Ar was released. The apparent age represented by these steps is interpreted to be the maximum possible age.

Chapter 4: Interpretation

Because most of the Ar spectra obtained were discordant to some extent, $^{40}Ar/^{39}Ar$ spectra interpreted as geochronologically insignificant are discussed first to identify sources of error or erroneous results which may have affected the shape of spectra interpreted as geochronologically significant.

4.1: Geochronologically insignificant spectra

Three of the four amphibole spectra obtained are regarded as inconclusive because they are highly discordant, with apparent ages ranging from *ca.* 100-700 Ma. Amphibole spectra typically have high initial apparent ages, followed by 2-4 heating steps through which *ca.* 50% of the ^{39}Ar is evolved before attaining the lowest apparent age. The high temperature parts of the spectra are again characterized by high apparent ages. The discordant spectra could result from sample contamination, compositional effects on argon systematics (although alone it is unlikely to produce discordance), the presence of excess ^{40}Ar, or indicate a complex tectonic or thermal history related to possible reheating events and partial resetting of the amphiboles with respect to argon.

The $^{37}Ar/^{39}Ar$ spectra indicate little to no contamination of the amphibole analyses by biotite or any other phase. Microprobe analysis of amphiboles obtained from the same samples revealed no significant chemical zoning (Appendix C), although a number of samples contain Fe- and K-rich amphiboles. A complex thermal history may be represented by highs and lows in an argon analysis spectrum, whereas excess argon is typically represented by a U-shaped spectrum. Amphibole spectra obtained in this study appear to exhibit both of these patterns. Excess argon, if present, may have been obtained from hydrothermal fluids circulating throughout the brittle upper crust and exhumed mid-crustal rocks.

Because the high temperature parts of amphibole spectra are generally U-shaped, excess ^{40}Ar was suspected. Inverse isochron plots of the amphibole data produced discordant results, indicating that the possibility of irradiation-induced excess argon as a source of error in amphibole analyses is unlikely.

Inverse isochron plots were not constructed from muscovite data.

High ages at high the high temperature end of the spectrum may be a relict of Proterozoic history, since protoliths of the Malton Gneiss are Proterozoic (Parrish and Armstrong, 1983). Incomplete resetting in Mesozoic time, possibly combined with excess argon at low temperature steps, may account for the observed complexity.

The majority of the muscovite spectra were also discordant, although the analyses were generally less discordant than those for amphiboles. However, not all muscovite analyses were conclusive. For example, an apparent age of 83 My was obtained from sample TJ79, located in the area of Tête Jaune Cache. This apparent age represents only 11% of ^{39}Ar evolved over two heat steps. The remainder of the spectrum suggests the presence of excess ^{40}Ar (Figure 18). Because petrographic analysis revealed the presence of recrystallized muscovite, at best the lowest temperature step may be interpreted as a maximum apparent age of cooling, and the upper step the minimum age of crystallization. Nevertheless, the apparent age obtained from analysis of this sample is within 5 Ma of that reported for a muscovite cooling age (78 ±2 Ma) from the same locality by Van Den Driessche and Maluski (1986) who interpreted it to reflect timing of deformation on the Valemount strain zone (McDonough and Simony, 1989) during post-middle Cretaceous strike-slip along faults in the Northern Rocky Mountain Trench. The data from Van Den Driessche and Maluski (1986) also show discordant apparent age spectra.

Discordant spectra were also obtained from muscovite samples RM26, RM42, and RM55. These spectra are characterized by high initial apparent ages, followed by three contiguous heat steps which are the lowest temperature steps, and ending with an increasing age gradient. The minimum apparent ages for these samples range between 61 and 65 Ma and are interpreted as upper cooling age limits. As for amphibole samples MG1B, MG5, and RM52, the extent to which excess argon has affected these samples (if at all) is unknown. As a result of discordance, and the possibility of the presence of excess argon,

these data cannont be relied upon as a basis for geological interpretation.

4.2: Geochronologically significant spectra

Interpretation of $^{40}Ar/^{39}Ar$ spectra in terms of cooling vs. growth or resetting with respect to ^{39}Ar is a must before the geologic significance of the apparent age is defined. This is accomplished by constraining temperature of growth and/or recrystallization as closely as possible based on a combination of petrography, mineral assemblage, and microstructure. Photos of thin sections and petrographic descriptions are included in Appendix A. The ages and locations of samples that yielded geogchronologically significant results are shown on cross sections A-A' and B-B' in Figures 20 and 21.

4.2.1: Interpretation of the $^{40}Ar/^{39}Ar$ spectra

In order to be considered geochronologically significant, muscovite and amphibole analyses should display a plateau in which 50% or more of the ^{39}Ar was evolved over a series of contiguous heat steps in which the error did not exceed the 1 sigma level. Samples MG16, MG65, CA78A, and RM43 meet this criterion. It is unclear if some discordance inherent in these spectra are the result of partial resetting or the presence of excess argon. Except for sample CA70B, amphibole analyses are excluded from this discussion for reasons identified above.

Malton Gneiss- Muscovite sample MG16 was obtained from the footwall of the NTAF. Texturally, the Malton Gneiss exhibits only minor post-peak metamorphic recrystallization. Two generations of muscovite identified in thin section are the probable cause of minor variations in the apparent age spectrum. The first generation of muscovite is most abundant in the sample and was most likely the major contributor to the results of the analysis. However, the finer second generation muscovite is interpreted as late stage and related to shearing. Based on mineral assemblage and texture, the age is interpreted to represent cooling through the muscovite closure temperature at 60 ±0.4 Ma.

Mica Creek succession- Two samples from this unit (CA70B and CA78A), obtained from the hanging wall of the NTAF, yielded interpretable ages. Sample CA70B was the only amphibolite to yield a relatively concordant spectrum from

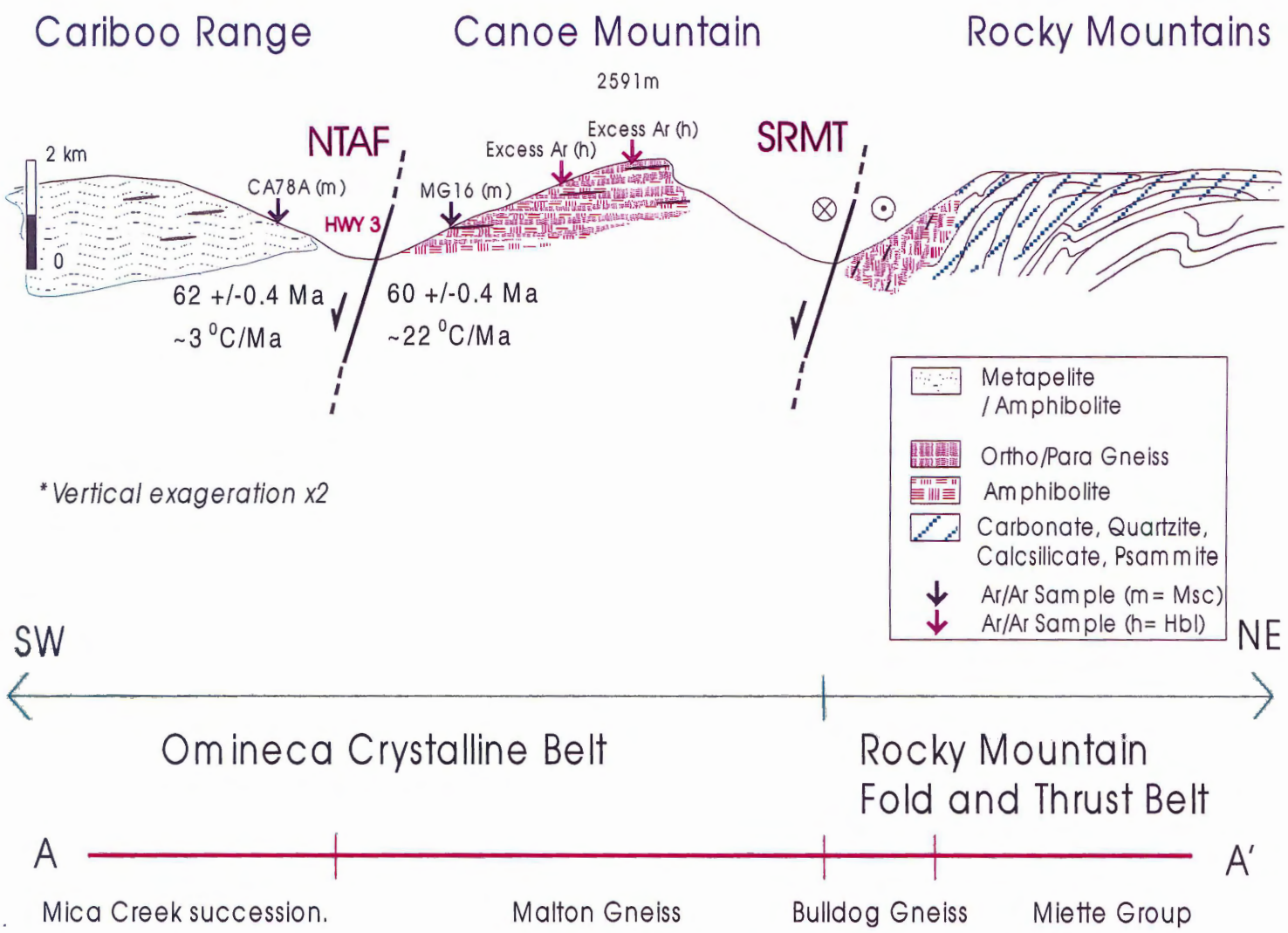

Figure 20: Schematic cross-section of A-A' locating the various units and locations of samples deemed analytically reliable based on evolution of ^{39}Ar in excess of 50% over contiguous steps within the 1 sigma error level.

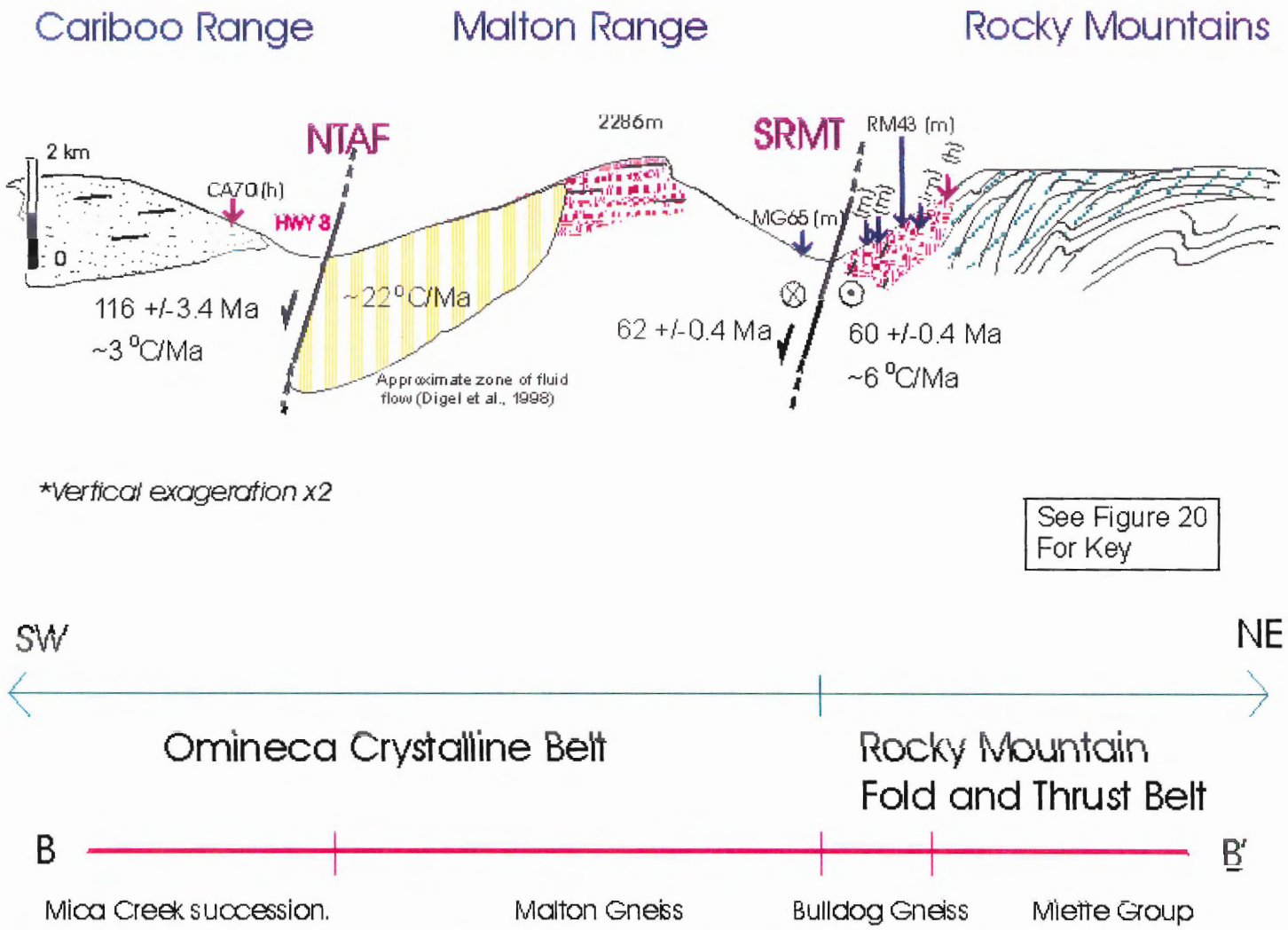

Figure 21: Schematic cross-section of B-B' locating the various units and locations of samples deemed analytically reliable based on evolution of ^{39}Ar in excess of 50% over contiguous steps within the 1 sigma error level.

hornblende at the same chronologic scale as the others. Recall, sample CA70B is highly recrystallized compared to other amphibole samples. Upon closer inspection, after initially high apparent ages, the lowest temperature step indicated an apparent age of 116 ±3.4 Ma and is followed by an increasing age gradient from 128-143 Ma in the latter part of the spectrum. A maximum apparent cooling age of 116 ±3.4 Ma is therefore interpreted for sample CA70B. The kyanite ± staurolite mineral assemblage (amphibolite facies) of muscovite sample CA78A (Chapter 2), partially recrystallized texture apparent in both samples, and largely discordant amphibole spectrum obtained for sample CA70B suggested partial resetting of amphibole and total resetting of muscovite with respect to ^{39}Ar. For the muscovite sample, 62 ±0.4 Ma. was interpreted as the maximum apparent age of cooling.

Bulldog Gniess- Muscovite sample RM43 was obtained from the immediate footwall of the RMF. Analysis of this sample provided the only acceptable spectrum obtained east of the RMF. Petrographic analysis indicated the protolith was syenitic, similar to the Malton Gneiss. There was no textural evidence in thin section of late stage recrystallization. Mineral assemblage and textural evidence suggested a metamorphic grade of middle amphibolite facies, and the apparent age of 60 ±0.4 Ma is therefore interpreted as a cooling age for muscovite.

Miette Group- Muscovite sample MG65 was obtained from wedge of pelitic schist, located at the exposed base of the Malton Gneiss, in the immediate hangingwall of the RMF (Figure 7). This sample was the source of mica for the only acceptable muscovite analysis from the Miette Group. Petrographic analysis revealed a mineralogy similar to sample TJ79 obtained from the Miette Group at Tête Jaune Cache, but indicated upper amphibolite facies metamorphism. Mica fish and low temperature shear zones which cross-cut the dominant fabric characterize the sample in thin section. Little retrogression is associated with the shear zones. Based on mineral assemblage and texture, the apparent age of 62 ±0.4 Ma is interpreted as a cooling age.

4.2.2: Geologic significance of the $^{40}Ar/^{39}Ar$ apparent ages

Previous geochronologic studies in the area of the Malton complex include U-Pb and apatite fission track (AFT) analyses by McDonough and Simony (1988) and McDonough et al. (1991, 1995, and references therein), and $^{40}Ar/^{39}Ar$ analyses of biotite and muscovite in the area of Tête Jaune Cache by Van Den Driessche and Maluski (1986). A summary of the results of these and other isotopic studies from the Omineca belt in the area of the Shuswap complex is available in Table 1. Results of previous geochronologic studies directly applicable to this study include K-Ar biotite ages from the staurolite-kyanite zone of the Bulldog Creek area, AFT results from a northeast-southwest directed transect across the Malton complex at about the same latitude as transects A-A' and B-B' of this study, and U-Pb data obtained from monazite, zircon, and titanite by Digel et al. (1998) in the northern Monashee Mountains. A cooling age of 112 Ma for biotite was recalculated from Wanless et al. (1968) by McDonough and Simony (1988). However, this analysis is inconsistent with results obtained in this study, possibly the result of unidentified excess argon and/or altered or relict biotite, and it is therefore excluded from the interpretation of results obtained in this study. However, the AFT results are included because of the location of the samples and because the results of the AFT analyses, performed at Dalhousie University, are much more recent (e.g., McDonough et al., 1995). The U-Pb data (Digel et al., 1998) are also included in support of the interpretation of the data obtained in this study.

Muscovite from the western Malton Gneiss cooled through 350 ±50 ^{0}C at 60 ±0.4 Ma. AFT analysis of samples obtained from the same latitude and structural level as samples from this study, further constrain the cooling of these rocks through 125 ±10 ^{0}C (Zentilli, 2000, personal correspondence) to 50 Ma (McDonough et al., 1995). The results of these analyses have been combined in a temperature vs. time plot (Figure 22) which yields an estimated linear cooling rate of *ca.* 22 $^{0}C/Ma$ for the western Malton Gneiss. Similarly, a temperature vs. time plot for muscovite (60 ±0.4) Ma and apatite (24 Ma) cooling ages from the

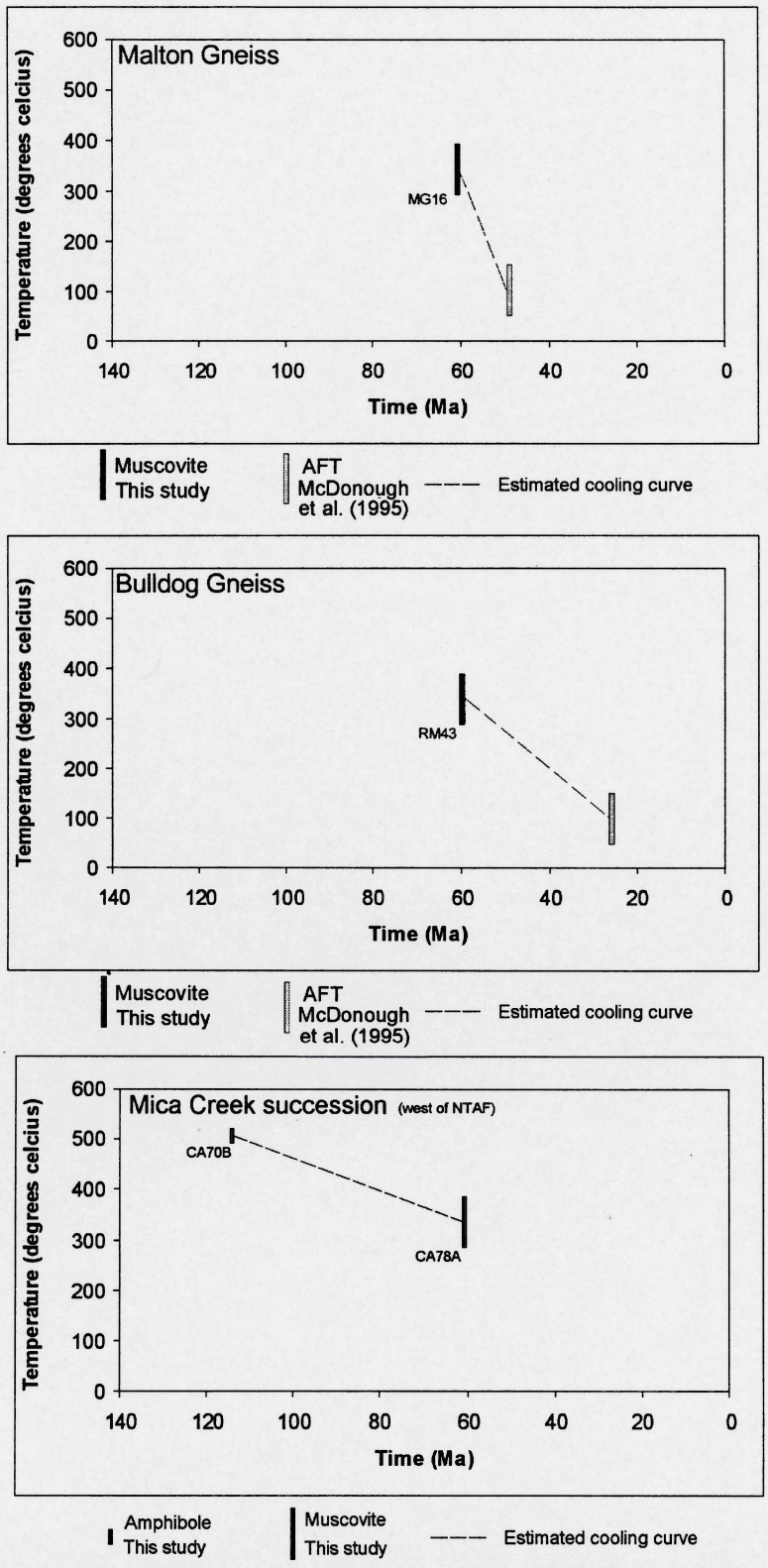

Figure 22: Temperature vs. time plots. Top – Malton Gneiss (~22 ^{0}C/Ma); Middle – Bulldog Gneiss (~6 ^{0}C/Ma); Bottom – Mica Creek succession (~3 ^{0}C/Ma). Note: peak metamorphism in Mica Creek succession (west of NTAF) ~170 Ma (Table 1 and sources therein). See text for U-Pb data.

Bulldog Gneiss (McDonough et al., 1995) provided an estimated linear cooling rate of *ca.* 6 ^{0}C/Ma.

A linear cooling rate of *ca.* 3 ^{0}C/Ma for samples from the Mica Creek succession was defined using amphibole (116 ±3.4 Ma) and muscovite (62 ±0.4 Ma) data. A muscovite cooling age of 62 ±0.4 Ma was obtained from Miette Group sample MG65, but because AFT analysis was not conducted at the same locality (McDonough et al., 1995) and the position of the outcrop suggested additional structural complexity related to the RMF, a cooling rate has not been determined. Estimated cooling rates are limited by the sparsity of data used in construction of the curves, resulting in a linear cooling rate. The rates are also limited in terms of geologic interpretation where data required to correlate rates across the faults are missing, particularly for high temperature minerals. Furthermore, sampling of muscovite and amphibole in the Mica Creek succession was separated by about 20 km, thereby excluding from interpretation any structural complications which lie between the two sample locations.

Muscovites from across the study area have similar apparent cooling ages. This indicates that the Malton complex, Mica Creek succession and Miette Group all cooled through 350 ±50^{0}C at about the same time, and suggests that the North Thompson-Albreda and Rocky Mountain faults underwent little or no relative vertical offset after *ca.* 60-62 Ma. However, AFT ages do differ, suggesting that an event occurred or was occurring approximately between 60 and 50 Ma. Digel et al. (1998) interpreted U-Pb ages of 65-59 Ma, obtained from a zone of pod sillimanite located in the footwall of the NTAF (Table 1), as relating to high temperature fluid flow along the NTAF in Paleocene time.

In extensional tectonic settings, slightly younger ages (2 Ma), characteristic of the footwalls of these normal faults, are to be expected where deeper, hotter rocks of the footwall are brought up relative to cooler rocks of the hanging wall. Based on the information obtained in this study, it is unlikely that the exact timing of fault motion could be constrained. However, because there is no notable offset of muscovite cooling ages across the faults at 60-62 Ma,

these ages may be interpreted as an upper age limit of fault motion within the study area.

Cooling rates are linked to how close a sample is to the surface, and provide an indirect constraint on the time or rate of exhumation. The high temperature cooling rate (500-350 ^{0}C) estimated for the Mica Creek succession , and the low temperature cooling rate (350-125 ^{0}C) estimated for the Bulldog Gneiss are comparable at 3-6 ^{0}C/Ma. However, low temperature cooling of the western Malton Gneiss (*ca.* 22 ^{0}C/Ma), in the footwall of the NTAF, is much faster than in the Bulldog Gneiss to the east. The estimated cooling rates are mainly controlled by AFT data (50 Ma vs 24-25 Ma) indicating earlier cooling through 125 ^{0}C for the Malton Gneiss at this locality. Since muscovite cooling ages are very similar, this suggests slow regional cooling below 350 ^{0}C prior to 60 Ma, followed by differential cooling between the Malton and Bulldog Gneisses at low temperature.

The estimated cooling rate established for the Mica Creek succession, because of the lack of directly comparable data across the NTAF, in particular, the lack of AFT data for this area, provides little insight into the exhumation history of the Malton Gneiss. However, there is evidence for high temperature fluid flow along the NTAF to the immediate south of the Malton Gneiss (Digel et al., 1998) which provides some insight into the processes which occurred during the exhumation of the Malton Gneiss.

There are a number of possible reasons for the faster low temperature cooling rate of the Malton Gneiss: a) differential (thrust) offset on the RMF or deeper level equivalent (sole thrust?); b) prolonged heating by magmatic activity or burial by sedimentary deposition; c) cooling by fluid flow along the faults, possibly linked to the presence of excess argon; d) differential vertical offset on the NTAF; e) differential erosion in Paleocene-Oligocene time. There are no data in this study to either support or dispute the validity of a) and there is little to no evidence in the area of the Malton complex in support of b). Based on evidence presented in this study, it is the author's opinion that the faster low

temperature cooling rate of the Malton Gneiss is the product of processes c) through e)..

If sufficient normal sense displacement along NTAF occurred after 60-62 Ma, prior to similar displacement along the RMF, a repository above the hanging wall may have formed and accommodated sediment input from the eroding cover of the Malton Gneiss. Combined with fluid flow along the NTAF, a rapid cooling rate of 22 ^{0}C/Ma relative to the Bulldog Gneiss (6 ^{0}C/Ma) would be established. Without the formation of a repository in response to normal-sense displacement along the (now present) RMF at or about the same time, exhumation would have proceeded more slowly as eroded sediment would less likely be transported elsewhere. Similar displacement along the RMF in Eocene (?) time would have exhumed the footwall of the RMF relative to the hanging wall. Cover sediments eroded from the footwall would have been deposited in a repository formed above the relatively lower hanging wall. The present day manifestation of this repository may be the Rocky Mountain Trench. This series of events is illustrated in Figure 23.

4.3: Implications for the Omineca belt

The North Thompson-Albreda and Rocky Mountain faults are high angle, west-side-down faults along which limited normal-sense displacement has been described (Chapter 2). Although this study suggests these faults appear to have played a role in the exhumation and cooling history of the Malton Gneiss, it is unlikely that they played any significant role in the exhumation of the Monashee complex, or any other complexes to the south. Vanderhaeghe and Teyssier (1997) compiled cooling ages from the Monashee complex and constructed a temperature vs. time plot, estimating cooling rates between 30-50 ^{0}C for high-grade mid- to lower crustal rocks and upper crustal rocks. Cooling rates were determined from analyses of zircon and monazite (U-Pb), white mica (Rb-Sr), hornblende, white mica, and biotite (K-Ar). High-grade rocks range in cooling age from 102-52 Ma (hornblende), and 52-44 Ma (biotite). Upper crustal rocks range

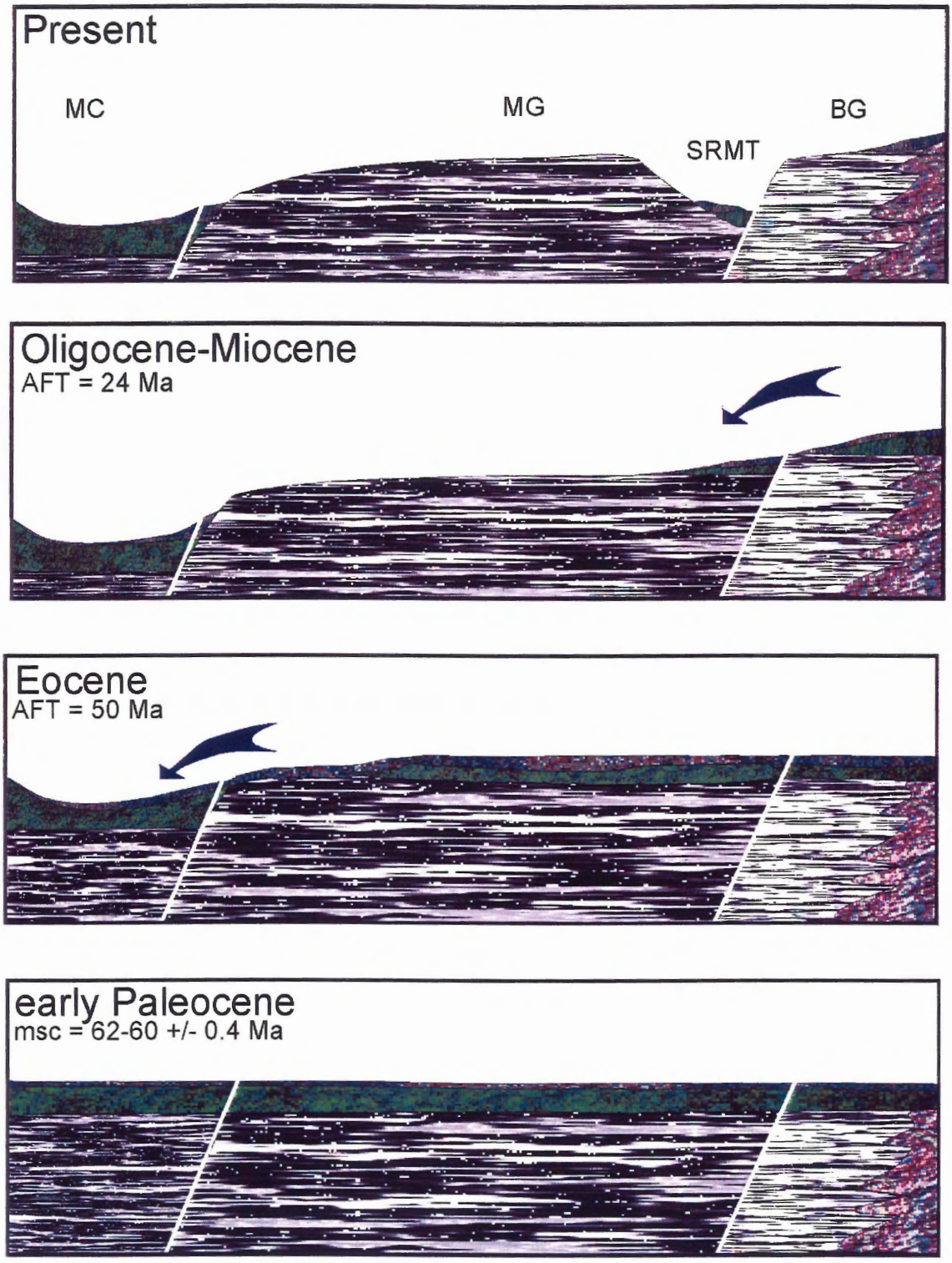

Figure 23: Possible exhumation history of the Malton Gneiss based on $^{40}Ar/^{39}Ar$ data obtained in this study and AFT data from McDonough et al. (1995). MC – Mica Creek succession; MG – Malton Gneiss; BG – Bulldog Gneiss; SRMT – Southern Rocky Mountain trench. Note: No implied vertical or horizontal scale.

in cooling age from 155 Ma (hornblende) to 147 (biotite). These rates are markedly faster and younger than those obtained in the area of the Malton Gneiss from this study, and suggest different differing mechanisms or rates of exhumation. Late orogenic extension linked to leucogranite intrusion has been described in the southern Shuswap complex (Carr, 1995; Vanderhaeghe and Teyssier, 1997), but does not appear to have played a role in the exhumation of the Malton Gneiss. In the area of the Malton gneiss, cooling rates are lower those reported in the Monashee complex, extensional offset is less than in the Monashee complex (narrowing to the north), exhumation of the Malton Gneiss is linked to steep rather than low-angle detachment faults, and there is no evidence for leucogranite intrusion in the Malton Gneiss.

Chapter 5: Conclusions

5.1: Summary and conclusions

The Shuswap complex of southeast British Columbia experienced a complex tectonic and thermal history, preserving evidence of Jurassic-Cretaceous compressional structures and peak metamorphism that are in turn overprinted by Late Cretaceous-Miocene extensional features (Coney and Harms, 1984; Tempelman-Kluit and Parkinson, 1986; Brown and Journeay, 1987; Parish et al., 1988). Much of the present day knowledge regarding the evolution of the Shuswap complex comes from numerous studies of the Monashee complex, one of three structural culminations within the Shuswap complex. Exhumation of the structural culminations within the Shuswap complex is widely believed to be the product of Paleocene-Miocene extension in the Omenica belt (Coney and Harms, 1984; Tempelman-Kluit and Parkinson, 1986; Brown and Journeay, 1987; van der Velden and Cook, 1996; Johnson and Brown, 1996). Comparison with data from other parts of the Omenica belt suggests that extension acted differently in terms of extent (Currie, 1988; Walker, 1989; van der Velden and Cook, 1994, 1996), timing (this study), and mechanisms (Parrish, 1988; Carr, 1989; Vanderhaeghe and Teyssier, 1997) in the area of the Malton complex.

The Malton complex, consisting of the Malton, Yellowjacket, and Bulldog gneisses, is located at the northern tip of the Shuswap complex. The North Thompson-Albreda Fault juxtaposes the Proterozoic middle amphibolite facies gneisses of the Malton Gneiss with the Neoproterozoic upper amphibolite facies metasediments of the Horsethief Creek Group cover strata to the west of the Shuswap complex. Leucogranite plutons, associated with the onset of extension in the Monashee complex (Parrish, 1988; Carr, 1989; Vanderhaeghe and Teyssier, 1997), have not been identified in the Malton complex.

To the east of the Shuswap complex, the Rocky Mountain Fault juxtaposes the Malton Gneiss with the Yellowjacket and Bulldog gneisses and their cover, Neoproterozoic strata of the Miette Group. The cover lithologies

comprise the Windermere Supergroup. Structure in the Windermere Supergroup is dominated by northeast-verging folds and faults, the result of Jurassic-Cretaceous compression.

$^{40}Ar/^{39}Ar$ analysis performed along two transects, oriented northeast-southwest, produced mainly discordant amphibole spectra from the Malton complex and Miette Group east of the Malton complex. Amphibole spectra are characterized by initially high apparent ages which precede the lowest temperature steps, and are followed by an increasing age gradient. These spectra are interpreted as representative of a complex tectonic and thermal history, possibly affected by excess argon, and provide no geochronologically significant information. An amphibole apparent cooling age of 116 ±3.4 Ma was obtained from sample CA70B from the Mica Creek succession of the Horsethief Creek Group. Muscovite spectra were generally less discordant and those identified as geochronologcially significant provided cooling ages of 62 ±0.4 Ma in the hanging walls and 60 ±0.4 Ma in the footwalls of the North Thompson-Albreda and Rocky Mountain faults.

Cooling rates were estimated for three parts of the study area based on temperature-time plots. Cooling rates of 22 ^{0}C/Ma and 6 ^{0}C/Ma for 350-125 ^{0}C were estimated for the western Malton Gneiss and Bulldog Gneiss respectively. A cooling rate of 3 ^{0}C/Ma over 500-350 ^{0}C and 116 ±3.4 to 62 ±0.4 Ma was estimated for samples from the Mica Creek succession, notably later (~50-60 Ma) than the peak metamorphic conditions reported at 174 and 163 Ma (Pigage, 1977; Gerasimoff, 1988; Mortensen et al., 1987). The muscovite cooling ages and cooling rates determined in the area of the Malton complex may possibly indicate that after mid Paleocene time, normal sense movement along the North Thompson-Albreda Fault resulted in the rapid exhumation of the Malton Gneiss relative to the Bulldog Gneiss. Normal sense movement along the Rocky Mountain Fault in Eocene (?) time then resulted in exhumation and cooling of the Bulldog Gneiss.

Previous workers have shown that cooling of the Monashee complex was

estimated at about 50 ^{0}C/Ma for high-grade mid- to lower-crustal rocks (biotite cooling ages reported at 52-44 Ma) and upper crustal rocks (biotite cooling age reported at 147 Ma). Results obtained in this study from the area of the Malton complex suggest relatively slower cooling for the northern Shuswap complex.

The extensional history of the northern Shuswap complex differs from that of the Monashee complex in terms of cooling ages, cooling rates, magnitude of extension, and exhumation process. In the area of the Malton Gneiss, muscovite cooling ages are older than those of muscovite from the Monashee complex by ~10 Ma, and the rate of cooling is notably slower than in the Monashee complex. Measurements of displacement along the North Thompson-Albreda and Rocky Mountain faults are considerably less than identified along the Okanagan Valley and Columbia River faults surrounding the Monashee Complex. Extension and subsequent exhumation in the northern Shuswap complex may have been accommodated by reactivation of thrust planes, unlike exhumation along detachment faults as described for the Monashee complex. Alternatively, ^{40}Ar/^{40}Ar evidence obtained in this study, combined with AFT analyses from McDonough et al. (1995) suggest that the Malton Gneiss cooled rapidly from the mid-Paleocene to recent time, possibly related to between 1-3 km of of west-side-down displacement along the NTAF (Currie, 1988; Walker, 1989). Comparable cooling data across the NTAF are required in order to test this hypothesis.

5.2: Recommendations for future work

A number of recommendations for future work are proposed to increase the body of knowledge surrounding the northern Shuswap complex. Additional mapping of structural features and metamorphic isograds is recommended to define better their interrelationship within the study area. Additionally, more detailed sampling is required across the entire study area in order to obtain a data set more representative of structural and stratigraphic relationships. Further sampling of amphibole is required to constrain the high temperature cooling history for the Malton complex. Additional sampling of amphibole and muscovite

is required to constrain the cooling history of the Miette Group east of the Malton complex. Comparable data, whether U-Pb, $^{40}Ar/^{39}Ar$, or AFT, is required across the NTAF and RMF in order to constrain better the timing of displacement along the faults. Argon laser analyses of muscovites (mica fish) may yield additional information relating to the timing of post-peak metamorphism or late stage deformation. Investigation of the geobarometry of the various units of the study area may yield important constraints on the depths from which the exposed rocks were exhumed. Combined with cooling ages and rates of cooling, further interpretation of the thermal history of the Malton Gneiss may be possible. This information may also clarify the significance of the amphibole data obtained in this study.

Appendix A

Petrography and micro photographs
of $^{40}Ar/^{39}Ar$ samples

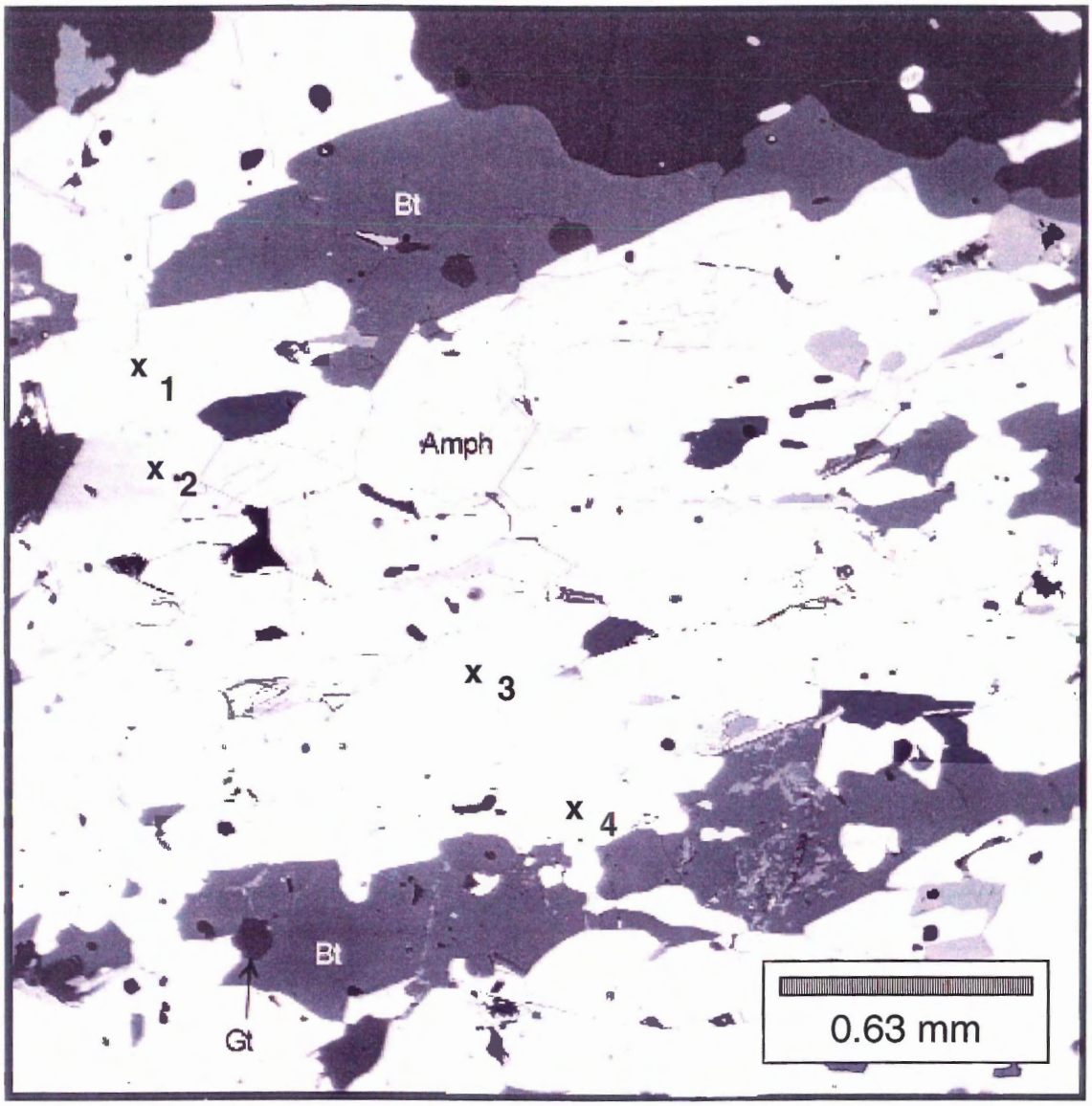

CA70B – BSI, parallel the lineation. Amphiboles were obtained from an outcrop of amphibolite located in the Mica Creek succession of the Cariboo Range, west of the North Thompson-Albreda Fault. L_1 is defined by preferentially aligned biotite. Garnet porphyroblasts up to 3.5 mm in diameter are common in hand sample. In thin section, recrystallized amphibole is preferentially oriented parallel to L_1. Garnets are poikiloblastic, containing quartz, feldspar and minor clinozoisite inclusions. Feldspar is present, grain boundaries intersecting at 120^0 where preserved within garnet. Biotite is present, oriented parallel to the lineation and often intergrown with the amphibole. Perpendicular the lineation, sericite is easily identified as having replaced plagioclase and amphibole is oriented along the grain boundaries of the garnets. Mineral assemblage and mineral textures indicate uppera amphiblolite facies metamorphism. Bt – biotite; Gt – garnet; Amph – amphibole. **X** – site investigated to identify chemical zoning.

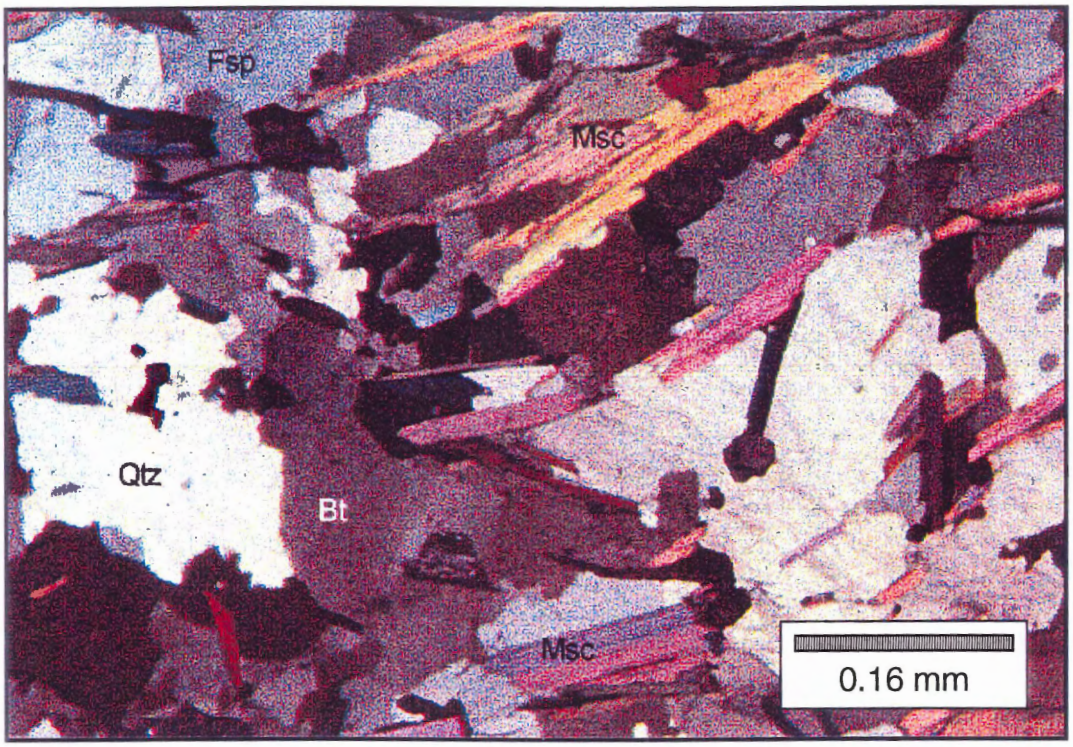

CA78A – Crossed-polars, parallel the lineation. Coarse-grained white mica was obtained from an outcrop of mica schist of the Mica Creek succession, located in the Cariboo Range, east of the North Thompson-Albreda Fault. Minor biotite and kyanite are visible in hand sample along with the white mica, interlayered with 2-3 cm thick layers of feldspar. Ductile deformation is identified by crenulation of S_1, defined by the white mica, and minor deformation of the felsic layers indicated by recrystallization. In thin section, coarse-grained white mica is intergrown with coarse-grained biotite. Coarse-grained white mica is also present in the feldspar dominated layers. Kyanite locally contains inclusions of rutile, garnet, and biotite. Kyanite, parallel to the flat-lying mica, is rimmed by fine-grained white mica. Incipient crenulation cleavage is apparent in the deformed mica-rich layers. Medium-grained idioblastic garnet porphyroblasts are also present. Quartz ribbons commonly contain sub-grains and new grains. Mineral assemblage and mineral texture indicates upper amphibolite facies metamorphism. Msc – muscovite; Bt – biotite, Qtz – quartz; Fsp – Feldspar.

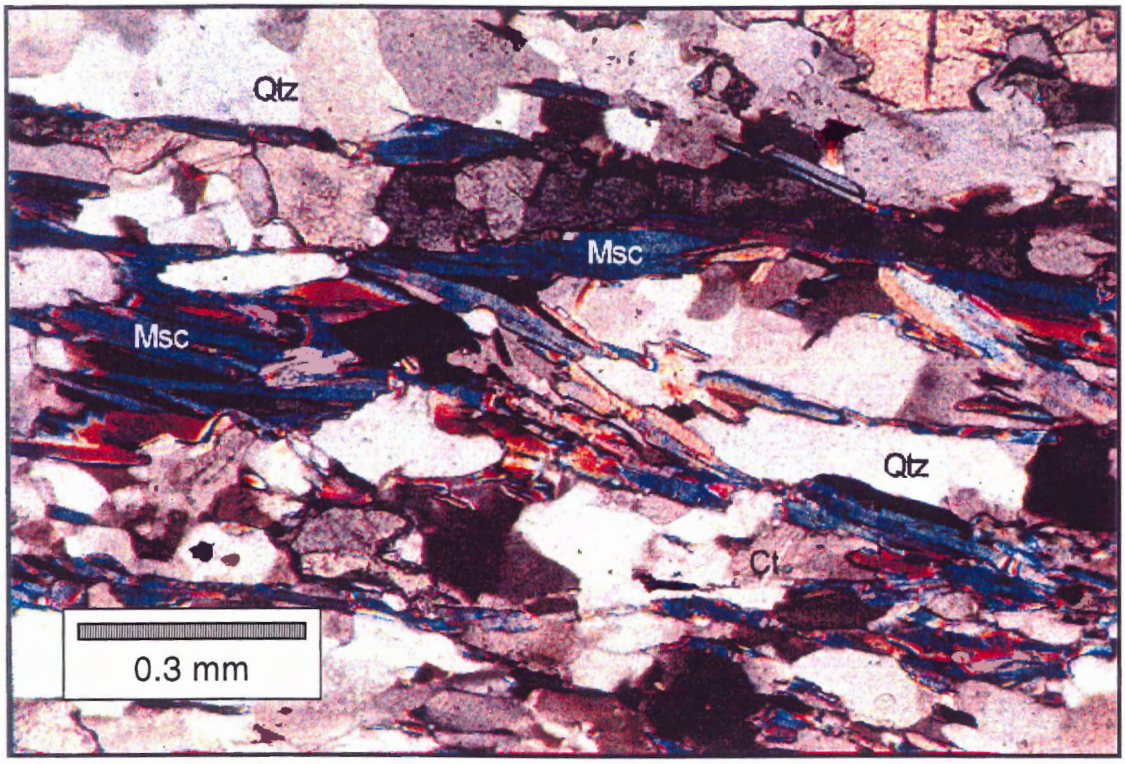

TJ79 – crossed-polars, parallel the lineation. Samples were obtained from an outcrop of psammite located at the northern end of the study area. The psammite is located in the Valemount Strain Zone, east of the Southern Rocky Mountain Trench, and represents the oldest metamorphosed or deformed set of sediments of the Miette Group within the study area. Quartzite beds contained evidence of preserved bedding. Fine-grained to coarse-grained white mica was used to define S_1. In thin section, mica fish are locally present, indicating some relatively lower temperature (post metamorphic peak) recrystallization. Biotite is commonly intergrown with muscovite. Mineral assemblage and texture indicates upper greenschist / lower amphibolite facies metamorphism. Qtz – quartz; Ct – carbonate; Msc – muscovite.

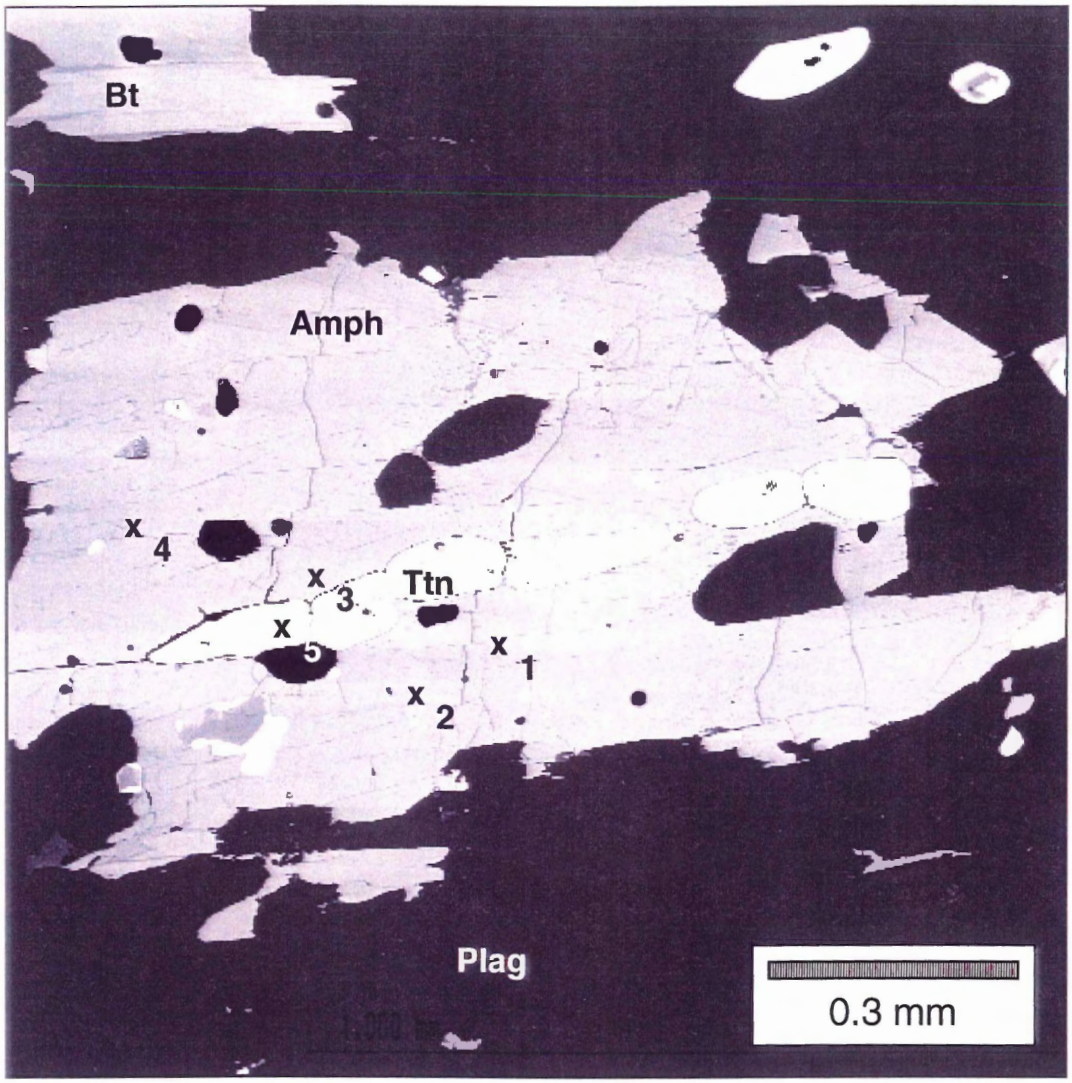

MG1B – BSI, parallel the lineation. Orthogneiss outcrops in the Malton Gneiss unit contain preferentially aligned amphibole, defining L_1. Layers dominated by variable proportions of amphibole and feldspar define shear foliation. In thin section, grain boundaries of the amphibole are highly variable. The amphibole commonly contains inclusions of titanite and epidote with some allanite cores. Biotite is common in the amphibole-rich layers, locally intergrown with chlorite. Perpendicular to the lineation, the shear foliation is only weakly defined by amphibole. The abundance of retrograde chlorite equals that of biotite. Plag – plagioclase; Amph – amphibole; Ttn – titanite; Bt – biotite. **X** – site investigated for chemical zonation.

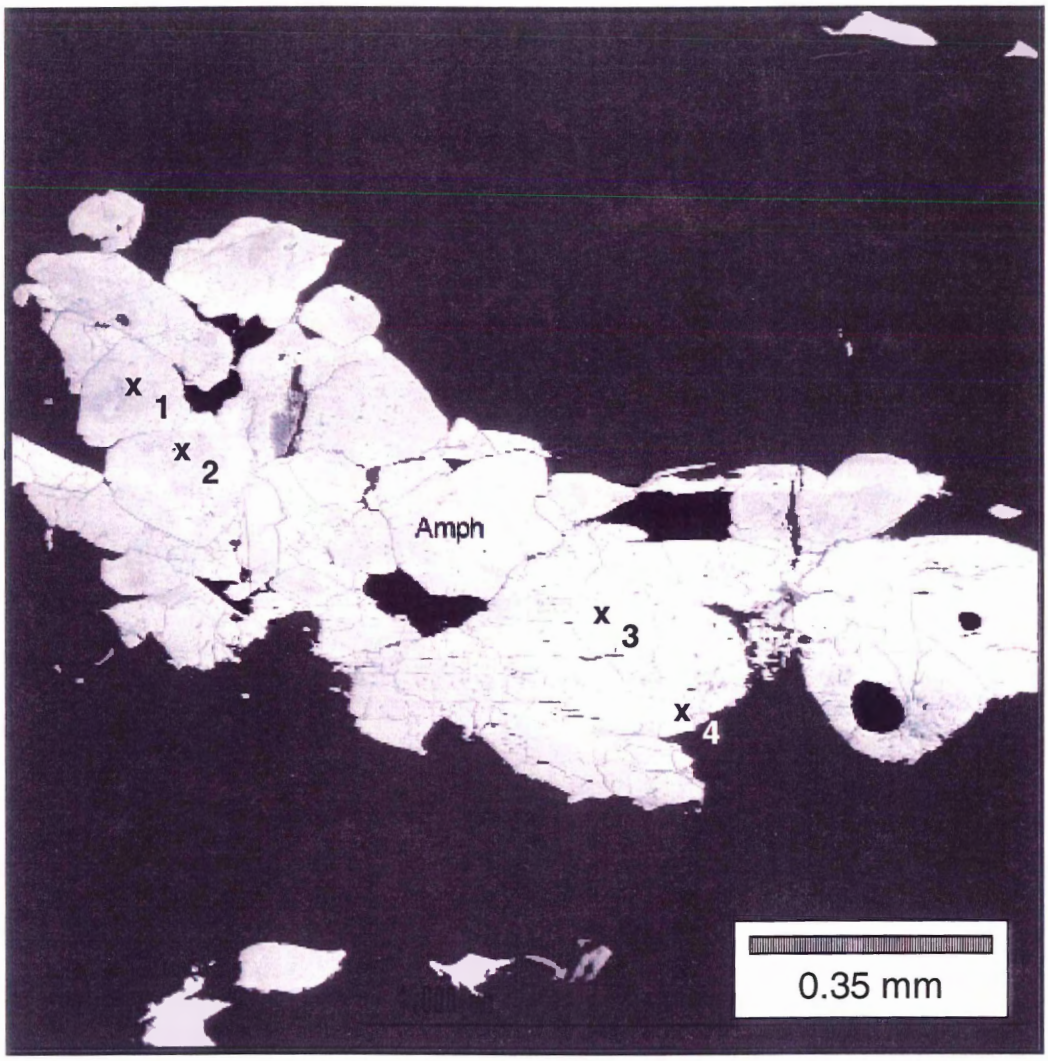

MG5 - BSI, parallel the lineation. Amphibole was obtained from a leucogneiss outcropping in the Malton Gneiss. Parallel amphiboles and stretched porphyroblasts of garnet define L_1. The shear foliation is defined by 1-2 cm thick layers of feldspar and moderately thicker layers of amphibole and feldspar. In thin section, amphiboles are subidioblastic. Porphyroblasts of poikiolitic garnets are present, commonly intergrown with amphibole. Other inclusions in the garnets include quartz and K-feldspar. Coarse-grained allenite locally relicts garnets. Amph – Amphibole. **X** – site investigated for chemical zonation.

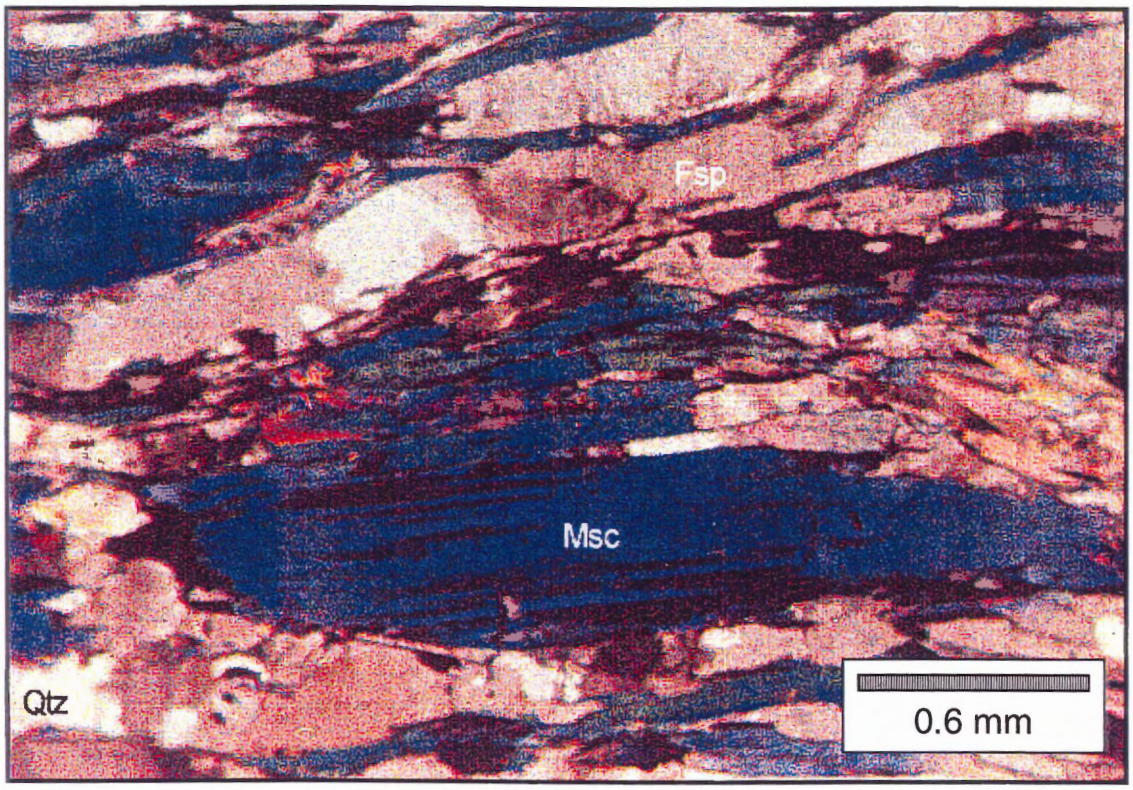

MG16 – Crossed-polars, parallel the lineation. Coarse-grained white mica defines both L_1 and the shear foliation in an outcrop of mica schist located in the Malton Gneiss. In hand sample the white mica is intergrown with oxides and interlayered with feldspar. In thin section the white mica is commonly intergrown with coarse-grained bladed biotite along the foliation and locally displays minor deformation features such as kinks. Epidote (locally containing allanite cores) and zoisite are common. Ductile deformation of the sample is indicated by quartz ribbons and quartz new grains in addition to preferentially aligned white mica and biotite a xenoblastic feldspar matrix. Plagioclase content greatly exceeds quartz content. Some fine-grained white mica is present, either the result of shearing the larger grains or as sericite after plagioclase. Msc – muscovite; Qtz – quartz; Fsp – feldspar.

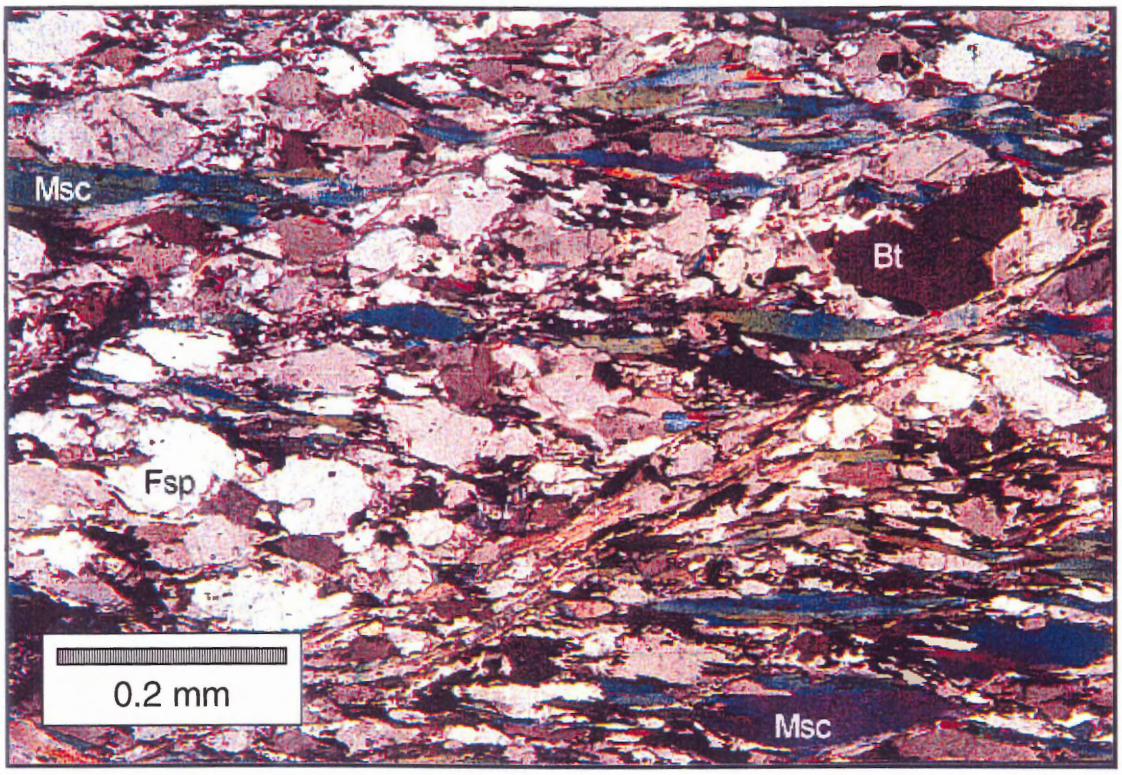

MG65 – Crossed-polars, parallel the lineation. Coarse-grained white mica was obtained from an outcrop of mica schist located along the northwest edge of the Malton Gneiss. L_1 is defined by stretched feldspar. In thin section coarse-grained white mica and biotite are preferentially oriented, defining the shear fabric (post peak metamorphic conditions). Biotite is intergrown with and/or rims the white mica. White mica displays evidence of weak deformation in the form of mica fish. Shear bands (7-10 mm in thickness, not in figure) of biotite contain abundant sphene and epidote group minerals as well as some white mica. A biotite-epidote shear zone is present in thinsection, but the effects of this deformation are restricted to the shear zone. This sample is similar in petrography to TJ79 but is less recrystallized. Msc – muscovite; Fsp – feldspar; Bt – biotite.

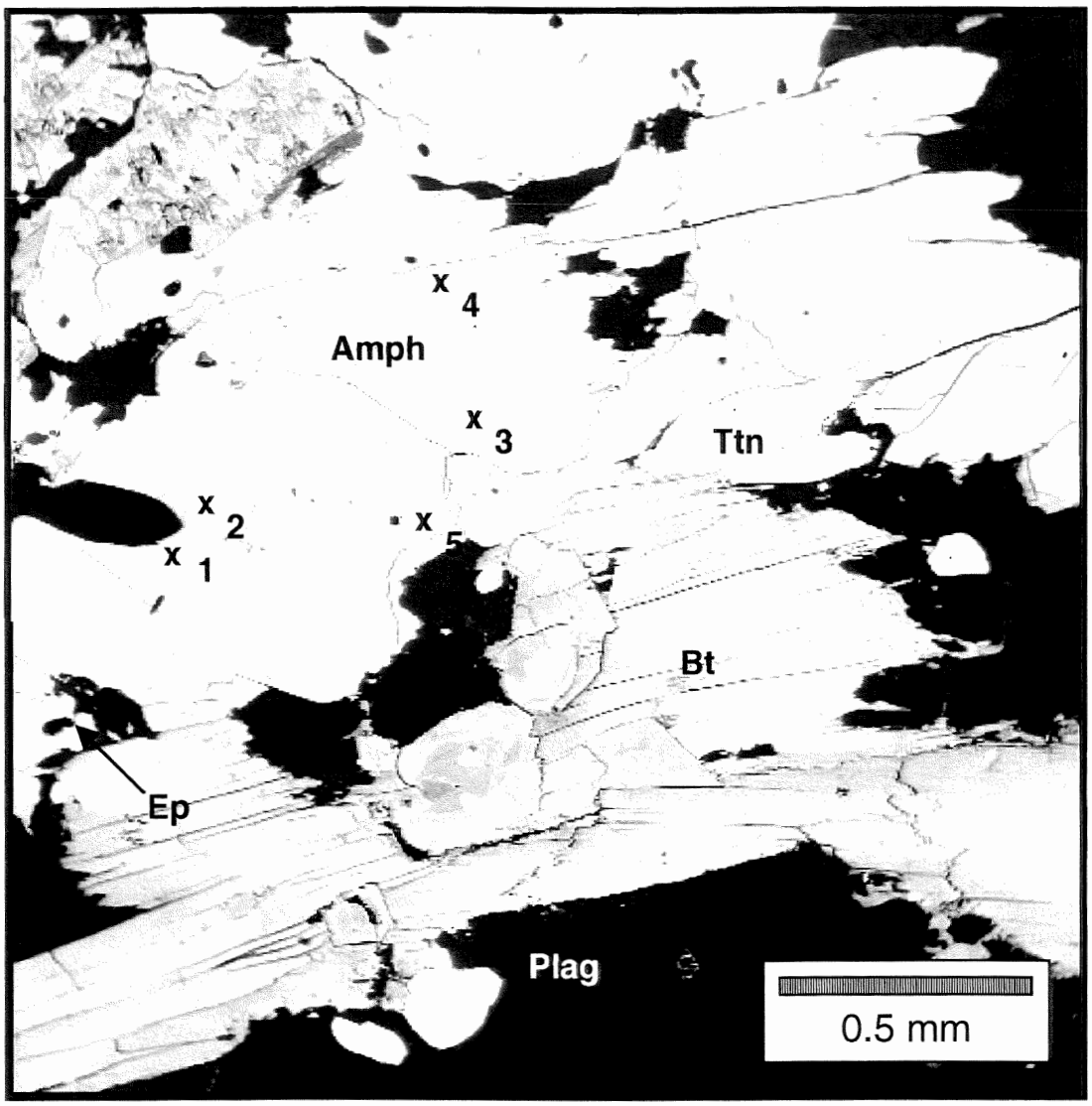

RM52 – BSI, parallel the lineation. Amphibole was obtained from an outcrop of amphibolite located in the Bulldog immediately east of the Rocky Mountain Fault. In outcrop quartz-feldspar veins cut the amphibolite along brittle deformation features. Feldspars present within the amphibolite is preferentially aligned and define L_1. In thin section, amphibole is coarse-grained and poikiloblastic, containing K-feldspar and plagioclase inclusions. The amphibole is commonly intergrown with idioblastic laths of biotite and subidioblastic sphene. Amph – amphibole; Ttn – titanite; Plag – plagioclase; Ep – epidote. **X** – site investigated for chemical zonation.

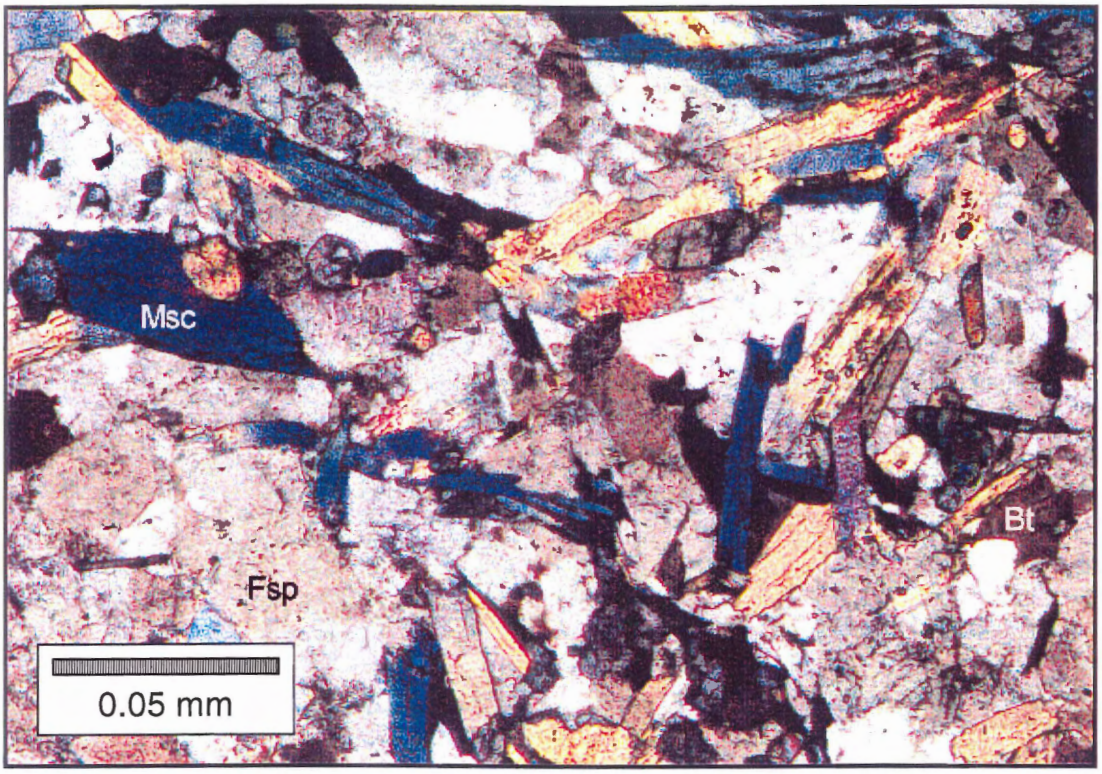

RM26 – Crossed-polars, parallel the lineation. Orthogneiss outcropping east of the Southern Rocky Mountain Trench provided the white mica used for $^{40}Ar/^{39}Ar$ analysis in this locality. Preferentially oriented white mica defines L_1 in hand sample and thin section. Augen shaped feldspars in hand sample suggest dextral-sense deformation in this area (see text, Chapter 2). K-feldspar megacrysts suggest an igneous protolith. Plagioclase is locally sericitized. Medium to coarse-grained biotite is oriented parallel to the white mica and is locally retrograded to chlorite. Epidote is common with some allanite cores. Titanite is generally abundant. Msc – muscovite; Fsp – Feldspar; Bt – biotite.

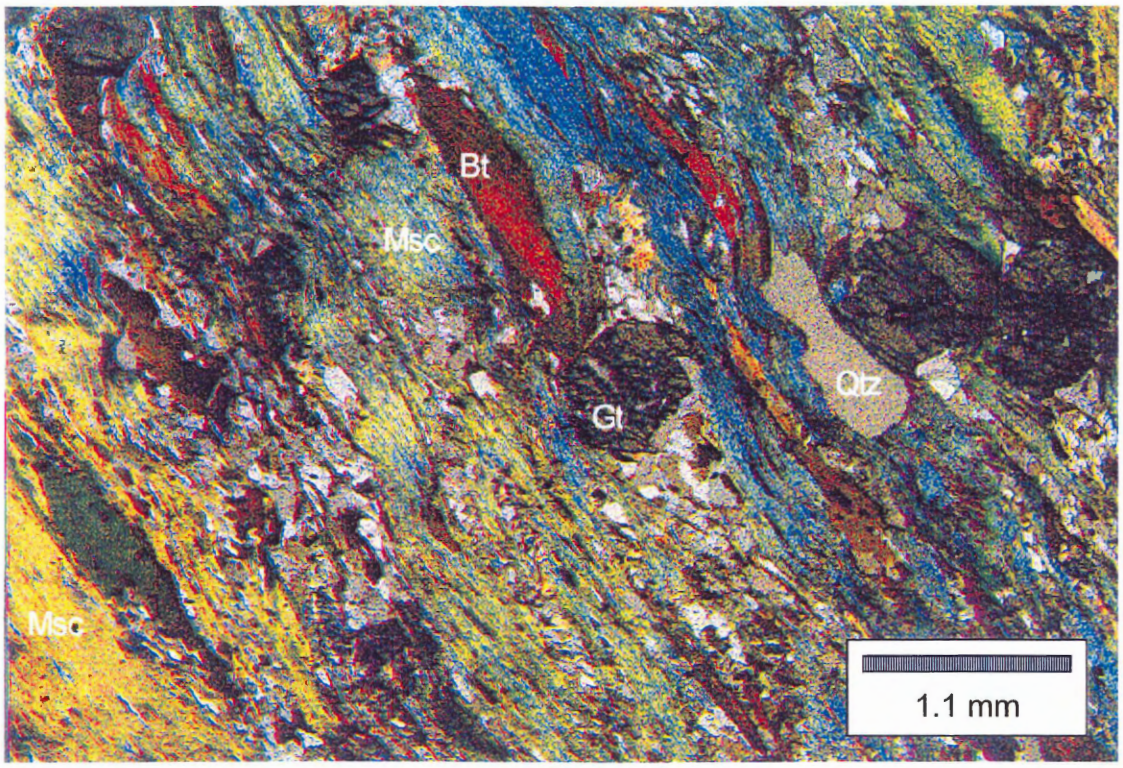

RM42 – Crossed-polars, parallel the lineation. East of the Rocky Mountain fault, coarse-grained parallel white mica defining S_1 was obtained from an outcrop of extremely fissile mica-schist. In thin section, white mica is weakly crenulated parallel to L_1, displaying incipient crenulation cleavage, perpendicular to L_1. White mica and biotite are locally intergrown. Fractured garnet porphyroclasts contain white mica oriented parallel S_1. Recrystallized white mica (post peak metamorphic conditions) commonly wraps around unfractured and fractured garnet porphyroblasts. Post-kinematic chlorite overgrows the fabric. Mineral assemblage indicates mid to upper amphibolite facies metamorphism. Msc – muscovite; Gt – garnet; Bt – biotite; Qz – quartz.

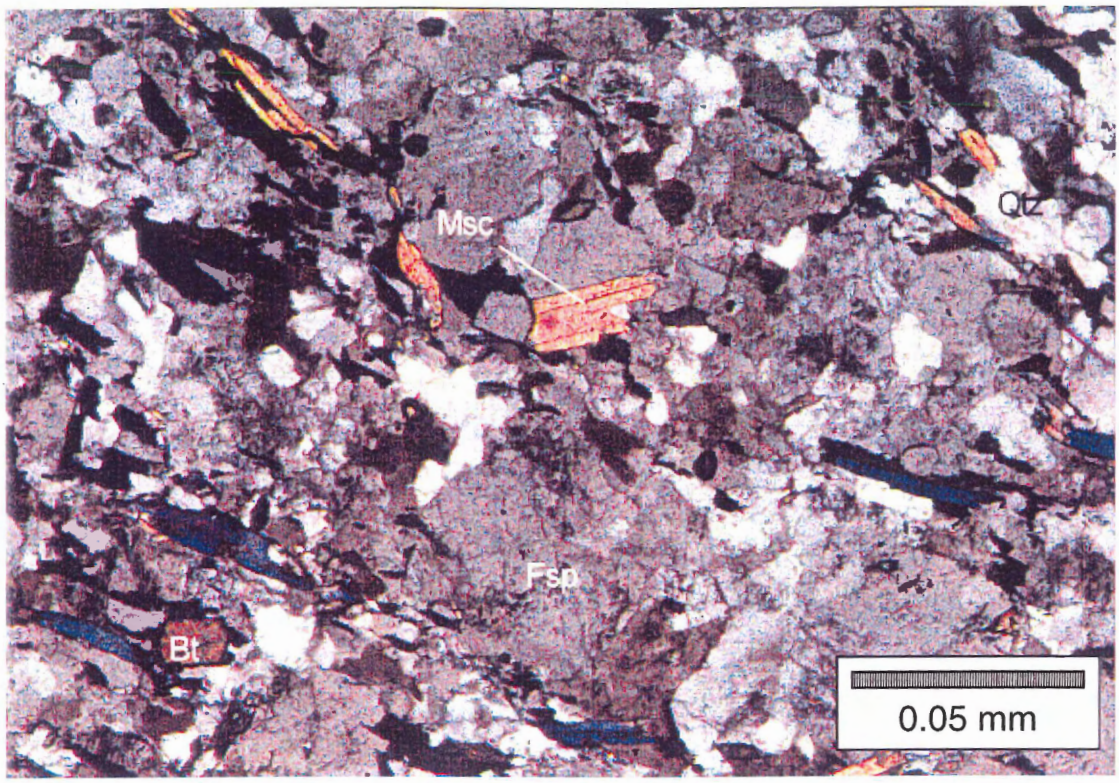

RM43 – Crossed-polars, parallel the lineation. Coarse-grained white mica was obtained from an outcrop of orthogneiss east of the Rocky Mountain fault. In thin section coarse-grained white mica and biotite clearly define S_1. Substantial retrogression is indicated by plagioclase altered to sericite and biotite altered to chlorite. Bulk composition suggests a syenitic protolith. A low temperature shear zone cross-cuts the sample in thinsection. Msc – muscovite; Bt – biotite; Fsp – feldspar; Qtz – quartz.

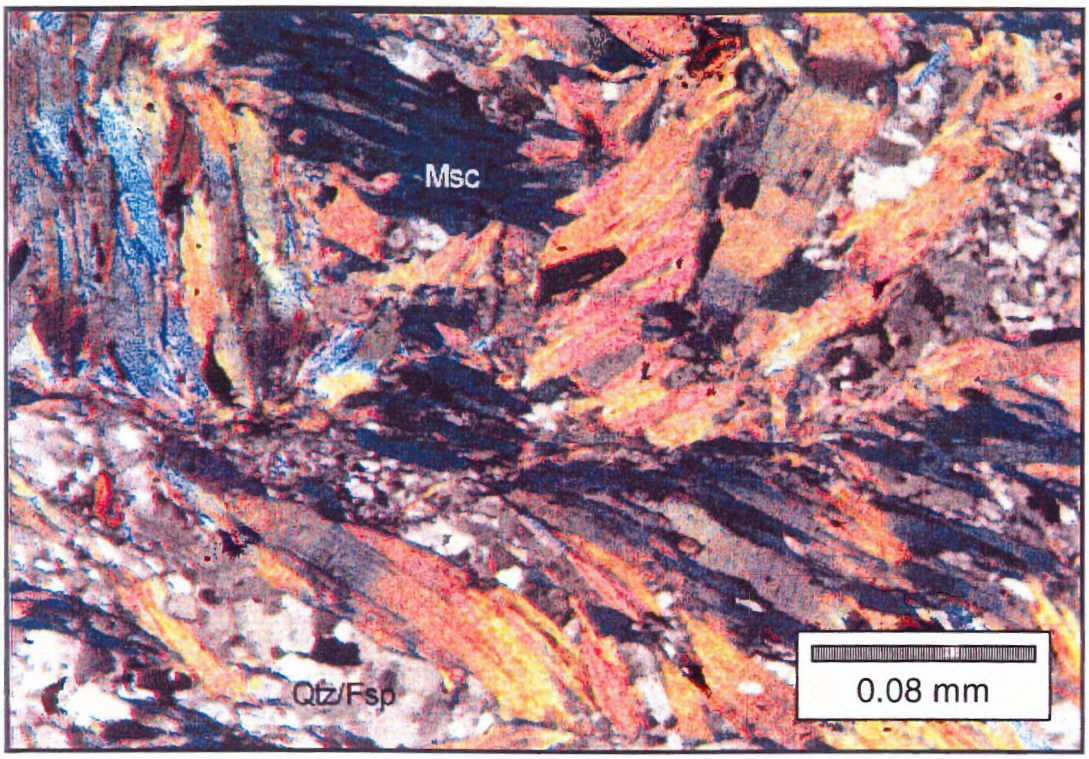

RM55 – Crossed-polars, perpendicular the lineation. Medium to coarse-grained white mica was obtained from a mica schist of the Miette Group, outcropping to the east of the Rocky Mountain fault. In hand sample S_1 is defined by weakly crenulated white mica. In thin section there is plenty of evidence of low temperature recrystallization. Coarse-grained white mica fish (generation 1) are interlayered with xenoblastic quartz and feldspar. Mica fish indicate a dextral sense of shear parallel L_1, defined by oriented white mica. Recrystllized (generation 2) white mica forms incipient crenulation cleavate. Perpendicular to L_1, incipient crenulation cleavage is visible. Msc – muscovite; Fsp – feldspar; Qtz – quartz.

Appendix B

Classification of amphiboles
from electron probe microanalyses

Ferropargasite*

		Oxide		Ions	Structure
MG1B	SiO2	39.99	Si	6.27	8.00
	TiO2	0.76	Ti	0.09	
	Al2O3	12.29	Al^{IV}	1.73	
	FeO	22.72	Al^{VI}	0.53	5.20
	MnO	0.57	Fe	2.98	
	MgO	6.52	Mn	0.08	
	CaO	11.24	Mg	1.52	
	Na2O	1.58	Ca	1.89	2.00
	K2O	1.84	Na^{M4}	0.11	
	Total	97.86	Na^{A}	0.37	
			K	0.37	0.73

Ferropargasite

		Oxide		Ions	Structure
MG5	SiO2	37.57	Si	6.13	8.00
	TiO2	0.65	Ti	0.08	
	Al2O3	12.59	Al^{IV}	1.87	
	FeO	30.46	Al^{VI}	0.55	5.21
	MnO	0.42	Fe	4.16	
	MgO	1.52	Mn	0.06	
	CaO	10.94	Mg	0.37	
	Na2O	1.37	Ca	1.91	2.00
	K2O	2.31	Na^{M4}	0.09	
	Total	98.31	Na^{A}	0.35	
			K	0.48	0.83

Tschermakite

		Oxide		Ions	Structure
CA70B	SiO2	42.66	Si	6.33	8.00
	TiO2	0.67	Ti	0.07	
	Al2O3	14.75	Al^{IV}	1.67	
	FeO	16.01	Al^{VI}	0.91	5.14
	MnO	0.23	Fe	1.99	
	MgO	9.64	Mn	0.03	
	CaO	11.77	Mg	2.13	
	Na2O	1.56	Ca	1.87	2.00
	K2O	0.75	Na^{M4}	0.13	
	Total	98.39	Na^{A}	0.32	
			K	0.14	0.46

Ferropargasite

		Oxide		Ions	Structure
RM52	SiO2	41.04	Si	6.22	8.00
	TiO2	0.61	Ti	0.07	
	Al2O3	14.41	Al^{IV}	1.78	
	FeO	19.28	Al^{VI}	0.79	5.23
	MnO	0.33	Fe	2.44	
	MgO	8.29	Mn	0.04	
	CaO	11.20	Mg	1.87	
	Na2O	1.99	Ca	1.82	2.00
	K2O	0.88	Na^{M4}	0.18	
	Total	98.44	Na^{A}	0.40	
			K	0.17	0.58

*Classifications based on Leake et al. (1997)

Ferropargasite

		Oxide		Ions	Structure
MG3	SiO_2	37.18	Si	6.11	8.00
	TiO_2	1.03	Ti	0.13	
	Al_2O_3	12.16	Al^{IV}	1.89	
	FeO	32.31	Al^{VI}	0.47	5.24
	MnO	0.52	Fe	4.44	
	MgO	0.54	Mn	0.07	
	CaO	10.54	Mg	0.13	
	Na_2O	1.59	Ca	1.86	2.00
	K_2O	2.19	Na^{M4}	0.14	
	Total	98.49	Na^{A}	0.36	
			K	0.46	0.82

Ferropargasite

		Oxide		Ions	Structure
MG2A	SiO_2	37.47	Si	6.22	8.00
	TiO_2	0.68	Ti	0.09	
	Al_2O_3	11.23	Al^{IV}	1.78	
	FeO	32.04	Al^{VI}	0.42	5.25
	MnO	1.68	Fe	4.45	
	MgO	0.24	Mn	0.24	
	CaO	10.01	Mg	0.06	
	Na_2O	1.98	Ca	1.78	2.00
	K_2O	2.30	Na^{M4}	0.22	
	Total	98.01	Na^{A}	0.42	
			K	0.49	0.91

Tschermakite

		Oxide		Ions	Structure
RM57	SiO_2	42.16	Si	6.22	8.00
	TiO_2	0.56	Ti	0.06	
	Al_2O_3	16.85	Al^{IV}	1.78	
	FeO	14.74	Al^{VI}	1.16	5.12
	MnO	0.11	Fe	1.82	
	MgO	9.38	Mn	0.01	
	CaO	11.54	Mg	2.07	
	Na_2O	1.77	Ca	1.82	2.00
	K_2O	0.55	Na^{M4}	0.18	
	Total	97.99	Na^{A}	0.33	
			K	0.10	0.44

Appendix C

electron probe microanalyses
of amphiboles

Analysis*		Oxide		Ions	Structure
1.00	SiO2	39.90	Si	6.00	8.00
	TiO2	4.71	Ti	0.53	
	Al2O3	13.55	Al^{IV}	2.00	
	FeO	10.34	Al^{VI}	0.40	5.07
	MnO	0.00	Fe	1.30	
	MgO	12.69	Mn	0.00	
	CaO	10.10	Mg	2.84	
	Na2O	2.63	Ca	1.63	1.63
	K2O	2.03	Na^{M4}	0.00	
	Total	95.94	Na^{A}	0.00	
			K	0.39	0.39

		Oxide		Ions	Structure
2.00	SiO2	41.22	Si	6.26	8.00
	TiO2	0.59	Ti	0.07	
	Al2O3	14.31	Al^{IV}	1.74	
	FeO	18.03	Al^{VI}	0.82	5.13
	MnO	0.25	Fe	2.29	
	MgO	8.48	Mn	0.03	
	CaO	11.47	Mg	1.92	
	Na2O	2.16	Ca	1.87	1.87
	K2O	0.87	Na^{M4}	0.00	
	Total	97.38	Na^{A}	0.00	
			K	0.17	0.17

		Oxide		Ions	Structure
	SiO2	41.49	Si	6.33	8.00
3.00	TiO2	0.69	Ti	0.08	
	Al2O3	13.58	Al^{IV}	1.67	
	FeO	18.20	Al^{VI}	0.77	5.11
	MnO	0.23	Fe	2.32	
	MgO	8.37	Mn	0.03	
	CaO	11.52	Mg	1.90	
	Na2O	1.97	Ca	1.88	1.88
	K2O	0.86	Na^{M4}	0.00	
	Total	96.91	Na^{A}	0.00	
			K	0.17	0.17

		Oxide		Ions	Structure
	SiO2	38.04	Si	6.21	8.00
4.00	TiO2	0.69	Ti	0.08	
	Al2O3	12.54	Al^{IV}	1.79	
	FeO	29.82	Al^{VI}	0.62	5.17
	MnO	0.36	Fe	4.07	
	MgO	1.42	Mn	0.05	
	CaO	10.73	Mg	0.34	
	Na2O	1.43	Ca	1.88	1.88
	K2O	2.23	Na^{M4}	0.00	
	Total	97.26	Na^{A}	0.00	
			K	0.46	0.46

*Missing analyses = probe analysis of a non-amphibole.

		Oxide		Ions	Structure
	SiO2	37.66	Si	6.20	8.00
7.00	TiO2	0.74	Ti	0.09	
	Al2O3	12.12	Al^{IV}	1.80	
	FeO	29.48	Al^{VI}	0.55	5.09
	MnO	0.31	Fe	4.06	
	MgO	1.40	Mn	0.04	
	CaO	10.83	Mg	0.34	
	Na2O	1.76	Ca	1.91	1.91
	K2O	2.33	Na^{M4}	0.00	
	Total	96.62	Na^{A}	0.00	
			K	0.49	0.49

		Oxide		Ions	Structure
	SiO2	38.12	Si	6.24	8.00
8.00	TiO2	0.66	Ti	0.08	
	Al2O3	12.22	Al^{IV}	1.76	
	FeO	29.67	Al^{VI}	0.60	5.14
	MnO	0.31	Fe	4.06	
	MgO	1.45	Mn	0.04	
	CaO	10.68	Mg	0.35	
	Na2O	1.58	Ca	1.87	1.87
	K2O	2.30	Na^{M4}	0.00	
	Total	97.00	Na^{A}	0.00	
			K	0.48	0.48

		Oxide		Ions	Structure
	SiO2	41.07	Si	6.37	8.00
9.00	TiO2	0.91	Ti	0.11	
	Al2O3	12.11	Al^{IV}	1.63	
	FeO	22.13	Al^{VI}	0.58	5.13
	MnO	0.47	Fe	2.87	
	MgO	6.54	Mn	0.06	
	CaO	11.37	Mg	1.51	
	Na2O	1.55	Ca	1.89	2.00
	K2O	1.70	Na^{M4}	0.11	
	Total	97.85	Na^{A}	0.36	
			K	0.34	0.69

		Oxide		Ions	Structure
	SiO2	40.68	Si	6.36	8.00
10.00	TiO2	0.80	Ti	0.09	
	Al2O3	11.99	Al^{IV}	1.64	
	FeO	22.00	Al^{VI}	0.57	5.11
	MnO	0.64	Fe	2.88	
	MgO	6.35	Mn	0.08	
	CaO	11.27	Mg	1.48	
	Na2O	1.83	Ca	1.89	2.00
	K2O	1.71	Na^{M4}	0.11	
	Total	97.26	Na^{A}	0.44	
			K	0.34	0.78

		Oxide		Ions	Structure
	SiO2	40.94	Si	6.38	8.00
11.00	TiO2	0.86	Ti	0.10	
	Al2O3	12.18	Al^{IV}	1.62	
	FeO	21.73	Al^{VI}	0.62	5.14
	MnO	0.51	Fe	2.83	
	MgO	6.52	Mn	0.07	
	CaO	11.24	Mg	1.52	
	Na2O	1.41	Ca	1.88	2.00
	K2O	1.69	Na^{M4}	0.12	
	Total	97.08	Na^{A}	0.30	
			K	0.34	0.64

		Oxide		Ions	Structure
	SiO2	40.83	Si	6.36	8.00
12.00	TiO2	0.58	Ti	0.07	
	Al2O3	12.19	Al^{IV}	1.64	
	FeO	22.62	Al^{VI}	0.59	5.17
	MnO	0.49	Fe	2.95	
	MgO	6.46	Mn	0.07	
	CaO	11.32	Mg	1.50	
	Na2O	1.56	Ca	1.89	2.00
	K2O	1.64	Na^{M4}	0.11	
	Total	97.68	Na^{A}	0.36	
			K	0.33	0.69

		Oxide		Ions	Structure
	SiO2	47.49	Si	7.03	8.00
13.00	TiO2	0.31	Ti	0.03	
	Al2O3	8.05	Al^{IV}	0.97	
	FeO	16.55	Al^{VI}	0.44	5.11
	MnO	0.26	Fe	2.05	
	MgO	11.57	Mn	0.03	
	CaO	12.13	Mg	2.55	
	Na2O	1.20	Ca	1.92	2.00
	K2O	0.27	Na^{M4}	0.08	
	Total	97.83	Na^{A}	0.27	
			K	0.05	0.32

		Oxide		Ions	Structure
	SiO2	40.97	Si	6.22	8.00
14.00	TiO2	0.67	Ti	0.08	
	Al2O3	14.52	Al^{IV}	1.78	
	FeO	18.12	Al^{VI}	0.82	5.15
	MnO	0.34	Fe	2.30	
	MgO	8.46	Mn	0.04	
	CaO	11.39	Mg	1.91	
	Na2O	2.08	Ca	1.85	2.00
	K2O	0.96	Na^{M4}	0.15	
	Total	97.51	Na^{A}	0.47	
			K	0.19	0.65

		Oxide		Ions	Structure
	SiO2	41.79	Si	6.32	8.00
15.00	TiO2	0.70	Ti	0.08	
	Al2O3	13.94	Al^{IV}	1.68	
	FeO	18.45	Al^{VI}	0.81	5.15
	MnO	0.18	Fe	2.33	
	MgO	8.45	Mn	0.02	
	CaO	11.24	Mg	1.91	
	Na2O	2.01	Ca	1.82	2.00
	K2O	0.97	Na^{M4}	0.18	
	Total	97.72	Na^{A}	0.41	
			K	0.19	0.60

		Oxide		Ions	Structure
	SiO2	41.82	Si	6.35	8.00
16.00	TiO2	0.66	Ti	0.08	
	Al2O3	13.72	Al^{IV}	1.65	
	FeO	18.23	Al^{VI}	0.80	5.15
	MnO	0.28	Fe	2.31	
	MgO	8.53	Mn	0.04	
	CaO	11.31	Mg	1.93	
	Na2O	1.96	Ca	1.84	2.00
	K2O	0.75	Na^{M4}	0.16	
	Total	97.27	Na^{A}	0.41	
			K	0.15	0.56

		Oxide		Ions	Structure
	SiO2	42.25	Si	6.39	8.00
18.00	TiO2	0.65	Ti	0.07	
	Al2O3	13.24	Al^{IV}	1.61	
	FeO	18.58	Al^{VI}	0.75	5.15
	MnO	0.37	Fe	2.35	
	MgO	8.53	Mn	0.05	
	CaO	11.37	Mg	1.92	
	Na2O	1.95	Ca	1.84	2.00
	K2O	0.77	Na^{M4}	0.16	
	Total	97.71	Na^{A}	0.42	
			K	0.15	0.57

		Oxide		Ions	Structure
	SiO2	41.77	Si	6.31	8.00
19.00	TiO2	0.68	Ti	0.08	
	Al2O3	13.89	Al^{IV}	1.69	
	FeO	18.23	Al^{VI}	0.78	5.12
	MnO	0.24	Fe	2.30	
	MgO	8.55	Mn	0.03	
	CaO	11.61	Mg	1.93	
	Na2O	2.11	Ca	1.88	2.00
	K2O	0.74	Na^{M4}	0.12	
	Total	97.81	Na^{A}	0.50	
			K	0.14	0.64

		Oxide		Ions	Structure
	SiO2	39.37	Si	6.39	8.00
20.00	TiO2	0.62	Ti	0.08	
	Al2O3	11.97	Al^{IV}	1.61	
	FeO	18.14	Al^{VI}	0.68	5.17
	MnO	0.32	Fe	2.46	
	MgO	7.89	Mn	0.04	
	CaO	10.81	Mg	1.91	
	Na2O	1.62	Ca	1.88	2.00
	K2O	0.84	Na^{M4}	0.12	
	Total	91.58	Na^{A}	0.39	
			K	0.17	0.56

		Oxide		Ions	Structure
	SiO2	42.06	Si	6.37	8.00
21.00	TiO2	0.53	Ti	0.06	
	Al2O3	13.85	Al^{IV}	1.63	
	FeO	18.40	Al^{VI}	0.84	5.13
	MnO	0.42	Fe	2.33	
	MgO	8.20	Mn	0.05	
	CaO	11.39	Mg	1.85	
	Na2O	2.01	Ca	1.85	2.00
	K2O	0.68	Na^{M4}	0.15	
	Total	97.54	Na^{A}	0.44	
			K	0.13	0.57

		Oxide		Ions	Structure
	SiO2	43.97	Si	6.51	8.00
22.00	TiO2	0.71	Ti	0.08	
	Al2O3	13.83	Al^{IV}	1.49	
	FeO	15.20	Al^{VI}	0.92	5.04
	MnO	0.26	Fe	1.88	
	MgO	9.62	Mn	0.03	
	CaO	11.98	Mg	2.12	
	Na2O	1.54	Ca	1.90	2.00
	K2O	0.48	Na^{M4}	0.10	
	Total	97.59	Na^{A}	0.34	
			K	0.09	0.43

		Oxide		Ions	Structure
	SiO2	42.72	Si	6.33	8.00
23.00	TiO2	0.81	Ti	0.09	
	Al2O3	14.78	Al^{IV}	1.67	
	FeO	16.16	Al^{VI}	0.91	5.10
	MnO	0.11	Fe	2.00	
	MgO	9.48	Mn	0.01	
	CaO	11.88	Mg	2.09	
	Na2O	1.59	Ca	1.89	2.00
	K2O	0.80	Na^{M4}	0.11	
	Total	98.33	Na^{A}	0.34	
			K	0.15	0.49

		Oxide		Ions	Structure
	SiO_2	43.01	Si	6.38	8.00
24.00	TiO_2	0.85	Ti	0.10	
	Al_2O_3	14.38	Al^{IV}	1.62	
	FeO	15.51	Al^{VI}	0.90	5.07
	MnO	0.23	Fe	1.92	
	MgO	9.60	Mn	0.03	
	CaO	11.96	Mg	2.12	
	Na_2O	1.64	Ca	1.90	2.00
	K_2O	0.65	Na^{M4}	0.10	
	Total	97.84	Na^{A}	0.37	
			K	0.12	0.50

		Oxide		Ions	Structure
	SiO_2	43.32	Si	6.46	8.00
25.00	TiO_2	0.51	Ti	0.06	
	Al_2O_3	13.90	Al^{IV}	1.54	
	FeO	15.14	Al^{VI}	0.91	5.08
	MnO	0.28	Fe	1.89	
	MgO	9.82	Mn	0.04	
	CaO	11.84	Mg	2.18	
	Na_2O	1.56	Ca	1.89	2.00
	K_2O	0.64	Na^{M4}	0.11	
	Total	97.02	Na^{A}	0.35	
			K	0.12	0.47

		Oxide		Ions	Structure
	SiO_2	36.82	Si	6.08	8.00
26.00	TiO_2	0.92	Ti	0.11	
	Al_2O_3	12.35	Al^{IV}	1.92	
	FeO	32.34	Al^{VI}	0.49	5.25
	MnO	0.50	Fe	4.47	
	MgO	0.47	Mn	0.07	
	CaO	10.67	Mg	0.12	
	Na_2O	1.44	Ca	1.89	2.00
	K_2O	2.20	Na^{M4}	0.11	
	Total	97.80	Na^{A}	0.35	
			K	0.46	0.81

Appendix D

$^{40}Ar/^{39}Ar$ analytical data

CA-70B HORNBLENDE ARGON SUMMARY

T°C	mV 39	% 39	AGE (Ma)±1s	% ATM	37/39	36/40	39/40	% IIC
650	5.2	.5	338.8 ± 26.2	43.3	3.31	.001468	.006208	.48
750	4.6	.4	182.3 ± 27.7	54.7	3.36	.001857	.009643	.75
850	5	.5	96.8 ± 17.7	54.3	4.63	.001852	.018738	1.72
900	8.6	.8	120.1 ± 10	33.1	6.58	.001132	.021948	2.05
950	23.4	2.3	116.2 ± 3.4	14.9	7.49	.000519	.028807	2.39
975	69.5	7	119.9 ± 1.4	8.8	7.73	.000309	.029877	2.41
1000	70.9	7.2	122.6 ± 1.3	6.8	7.85	.000245	.029806	2.4
1025	206.1	20.9	131.9 ± .8	2.5	7.25	.000095	.028959	2.09
1050	206.4	21	145 ± .8	1.6	6.91	.000063	.026494	1.85
1075	25.9	2.6	128.1 ± 3.4	7.5	7.57	.000276	.028244	2.23
1100	56.4	5.7	130.4 ± 1.6	5.5	7.5	.000203	.028352	2.18
1125	59.7	6	132.1 ± 1.6	5.8	7.52	.00021	.027905	2.16
1150	25.3	2.5	128.8 ± 3.6	12.6	7.43	.000441	.026583	2.18
1250	84.5	8.6	138.2 ± 1.3	8.7	7.1	.000303	.025846	1.97
1350	59.7	6	137.3 ± 1.9	21.6	7.15	.000735	.022378	2
1450	70.7	7.2	142.7 ± 2.1	33.6	7.04	.001141	.018196	1.91

TOTAL GAS AGE = 135.3 ± 1.1 Ma

J = .00226 ± .0000113 (.5 %)

37/39,36/40 AND 39/40 Ar RATIOS ARE CORRECTED FOR MASS SPECTROMETER DISCRIMINATION,INTERFERING ISOTOPES AND SYSTEM BLANKS

% IIC - INTERFERING ISOTOPES CORRECTION

CA-78A MU ARGON SUMMARY

T°C	mV 39	% 39	AGE (Ma)±1s	% ATM	37/39	36/40	39/40	% IIC
600	9	.4	64.4 ± 8.4	48.4	.01	.001646	.032098	0
650	13.1	.7	70.9 ± 5.7	34.8	0	.001182	.036761	0
700	26.1	1.3	58 ± 3.6	57.8	0	.001959	.029132	0
750	54.1	2.8	61 ± 2.1	51.7	0	.001753	.031617	0
775	283.1	15.1	62.7 ± .4	12.6	0	.000429	.055586	0
800	386.8	20.6	62.2 ± .3	2.7	0	.000091	.062456	0
825	269.6	14.4	62.3 ± .4	1.3	0	.000045	.063258	0
850	197.3	10.5	62.3 ± .4	1.2	0	.000043	.063354	0
875	139	7.4	62.3 ± .5	1.5	0	.000051	.063121	0
900	82.2	4.3	62.7 ± .8	2.2	0	.000077	.062261	0
925	55.9	2.9	63.1 ± 1.1	2.7	0	.000091	.061684	0
950	48.3	2.5	63.1 ± 1.2	3.4	0	.000116	.061244	0
975	45.3	2.4	63.3 ± 1.3	3.5	0	.000119	.060918	0
1000	42.7	2.2	62.1 ± 1.5	6.5	0	.000221	.06026	0
1050	78.2	4.1	62.1 ± .9	5.9	0	.000201	.060541	0
1150	112.4	6	61.9 ± .6	4.9	0	.000167	.061396	0
1250	18	.9	74 ± 4	27.2	.01	.000924	.039243	0
1450	8.9	.4	142.2 ± 15.4	69.6	0	.00236	.008345	0

MEAN AGE(750°C-1150°C)=62.4 ± .4 Ma (2s UNCERTAINTY,INCLUDING ERROR IN J)
J = .002255 ± .0000115 (.5 %)
37/39,36/40 AND 39/40 Ar RATIOS ARE CORRECTED FOR MASS SPECTROMETER DISCRIMINATION,INTERFERING ISOTOPES AND SYSTEM BLANKS
% IIC - INTERFERING ISOTOPES CORRECTION

TJ-79 MUSCOVITE ARGON SUMMARY

T°C	mV 39	% 39	AGE (Ma)±1s	% ATM	37/39	36/40	39/40%	IIC
600	38.7	1.9	105.6 ± 3.6	32.8	.18	.00111	.024994 0	
650	60.4	3	85.3 ± 2	16.5	.12	.00056	.038639	.02
700	96.2	4.7	82.9 ± 1.3	10.1	0	.000342	.04285	.07
750	119.3	5.9	83.2 ± 1	4.1	0	.000141	.045522	.07
800	166.3	8.2	86 ± .7	3 0		.000102	.044525	.07
850	274	13.6	88.8 ± .6	2.3	0	.000079	.043406	.06
875	228.5	11.3	89.1 ± .6	1.4	0	.00005	.043613	.06
900	150.6	7.4	88.5 ± .8	1.2	0	.000043	.044014	.06
925	131.5	6.5	89.4 ± .7	2.4	0	.000081	.043078	.06
950	125.7	6.2	90.8 ± .7	2.1	0	.000073	.042489	.06
975	134.5	6.6	91.7 ± 1.2	30		.00001	.042836	.06
1000	142.6	7	93.8 ± .9	-.2	0	-.000004	.04207	.06
1025	142.4	7	96.3 ± 1	.3	0	.000012	.040745	.06
1050	99.6	4.9	101.1 ± 1.3	.2	0	.000008	.038788	.05
1450	100	4.9 -	-	-	-	-	-	

J = .002245 ± 1.1225E-05 (.5 %)

37/39,36/40 AND 39/40 Ar RATIOS ARE CORRECTED FOR MASS SPECTROMETER DISCRIMINATION,INTERFERING ISOTOPES AND SYSTEM BLANKS

% IIC - INTERFERING ISOTOPES CORRECTION

MG-1B HB ARGON SUMMARY

T°C	mV 39	% 39	AGE (Ma)±1s	% ATM	37/39	36/40	39/40	% IIC
650	84.9	3.4	812.9 ± 3.7	4.1	.3	.000139	.00381	.02
750	128.8	5.3	210.2 ± 1.3	6.7	.31	.000228	.017075	.06
850	82.4	3.3	228.7 ± 1.7	7.1	1.11	.000242	.015539	.21
900	186.8	7.6	298.7 ± 1.5	3.4	2.72	.000116	.012132	.43
950	449.7	18.4	458 ± 2	1	2.98	.000037	.007741	.36
975	454.6	18.6	485.6 ± 2.1	.8	2.82	.000027	.007263	.33
1000	488	20	309.2 ± 1.4	1	2.8	.000035	.011974	.43
1025	300.2	12.3	202.6 ± 1.1	1	2.73	.000037	.018817	.56
1050	90.4	3.7	276.8 ± 1.5	1.3	2.77	.000048	.01345	.46
1075	32.6	1.3	587.5 ± 4.2	1.6	3.41	.000056	.00578	.37
1100	31.7	1.3	582.4 ± 4.2	1.9	3.67	.000067	.005819	.4
1125	12.4	.5	572.1 ± 10.4	3.5	3.22	.000123	.005844	.35
1150	18.5	.7	529.3 ± 6.6	4.3	3.01	.000149	.006345	.34
1175	10.2	.4	476.6 ± 11.2	10.8	2.87	.000367	.006675	.34
1200	5.9	.2	462.8 ± 18.8	22.6	2.85	.000767	.005991	.35
1250	8.8	.3	467.1 ± 13.5	22.2	3.19	.000752	.005958	.39
1300	13.7	.5	466.9 ± 10.4	17.4	3.14	.000592	.006321	.38
1350	10.8	.4	442.2 ± 12.4	26	3.35	.000881	.006029	.42
1450	20.4	.8	421 ± 7.1	32.5	3.32	.001102	.005805	.43

TOTAL GAS AGE = 384.1 ± 2.2 Ma

J = .002263 ± 1.1315E-05 (.5 %)

37/39,36/40 AND 39/40 Ar RATIOS ARE CORRECTED FOR MASS SPECTROMETER DISCRIMINATION,INTERFERING ISOTOPES AND SYSTEM BLANKS

% IIC - INTERFERING ISOTOPES CORRECTION

MG-5 HB ARGON SUMMARY

T°C	mV 39	% 39	AGE (Ma)±1s	% ATM	37/39	36/40	39/40	% IIC
650	38.8	2.4	496.6 ± 4.56	.7	4	.000203	.006728	.08
750	563.5	2	59.9 ± 2	6.5	1.24	.000222	.013678	.21
850	64.7	41	50.2 ± 1.6	7.7	1.66	.000265	.024076	.43
900	487.8	30.4	241.9 ± 1.1	1.1	2.05	.00004	.015615	.37
950	664.2	41.5	161.5 ± .7	.8	2.03	.000031	.023989	.5
975	55.5	3.4	151 ± 1.6	3.3	1.91	.000118	.025081	.49
1000	41.1	2.5	163 ± 2.2	3.8	1.98	.000136	.023038	.48
1025	54	3.3	190.8 ± 1.7	2.2	1.98	.000081	.01985	.43
1050	47.8	2.9	208.8 ± 2.3	2.5	1.92	.000089	.018006	.39
1075	30.3	1.8	261.9 ± 4.5	3.2	1.85	.000114	.014037	.32
1100	11.9	.7	232.6 ± 6.7	9.1	1.53	.000311	.014992	.28
1125	6.4	.4	233.6 ± 13.9	10.5	1.27	.000361	.014707	.24
1150	6.4	.4	215.7 ± 14.4	15.9	1.34	.000544	.015035	.26
1175	5	.3	210.2 ± 17.1	23.5	1.7	.000802	.014066	.34
1250	2.3	.1	213.2 ± 405	31.3	1	.001804	.008528	.26
1350	27	1.6	200.2 ± 4.2	23.5	1.94	.000799	.014772	.4

TOTAL GAS AGE = 204.1 ± 1.4 Ma

J = .002269 ± 1.1345E-05 (.5 %)

37/39,36/40 AND 39/40 Ar RATIOS ARE CORRECTED FOR MASS SPECTROMETER DISCRIMINATION,INTERFERING ISOTOPES AND SYSTEM BLANKS

% IIC - INTERFERING ISOTOPES CORRECTION

MG-16 MU ARGON SUMMARY

T°C	mV 39	% 39	AGE (Ma)±1s	% ATM	37/39	36/40	39/40	% IIC
600	27.3	1.1	81.3 ± 2.4	19.7	.02	.00067	.042135	.01
650	37.4	1.6	67.4 ± 1.7	22.3	.01	.000758	.049338	0
700	55.1	2.4	62.7 ± 1.5	40.2	.01	.001362	.040869	0
750	82.1	3.5	62.8 ± .9	21.2	0	.00072	.053763	0
775	85.5	3.7	62.4 ± .8	17.6	0	.000596	.056615	0
800	182.1	7.9	60.8 ± .4	7.1	0	.000241	.0655	0
825	269.6	11.7	59.7 ± .3	2.7	0	.000092	.069912	0
850	305.8	13.3	59.1 ± .3	1.4	0	.00005	.071548	0
875	247.3	10.7	59.1 ± .3	1.4	.01	.000048	.071567	0
900	173.7	7.5	59.6 ± .4	1.5	.01	.000051	.070856	.01
925	143	6.2	62 ± .5	2	.03	.000069	.067781	.02
950	130	5.6	61.6 ± .5	1.9	.06	.000066	.068289	.04
975	138.3	6	58.9 ± .4	1.7	.02	.000058	.071666	.01
1000	145.4	6.3	58.2 ± .4	.9	0	.000032	.073024	0
1050	209.4	9.1	58.8 ± .4	.4	.02	.000016	.072619	.01
1150	53.5	2.3	74.8 ± 1	3.6	.19	.000126	.05506	.09
1250	5.8 .	2	345.9 ± 16.1	23.5	1.46	.000797	.008765	.22
1450	2	0	1114 ± 84.1	51.7	3.77	.001751	.001367	.32

MEAN AGE(800°C-1050°C)= 59.7 ± .4 Ma (2s UNCERTAINTY,INCLUDING ERROR IN J)

J = .00242 ± .0000121 (.5 %)

37/39,36/40 AND 39/40 Ar RATIOS ARE CORRECTED FOR MASS SPECTROMETER DISCRIMINATION,INTERFERING ISOTOPES AND SYSTEM BLANKS

% IIC - INTERFERING ISOTOPES CORRECTION

MG-65 MUSCOVITE ARGON SUMMARY

T°C	mV 39	% 39	AGE (Ma)±1s	% ATM	37/39	36/40	39/40	% IIC
600	8.9	.4	81.5 ± 16.5	87.4	.06	.002961	.006103	.02
650	19.9	.9	68.8 ± 5.6	77.8	.02	.002636	.012816	.01
700	38.6	1.7	60.2 ± 2.9	70.5	.01	.002387	.019543	0
750	74.9	3.3	66.7 ± 1	34.2	0	.001158	.039335	0
775	112.7	5	65.8 ± .6	22.2	0	.000752	.047106	0
800	175.3	7.9	64.1 ± .4	12.3	0	.000418	.05453	0
825	253.7	11.4	63.3 ± .6	8	0	.000272	.057949	0
850	266.4	12	62 ± .3	5.2	0	.000177	.061043	0
875	240.2	10.8	61.8 ± .3	4.8	0	.000163	.061474	0
900	168.2	7.6	62.2 ± .4	6.2	0	.00021	.060163	0
950	245.4	11	62.6 ± .3	7.3	.01	.000249	.059094	0
1000	290.9	13.1	62.3 ± .3	5.9	0	.000201	.060255	0
1050	264.7	11.9	62 ± .3	3.5	0	.00012	.062092	0
1100	35	1.5	73.3 ± 1.2	10.2	.05	.000348	.048768	.02
1250	14.6	.6	98.7 ± 4	41.2	.5	.001398	.023528	.18
1450	1.9	0	93.1 ± 124	95.6	3.7	.003238	.001859	1.42

MEAN AGE(850°C-1050°C)= 62.1 ± .4 Ma (2s UNCERTAINTY,INCLUDING ERROR IN J)

J = .002253 ± .0000115 (.5 %)
37/39,36/40 AND 39/40 Ar RATIOS ARE CORRECTED FOR MASS SPECTROMETER DISCRIMINATION,INTERFERING ISOTOPES AND SYSTEM BLANKS
% IIC - INTERFERING ISOTOPES CORRECTION

RM-52 HB ARGON SUMMARY

T°C	mV 39	% 39	AGE (Ma)±1s	% ATM	37/39	36/40	39/40	% IIC
650	38.9	2.9	1079.9 ± 6.2	3.4	.65	.000117	.002637	.05
750	50.5	3.8	503.7 ±3.1	6.3	.67	.000216	.006509	.07
850	39.1	2.9	486.2 ±3.5	5.3	1.76	.000182	.006851	.21
900	56.4	4.2	411.3 ±2.7	3.6	3.8	.000123	.008427	.49
950	181.5	13.6	510.4 ±2.3	1.2	5.31	.000043	.00676	.61
975	209.3	15.7	641.4 ±2.8	15.6	1	.000036	.005188	.58
1000	224.1	16.9	605 ± 2.6	1.15	.61	.000038	.005557	.6
1025	138.3	10.4	362.9 ±1.8	1.1	5.44	.000042	.009922	.76
1050	77.5	5.8	288.4 ±1.8	1.1	5.28	.000043	.012752	.85
1075	45.8	3.4	421.8 ±2.9	15.7	6	.000041	.0084	.74
1100	49.8	3.7	532 ± 3.2	1.3	6.13	.000049	.006435	.7
1125	34.3	2.5	680.4 ±4.8	1.7	6.12	.000062	.004798	.62
1150	21.9	1.6	636.3 ±5.7	3.3	6.1	.000115	.005116	.63
1175	13.1	.9	622.4 ±8.6	8.4	6.2	.000286	.004978	.65
1200	11.6	.8	580.4 ±10.5	11.6	6.08	.000395	.005213	.66
1250	12.3	.9	603.2 ±11.3	15.1	6.13	.000512	.004789	.65
1300	32.4	2.4	517.6 ±4.2	8.9	5.77	.000302	.006138	.66
1350	29.6	2.2	498 ± 4.3	11.5	5.77	.00039	.006232	.68
1450	58	4.3	505.9 ±3.4	14.9	5.7	.000506	.005883	.66

TOTAL GAS AGE = 542.6 ± 2.9 Ma

J = .00224 ± .0000112 (.5 %)

37/39,36/40 AND 39/40 Ar RATIOS ARE CORRECTED FOR MASS SPECTROMETER DISCRIMINATION,INTERFERING ISOTOPES AND SYSTEM BLANKS

% IIC - INTERFERING ISOTOPES CORRECTION

RM-26 MU ARGON SUMMARY

T°C	mV 39	% 39	AGE (Ma)±1s	% ATM	37/39	36/40	39/40	% IIC
600	40.8	1.4	114.6 ± 2.4	11.6	.07	.000394	.030287	.0
650	62.6	2.1	76.2 ± 1.3	5.9	.06	.0002	.04904	.02
700	98.2	3.3	64.6 ± .9	7.1	.01	.000243	.057185	0
750	145.4	4.9	68.4 ± .6	4.4	0	.000149	.055563	0
775	155.8	5.3	70.6 ± .6	2.7	0	.000094	.054743	0
800	260.8	8.9	68.1 ± .4	2.4	0	.000084	.056941	0
825	338	11.6	65.9 ± .4	2.3	0	.000081	.058874	0
850	327.7	11.2	64.9 ± .4	1.7	0	.00006	.060172	0
875	331.5	11.3	65.4 ± .4	1.6	0	.000055	.059861	0
900	263.8	9	66.7 ± .4	1.9	0	.000067	.058415	0
925	218.9	7.5	69.2 ± .5	1.9	.01	.000067	.056324	0
950	197	6.7	73.5 ± .5	1.7	.01	.000059	.053034	0
975	187.4	6.4	78.7 ± .5	1.3	0	.000046	.049686	0
1000	14	6.4	85.6 ± .6	.3	0	.000012	.046086	0
1050	96.1	3.3	109.2 ± .9	0.02		.000001	.035995	0
1150	22.7	.7	407.6 ± 4.3	.9	.25	.000033	.008777	.03
1250	13.4		477.8 ± 7.4	5.4	.16	.000185	.007006	.01
1450	4.6	.1	1110.9 ± 48	29.6	.21	.001004	.001857	.01

MEAN AGE(825°C-875°C)= 65.4 ± .5 Ma (2s UNCERTAINTY,INCLUDING ERROR IN J)

J = .002247 ± .0000112 (.4 %)

37/39,36/40 AND 39/40 Ar RATIOS ARE CORRECTED FOR MASS SPECTROMETER DISCRIMINATION,INTERFERING ISOTOPES AND SYSTEM BLANKS

% IIC - INTERFERING ISOTOPES CORRECTION

RM-42 MUSCOVITE ARGON SUMMARY

T°C	mV 39	% 39	AGE (Ma)±1s	% ATM	37/39	36/40	39/40	% IIC
600	26. 1	1	74.8 ± 1.8	5.3	0	.00018	.050435	.08
650	64.7	2.7	70.5 ± .8	3.8	0	.000129	.054407	.08
700	142.1	6	66.5 ± .5	7.5	0	.000254	.055499	.09
750	278	11.7	64.9 ± .3	1.5	0	.000052	.060563	.09
800	481.8	20.3	65.4 ± .3	1.3	0	.000044	.060164	.09
825	378.9	16	65.3 ± .3	1.6	0	.000056	.060115	.09
850	283.7	12	65.8 ± .3	1.3	0	.000044	.059808	.09
875	169.6	7.1	67.1 ± .4	1.8	.01	.000061	.058352	.08
900	91.3	3.8	69.1 ± .6	2.5	.02	.000085	.056256	.07
925	59.2	2.5	70.8 ± .8	2.3	.01	.000078	.055014	.07
950	55	2.3	68.7 ± .9	2.9	.01	.0001	.056342	.08
1000	60.7	2.5	69.6 ± .8	.4	.01	.000016	.05698	.08
1025	81.1	3.4	67.8 ± .6	.9	.01	.000032	.058248	.08
1050	87.7	3.7	67.8 ± .6	1.4	.01	.00005	.057976	.08
1075	35.6	1.5	71.3 ± 1.3	3.1	.02	.000107	.054138	.07
1100	6.8	.2	97 ± 7.1	14.8	.15	.000504	.034896	0
1150	2.8	.1	140.3 ± 23	49.7	.66	.00169	.014069	.13
1250	.8	0	795.7 ± 231	63.7	5.02	.00216	.001478	.47
1450	.5	0	2653.9 ± 456	59.7	2.81	.002023	.00027	.19

MEAN AGE(750°C-825°C)= 65.2 ± .5 Ma (2s UNCERTAINTY,INCLUDING ERROR IN J)

J = .002256 ± .0000115 (.5 %)
37/39,36/40 AND 39/40 Ar RATIOS ARE CORRECTED FOR MASS SPECTROMETER DISCRIMINATION,INTERFERING ISOTOPES AND SYSTEM BLANKS
% IIC - INTERFERING ISOTOPES CORRECTION

RM-43 MUSCOVITE ARGON SUMMARY

T°C	mV 39	% 39	AGE (Ma)±1s	% ATM	37/39	36/40	39/40	% IIC
600	10.9	.5	87.9 ± 10.2	65.6	.01	.002224	.015487	0
650	22.7	1.1	64 ± 6.1	74.5	0	.002525	.01581	0
700	41	2	68.8 ±3.1	61.3	0	.002077	.022337	0
750	83.9	4.1	66.8 ±1.4	41.1	0	.001394	.035013	0
775	116.1	5.7	63.9 ± .8	23.6	0	.0008	.047563	0
800	188.5	9.3	62.3 ± .5	13.6	0	.000461	.055193	0
825	254.4	12.5	60.9 ± .4	7.5	0	.000254	.060522	0
850	271.9	13.4	60.2 ± .4	4.5	0	.000153	.063231	0
875	267.4	13.1	60.1 ± .4	4.1	0	.000139	.063555	0
900	170.1	8.3	60.5 ± .5	4.6	0	.000156	.06283	0
925	123.4	6	60.6 ± .6	6.2	0	.000211	.061641	0
950	116.3	5.7	60.6 ± .6	5.9	0	.0002	.06189	0
975	115.3	5.6	60.2 ± .6	4.2	0	.000144	.063362	0
1000	100.4	4.9	60 ± .6	1.3	0	.000047	.065509	0
1050	89.5	4.4	60 ± .6	1.1	0	.000039	.065648	0
1150	38.8	1.9	60.6 ±1.7	12	0	.00041	.057903	0
1250	14.2	.7	64.5 ±5.5	45.2	0	.001534	.0339	0
1450	1.8	0	117.2 ± 1	45	94.20	.003193	.001929	0

MEAN AGE(850°C-1150°C)= 60.3 ± .4 Ma (2s UNCERTAINTY,INCLUDING ERROR IN J)

J = .002248 ± .0000112 (.4 %)
37/39,36/40 AND 39/40 Ar RATIOS ARE CORRECTED FOR MASS SPECTROMETER DISCRIMINATION,INTERFERING ISOTOPES AND SYSTEM BLANKS
% IIC - INTERFERING ISOTOPES CORRECTION

RM-55 MU ARGON SUMMARY

T°C	mV 39	% 39	AGE (Ma)±1s	% ATM	37/39	36/40	39/40	% IIC
600	20.1	.8	88.1 ± 3	9.3	0	.000317	.040793	0
650	42.8	1.8	69.2 ± 1.5	9.3	0	.000315	.052149	0
700	82.6	3.4	63.8 ± .8	6.5	0	.000222	.058356	0
750	125.7	5.2	62 ± .6	5.2	0	.000176	.060949	0
775	111.3	4.6	63.3 ± .6	3.7	0	.000127	.060579	0
800	164.8	6.9	63.2 ± .5	2.6	0	.000088	.061431	0
825	260	10.9	61.3 ± .3	1.1	0	.000039	.064229	0
850	264.7	11.1	60.6 ± .3	.4	0	.000015	.065514	0
875	220.5	9.2	61.1 ± .3	.2	0	.000008	.065031	0
900	157.1	6.6	62.4 ± .4	.3	0	.000012	.063659	0
925	127.8	5.3	63.8 ± .5	.6	0	.000021	.062094	0
950	118.6	4.9	64.6 ± .5	.4	0	.000014	.061439	0
975	126.5	5.3	64.5 ± .5	.6	0	.000022	.061379	0
1000	137.3	5.7	63.4 ± .5	.5	0	.00002	.062509	0
1050	220.2	9.2	61.7 ± .4	.3	0	.000013	.064329	0
1150	188.5	7.9	67.1 ± .5	1.1	.02	.000039	.058584	.01
1250	2.9	.1	1042.5 ± 33.3	10.3	2.32	.000349	.00258	.2
1450	.9	0	3370.1 ± 116	24.7	10.21	.000837	.000309	.69

MEAN AGE(825°C-875°C)= 61 ± .5 Ma (2s UNCERTAINTY,INCLUDING ERROR IN J)

J = .002249 ± .0000112 (.4 %)
37/39,36/40 AND 39/40 Ar RATIOS ARE CORRECTED FOR MASS SPECTROMETER DISCRIMINATION,INTERFERING ISOTOPES AND SYSTEM BLANKS
% IIC - INTERFERING ISOTOPES CORRECTION

References

Archibald, D. A., Glover, J. K., Price, R. A., Farrar, E., and Carmichael, D. M., 1983. Geochronology and tectonic implications of magmatism and metamorphism, southern Kootenay Arc and neighboring regions, southeastern British Columbia. Part I: Jurassic to Mid-Cretaceous. Canadian Journal of Earth Sciences, **20**: 1891-1913.

Archibald, D. A., Krough, T. E., Armstrong, R. L., Farrar, E., 1984. Geochronology and tectonic implications of magmatism and metamorphism, southern Kootenay Arc and neighboring regions, southeastern British Columbia. Part II: Mid-Cretaceous to Eocene. Canadian Journal of Earth Sciences, **21**: 567-583.

Armstrong, R. L., Taubeneck, W. H., Hales, P. Q., 1977. Rb/Sr and K-Ar geochronomtery of Mesozoic granitic rocks and their Sr isotopic composition, Oregon Washington, and Idaho. Geological Society of America Bulletin, **88**: 397-411.

Armstrong, R. L., 1982. Cordilleran metamorphic core complexes - From Arizona to southern Canada: Annual Review of Earth and Planetary Sciences, **10**: 129-154.

Bally, A. W., Gordy, P. L., Stewart, G. A., 1966. Structure, seismic data, and orogenic evolution of southern Canadian Rocky Mountains. Bull. Can. Pet. Geol., **14**: 337-381.

Bardoux, M., Mareschal, J. C., 1994. Extension in south-central British Columbia: mechanical and thermal controls. Tectonophysics, **238**: 451-470.

Brown, R. L., Carr, S. D., Johnson, B. J., Coleman, V. J., Cook, F. A., Varsek, J. L., 1992. The Monashee decollement of the southern Canadian Cordillera: a crustal-scale shear zone linking the Rocky Mountain Foreland Belt to lower crust beneath accreted terranes. *In* McClay, K. R. (Ed), Thrust Tectonics. Chapman and Hall, London, 357-364.

Brown, R. L., Journeay, M. J., 1987. Tectonic denudation of the Shuswap metamorphic terrane of southeastern British Columbia. Geology, **15**: 142-146.

Brown, R. L., Journeay, M. J., Lane, L. S., Murphy, D. C., and Rees C. J., 1986. Obduction, backfolding and piggyback thrusting in the metamorphic hinterland of the southeastern Canadian Cordillera. Journal of Structural Geology, **8**, nos. 3/4: 255-268.

Brown, R. L., McDonough, M. R., Crowley, J. L., Johnson, B. J., Mountjoy, E. W., Simony, P. S., 1993. Cordilleran Transect, Rocky Mountain Foreland and Omineca Hinterland, southeastern British Columbia. Geological Association of Canada, Mineralogical Association of Canada, Joint Annual Meeting, Field Trip B-9, Guidebook: 60.

Brown, R. L., McNicoll, V. J., Parrish, R. R., and Scammell, R., 1992. Middle Jurassic plutonism in the Kootenay terrane, northern Selkirk Mountains, British Columbia. *In* Radiogenic age and isotopic studies: Report 5. Geological Survey of Canada, Paper 91-2: 135-141.

Brown, R.L., Read, P.B., 1983. Shuswap terrane of British Columbia: A Mesozoic "core complex": Geology, **11**, pp. 164-168.

Campbell, R. B., 1968. Geology of the Canoe River, British Columbia. Geological Survey of Canada, Map 15-1967.

Carr, S. D., 1989. Implications of Early Eocene Ladybird granite in the Thor-Odin/Pinnacles area, southern British Columbia. Papers of the Geological Survey of Canada, **89-1E**: 69-77.

_____ 1990. Late Cretaceous - early Tertiary tectonic evolution of the southern Omineca Belt, Canadian Cordillera [Ph.D. thesis]: Ottawa, Ontario, Carleton University, 220.

_____ 1992. Tectonic setting and U-Pb geochronology of the early Tertiary Ladybird leucogranite suite, Thor-Odin - Pinnacles area, southern Omineca Belt, British Columbia. Tectonics, **11**: 258-278.

_____ 1995. The southern Omineca belt, British Columbia: new perspectives from the LITHOPROBE Geoscience Program. Canadian Journal of Earth Sciences, **32**: 1720-1739.

Carr, S. D., Brown, R. L., 1990. Southern Cordillera LITHOPROBE lines 6 to 10: Crustal structure and tectonic chronology, presented at Project LITHOPROBE Southern Canadian Cordillera Transect Workshop, University of Calgary, Calgary, Alberta, March 3-4.

Chamberlain, V. E., Lambert, R. St J., Holland, J. G., 1980. The Malton Gneiss: Archean gneisses in British Columbia. Precambrian Research, **11**: 297-306.

Cliff, R. A., 1985. Isotopic dating in metamorphic belts. The Journal of the Geological Society of London, **142**: 97-110.

Clowes, R. M., Brandon, M., Green, A. G., Yorath, C., J., Sutherland Brown, A., Kanasewich, E. R., Spencer, C. S., 1987. LITHOPROBE southern Vancouver Island: Cenozoic subduction complex image by deep seismic reflections. Canadian Journal of Earth Sciences, **24**: 31-51.

Colpron, M., 1996. $^{40}Ar/^{39}Ar$ thermochronology along the western flank of the Selkirk fan structure, SE British Columbia. *In* LITHOPROBE Slave - Northern Cordillera Lithospheric Evolution (SNORCLE) and Cordilleran Tectonics Workshop. University of Calgary, Calgary, Alberta. *Compiled by* Cook, F., Erdmer, P., LITHOPROBE Report 50: 182-183.

Coney, P. J., 1979. Tertiary evolution of Cordilleran metamorphic core complexes. *In* Armentrout, J. M., Cole, M. R., Terbest, H, Jr. (Ed), Cenozoic paleogeography of western United States. Society of Economic Paleontologists and Mineralogists, Pacific Section, Pacific Coast Paleogeography Symposium 3: 15-28.

Coney, P. J., and Harms, Tekla A., 1984. Cordilleran metamorphic core complexes: Cenozoic extensional relics of Mesozoic compression. Geology, **12**: 550-554.

Cook, F. A., 1995. The reflection Moho beneath the southern Canadian Cordillera. Canadian Journal of Earth Sciences, **32**: 1520-1530.

Cook, F. A., Green, A. G., Simony, P. S., Price, R. A., Parrish, R. R., Milkereit, B., Gordy, P. L., Brown, R. L., Coflin, K. C., Patenaude, C., 1988. LITHOPROBE seismic reflection structure of the southeastern Canadian Cordillera: Initial results. Tectonics, **7**: 157-180.

Cook, F. A., Varsek, J. L., Clowes, R. M., Kanasewich, E. R., Spencer, C. S., Parrish, R. R., Brown, R. L., Carr, S. D., Johnson, B. J., Price, R. A., 1992. LITHOPROBE crustal reflection cross section of the southern Canadian Cordillera, 1, foreland thrust and fold belt to Fraser River fault. Tectonics, **11**, no. 1: 12-35.

Crowley, J. L., Parrish, R. R., 1999. U-Pb isotopic constraints on diachronous metamorphism in the northern Monashee complex, southern Canadian Cordillera. Journal of Metamorphic Geology, **17**: 483-502.

Currie, L. D., 1988. Geology of the Allen Creek area, Cariboo Mountains, British Columbia [M.Sc. thesis]: Calgary, Alberta, The University of Calgary.

Digel, Scott G., Ghent, Edward D., Carr, Sharon D., and Simony, Philip S., 1998. Early Cretaceous kyanite-sillimanite metamorphism and Paleocene sillimanite overprint near Mount Cheadle, southeastern British Columbia:

geometry, geochronology, and metamorphic implications. Canadian Journal of Earth Sciences, **35**: 1070-1087.

Dodson, M. H., 1973. Closure temperature in cooling geochronological and petrologic system. Contributions to Minearlogy and Petrology, **40**: 259-274.

Engebretson, D. C., Cox, A., Gordon, R. G., 1985. Relative motions between oceanic and continental plates in the Pacific basin. Geological Society of America, **206**: 59.

England, P., 1982. Some numerical investigations of large scale continental deformation. *In* Hsu, K. J. (Ed), Mountain building processes: New York, Academic Press, 129-139.

Gabrielse, H., 1985. Major dextral transcurrent displacements along the Northern Rocky Mountain Trench and related lineaments in north-central British Columbia. Geological society of America Bulletin, **96**: 1-14.

Gerasimoff, M. D., 1988. The Hobson Lake pluton, Cariboo Mountains, and its significance to Mesozoic and Early Tertiary Cordilleran tectonics [M.Sc. Thesis]: Kingston, Ontario, Queen's University.

Ghent, E. D., Knittler, C. C., Raeside, R. P., Stout, M. Z., 1982. Geothermometry and geobarometry of pelitic rocks, upper kyanite and sillimanite zones, Mica Creek, British Columbia. Canadian Mineralogist, **20**: 295-305.

Gibson, H. D., Brown, R. L., Parrish, R. R., 1999. Deformation-induced inverted metamorphic field gradients: an example from the southeastern Canadian Cordillera. Journal of Structural Geology, **21**: 751-767.

Hanmer, S., Passchier, C., 1991. Shear-sense indicators: a review. Geological Survey of Canada, Paper 90-17: 72.

Harrison, T. M., McDougall, I., 1982. The thermal significance of potassium feldspar K-Ar ages inferred from $^{40}Ar/^{39}Ar$ age spectrum results. Geochim. Cosmochim. Acta, **46**: 1811-1820.

Heizler, M. T., Lux, D. R., Decker, E. R., 1988. The age and cooling history of the Chain of Ponds and Big Island Pond plutons and the Spider Lake granite, west-central Main and Quebec. American Journal of Science, **288**: 925-952.

Johnson, B. J., Brown, R. L., 1996. Crustal Structure and early Tertiary extensional tectonics of the Omineca belt at 51^{0}N latitude, southern

Canadian Cordillera. Canadian Journal of Earth Sciences, **33**: 1596-1611.

Journeay, J. M., 1985. Thermal-tectonic evolution of the Monashee complex: A basement duplex, Omineca belt, British Columbia: Geological Society of America, Abstracts with Programs, **17**, 364.

_____ 1986. Stratigraphy, internal strain and thermo-tectonic evolution of northern Frenchman Cap dome: An exhumed duplex structure, Omineca hinterland, S.E. Canadian Cordillera [Ph.D. thesis]: Kingston, Ontario, Queen's University, 350.

Leake, B. E., Woolley, A. R., Arps, C. E. S., Birch, W. D., Gilbert, M. C., Grice, J. D., Hawthorne, F. C., Kato, A., Kisch, H. J., Krivovichev, V. G., Linthout, K., Laird, J., Mandarino, J. A., Maresch, W. V., Nickel, E. H., Rock, N. M. S., Schumacher, J. C., Smith, D. C., Stephenson, N. C. N., Ungaretti, L., Whittaker, E. J. W., Youzhi, G., 1997. Nomenclature of amphiboles: Report of the Subcommittee on Amphiboles of the International Mineralogical Association, Commission on New Minerals and Mineral Names. American Mineralogist, **82**: 1019-1037.

Lister, G. S., Baldwin, S. L., 1996. Modelling the effect of arbitrary P-T-t histories on argon diffusion in minerals using the MacArgon program for the Apple Macintosh. Tectonophysics, **253**: 83-109.

Mathews, W. H., 1981. Early Cenozoic resetting of potassium-argon dates and geothermal history of north Okanagan area, British Columbia. Canadian Journal of Earth Sciences, **18**, 1310-1319.

McDonough, M. R., 1984. Structural evolution and metamorphism of basement gneisses and Hadrynian cover, Bulldog Creek area, British Columbia [M.Sc. thesis]: Calgary, Alberta, The University of Calgary.

McDonough, M. R., Morrison, M. L., 1990. Ptarmigan Creek West-half, British Columbia (83D/10), Geological Survey of Canada, Open File Report, 1:50 000 scale.

McDonough, M. R., Morrison, M. L., Currie, L. D., Walker, R. T., Pell, J., Murphy, D. C., 1991[a]. Canoe Mountain, British Columbia (83D/11), Geological Survey of Canada, 1:50 000 scale.

McDonough, M. R., Mountjoy, E. W., 1990. Lucerne West-half, British Columbia (83D/15), Geological Survey of Canada, Open File Report, 1:50 000 scale.

McDonough, M. R., Murphy, D. C., 1994. Geology and structure cross-sections, Valemount, British Columbia; Geological Survey of Canada, Map 1843A, 1:50 000 scale.

McDonough, M. R., Parrish, R. R., 1991. Proterozoic gneisses of the Malton Complex, near Valemount, British Columbia: U-Pb ages and Nd isotopic signatures. Canadian Journal of Earth Sciences, **28**: 1202-1216.

McDonough, M. R., Simony, P. S., 1988. Structural evolution of the basement gneisses and Hadrynian cover, Bulldog Creek area, Rocky Mountains, British Columbia. Canadian Journal of Earth Sciences, **25**: 1687-1702.

_____ 1989. Valemount strain zone: A dextral oblique-slip thrust system linking the Rocky Mountain and Omineca belts of the southeastern Canadian Cordillera. Geology, **17**: 237-240.

McDonough, M. R., Simony, P. S., Morrison, M. L., Oke, C., Sevigny, J. H., Robbins, D. B., Digel, S. G., Grasby, S. E., 1991[b]. Howard Creek, British Columbia (83D/7). Geological Survey of Canada, Open File Report, 1:50 000 scale.

McDonough, M. R., Stockmal, G. S., Issler, D. R., Grist, A. M., Zentilli, M., and Archibald, D. A., 1995. Apatite Fission Track and ^{40}Ar-^{39}Ar Analysis of the External Zone of the Canadian Rockies Near Jasper, Alberta: Implications for Thermal Maturity. Oil and Gas Forum Proceedings, GSC Open File 3058: 83-88.

McDougall, I., Harrison, T. M., 1988. Geochronology and Thermochronology by the $^{40}Ar/^{39}Ar$ Method. Oxford Monographs on Geology and Geophysics No. 9, Oxford University Press, New York.

Merrihue, C., Turner, G., 1966. Potassium-Argon Dating by Activation with Fast Neutrons. *In* Harper, C. T. (Ed), Geochronology : Radiometric Dating of Rocks and Minerals. Benchmark Papers in Geology: 396-401.

Molnar, P., Chen, Weng-Ping, 1983. Focal depths and fault plane solutions of earthquakes under the Tibetan Plateau. Journal of Geophysical Research, **88**: 1180-1196.

Monger, J. W. H., 1993. Canadian Cordilleran tectonics: From geosynclines to crustal collage. Canadian Journal of Earth Sciences, **30**: 209-231.

Monger, J. W. H., Price, R. A., and Tempelman-Kluit, D. J., 1982. Tectonic accretion and the origin of the two major metamorphic and plutonic welts in the Canadian Cordillera. Geology, **10**: 70-75.

Morrison, M. L., 1979. Structure and petrology of the southern portion of the Malton Gneiss, British Columbia. *In* Current research, part B. Geological Survey of Canada, Paper 79B-1: 407-410.

Mortensen, J. K., Montgomery, J. R., Fillipone, J., 1987. U-Pb zircon, monazite, and sphene ages for granitic orthogneiss of the Barkerville terrane, east-central British Columbia. Canadian Journal of Earth Sciences, **24**: 1261-1266.

Murphy, D. C., McDonough, M. R., 1990. Sub-Windermere and older unconformities on crystalline basement, Cariboo Mountains, and depositional setting of the Late Proterozoic middle Miette Group, Rocky Mountains, British Columbia. *In* Aitken, J. D., McDonough, M. R. (Ed): Later Proterozoic Glaciation, Rifting and Eustasy, as Illustrated by the Windermere Supergroup. Geological Association of Canada, Nuna Research Conference, Fieldtrip Guidebook: 10.1-10.27.

Parrish, R. R., Armstrong, R. L., 1983. U-Pb zircon age and tectonic significance of gneisses in structural culminations of the Omineca Crystalline Belt, British Columbia. Geological Society of America, Abstracts with Programs, **15**: 324.

_____ 1987. The *ca.* 162 Ma Galena Bay stock and its relationship to the Columbia River fault zone, southeast British Columbia. *In* Radiogenic age and isotopic studies: Report 1. Geological Survey of Canada, Paper 87-2: 25-32.

Parrish, R. R., Carr, S. D., Parkinson, D. L., 1988. Eocene extensional tectonics and geochronology of the southern Omineca belt, British Columbia and Washington. Tectonics, **7**, no. 2: 181-212.

Pell, J., Simony, P. S., 1987. New correlations of Hadrynian strata, south-central British Columbia. Canadian Journal of Earth Sciences, **24**: 302-313.

Pigage, L. C., 1977. Rb-Sr dates for granodiorite intrusions in the northeastern margin of the Shuswap metamorphic complex, Cariboo Mountains, British Columbia. Canadian Journal of Earth Sciences, **14**: 1690-1695.

Price, R. A., Monger, J. H., Roddick, J. A., 1985. Cordilleran cross section, Calgary to Vancouver. *In* Tempelman-Kluit (Ed), Field Guides to Geology and Mineral Deposits in the Southern Canadian Cordillera. Geological Society of America Cordilleran Section, Boulder, Colorado: 3-1 to 3-85.

Price, R. A., Carmichael, D. M., 1986. Geometric test for Late Cretaceous-Paleogene intracontinental transform faulting in the Canadian Cordillera.

Geology, **14**: 468-471.

Price, R. A., Mountjoy, E. W., 1970. Geological structure of the Canadian Rocky Mountains between Bow and Athabasca rivers - a progress report. *In* Wheeler, J. O. (Ed), Structure of the southern Canadian Cordillera. The Geological Association of Canada, Special Paper Number 6.

Reynolds, P. H., 1992. Low Temperature Thermochronology the the $^{40}Ar/^{39}Ar$ Method. *In* Zentilli, M., Reynolds, P. H., (Ed), Short Course Handbook on Low Temperature Thermochronology. Mineralogical Association of Canada: 3-19.

Ross, G. M., 1991. Tectonic setting of the Windermere grit system. Geology, **19**: 1125-1128.

Samson, S. D., Alexander, E. C. Jr., 1987. Calibration of the interlaboratory ^{40}Ar-^{39}Ar dating standard, Mmhb-1. Chemical Geology (Isotopic Geology Section), **66**: 27-34.

Scammell, R. J., 1991. Structure and U-Pb geochronology of the southern Scrip Range, southern Omineca belt, British Columbia: a progress report. LITHOPROBE Southern Canadian Cordillera Transect Report: 85-96.

_____ 1992. Composite deformation, intradeformational leucogranite magmatism and thermal history, northern Monashee Mountains, Omineca belt, B.C. LITHOPROBE Southern Canadian Cordillera Transect Report 24: 5-11.

_____ 1993. Mid Cretaceous - Tertiary thermotectonic history of former mid-crustal rocks, southern Omineca Belt, Canadian Cordillera [Ph.D thesis]: Kingston, Ontario, Queen's University.

Schaeffer, O. A., 1982. Laser Microporbe Argon-39-Argon-40 Dating of Individual Mineral Grains. *In* Comstock, M. J. (Ed), Nuclear and Chemical Dating Techniques: Interpreting the Environmental Record. ACS Symposium Series: 139-148.

Sevigny, J. H., 1988. Geochemistry of Later Proterozoic amphibolites and ultramafic rocks, southeastern Canadian Cordillera. Canadian Journal of Earth Sciences, **25**: 1323-1327.

Sevigny, J. H., Ghent, E. D., 1989. Pressure, temperature and fluid composition during amphibolite facies metamorphism of graphic metapelites, Howard Ridge, British Columbia. Journal of Metamorphic Geology, **7**: 497-505.

Sevigny, J. H., Parrish, R. R., Ghent, E. D., 1988. Petrogenesis of peraluminous granites, Monashee Mountains, southeastern Canadian Cordillera. Journal of Petrology, **30**: 557-581.

Sevigny, J. H., Parrish, R. R., Donelick, R. A., Ghent, E. D., 1990. Northern Monashee Mountains, Omineca Crystalline Belt, Brithish Columbia: Timing of metamorphism, anatexis, and tectonic denudation. Geology, **18**: 103-106.

Simony, P. S., Ghent, E. D., Craw, D., Mitchell, W., Robbins, D. B., 1980. Structural and metamorphic evolution of northeast flank of Shuswap Complex, southern Canoe River area, British Columbia. *In* Crittenden, M. D., Coney, P. J., Davis, G. H., (Ed), Cordilleran metamorphic core complexes. Geological Society of America, Memoir 153: 445-461.

Simpson, C., Schmid. S. M., 1983. An evaluation of criteria to deduce the sense of movement in sheared rocks. Geological Society of America Bulletin. 94**; 11**: 1281-1288.

Struik, L. C., 1993. Intersecting intracontinental Tertiary transform fault systems in the North American Cordillera. Canadian Journal of Earth Sciences, **30**: 1262-1274.

Tempelman-Kluit, D., Parkinson, D., 1986. Extension across the Eocene Okanagan crustal shear in southern British Columbia. Geology, **14**: 318-321.

Van Den Driessche, J., Maluski, H., 1986. Mise en évidence d'un cisaillement ductile dextre d'âge crétacé moyen dans la région de Tête Jaune Cache (nord-est du complexe métamorphique Shuswap, Columbie-Britannique). Canadian Journal of Earth Sciences, **23**: 1331-1342.

van der Velden, A. J., Cook, F. A., 1994. Displacement of the Lewis thrust sheet in southwestern Canada: New evidence from seismic reflection data. Geology, **22**: 819-822.

_____ 1996. Structure and tectonic development of the southern Rocky Mountain trench. Tectonics, **15**, No. 3: 517-544.

Vanderhaeghe, O., 1997. Role of partial melting during late-orogenic collapse [Ph.D. thesis]: Minneapolis, Minnesota, University of Minnesota.

Vanderhaeghe, O., Teyssier, C., 1997. Formation of the Shuswap metamorphic core complex during late-orogenic collapse of the Canadian Cordillera: Role of ductile thinning and partial melting of the mid-to lower crust.

Geodinamica Acta (Paris), **10**: 41-58.

Varsek, J. L., Cook. F. A., 1991. Seismic reflection geometry of a folded and detached accretionary complex, Kootenay Arc, British Columbia. Geology, **19**: 159-162.

Walker, R. T., 1989. Geology of the Mt. Lulu area, southern Cariboo Mountains, British Columbia [M.Sc. thesis]: Calgary, Alberta, The University of Calgary.

Wanless, R. K., Stevens, R. D., Lachance, G. R., Edmonds, C. M., 1968. Age determinations and geological studies, K - Ar isotopic ages, report 8. Geological Survey of Canada, Paper 67-2A: 1-53.